Aus dem Max von Pettenkofer-Institut für Hygiene und Medizinische Mikrobiologie der
Ludwig-Maximilians-Universität München

Lehrstuhl: Bakteriologie
Komm. Vorstand: Prof. Dr. Rainer Haas

Phosphoinositide Modulation during *Legionella pneumophila* Infection

Dissertation
to Attain the Doctor degree in Natural Sciences at the Medical Faculty of the Ludwig-Maximilians-Universität München

Presented by

Stephen Douglas Weber

from Ottawa

Printed with the Permission of the Medical Faculty
of the Ludwig-Maximilians-Universität München

Supervisor: Prof. Dr. Hubert Hilbi

2nd Examiner: Prof. Dr. Alexander Dietrich

Dean of the Medical Faculty (Dekan)
Prof. Dr. med. Dr. h.c. Maximilian Reiser, FACR, FRCR

Date of the oral examination: 25.06.2015

Eidesstattliche Versicherung

Ich, Stephen Douglas Weber, erkläre hiermit an Eides statt, dass ich die vorliegende Dissertation mit dem Thema selbständig verfasst, mich außer der angegebenen keiner weiteren Hilfsmittel bedient und alle Erkenntnisse, die aus dem Schrifttum ganz oder annähernd übernommen sind, als solche kenntlich gemacht und nach ihrer Herkunft unter Bezeichnung der Fundstelle einzeln nachgewiesen habe. Ich erkläre des Weiteren, dass die hier vorgelegte Dissertation nicht in gleicher oder in ähnlicher Form bei einer anderen Stelle zur Erlangung eines akademischen Grades eingereicht wurde.

_____ _____

Ort, Datum Unterschrift

TABLE OF CONTENTS

Abbreviations

AA	amino acid
Amp	ampicillin
AYE	ACES Yeast Extract
BLAST	Basic Local Alignment Search Tool
BPP	β-propeller phytase
BS	blasticidin-S
Cam	chloramphenicol
CCD	charge coupled device
CFU	colony forming units
CMOS	complementary metal-ion-semiconductor
CnxA	calnexin
CPhy	cysteine phytase
CYE	charcoal yeast extract
DAG	diacylglycerol
Dot	defective organelle trafficking
EE	early endosome
ER	endoplasmic reticulum
ERES	endoplasmic reticulum exit site
FYVE	Fab 1, YOTB, Vac 1, and EEA1
G418	genetecin
GAP	GTPase-activating protein
GDF	GDI displacement factor
GDI	GDP dissociation inhibitor
GEF	guanine nucleotide exchange factor
GFP	green fluorescence protein
GST	glutathione S-transferase

HAP	histidine acid phosphatase
HRPO	horseradish peroxidase
Icm	intracellular multiplication
Ins	inositol
Ins(x)P_x	inositol phosphate
InsP_6	phytic acid (phytate)
IPTG	isopropyl-1-thio-D-galactopyranoside
Kan	kanamycin
LCV	*Legionella*-containing vacuole
LE	late endosome
LppA	*Legionella pneumophila* phytase A
LPS	lipopolysaccharide
Lqs	*Legionella* quorum sensing
LYS	lysosome
MCV	*Mycobacterium*-containing vacuole
MOI	multiplicity of infection
mRFP	monomer red fluorescence protein
MVB	multivesicular body
Neo	neomycin
OCRL	oculocerebrolrenal syndrome of Lowe
OD_x	optical density at x nm
PA	Phosphatidic acid
PAP	purple acid phosphatase
PBS	phosphate-buffered saline
PC	phosphatidylcholine
PFA	paraformaldehyde
PH	Pleckstrin homology
PI	phosphoinositide

PI3K	phosphatidylinositol 3-kinase
PI4K	phosphatidylinositol 4-kinase
PLC	phospholipase C
PM	plasma membrane
PTEN	phosphatase and tensin homologue on chromosome ten
PtdIns	phosphatidylinositol
PtdIns(x)P_x	phosphatidylinositol phosphate
PTP	protein tyrosine phosphatase
PX	phox
R	resistant
RT	room temperature
RBS	ribosomal binding site
SCV	*Salmonella*-containing vacuole
SHIP	SRC Homology 2 Domain-containing Inositol-5-Phosphatase
SNX	sorting nexin
SPI-1	*Salmonella* pathogenicity island 1
SPI-2	*Salmonella* pathogenicity island 2
TBS	tris-buffered saline
TEN	tubular endosomal network
TGN	trans-Golgi network
T3SS	type III secretion system
T4SS	type IV secretion system
V-ATPase	vacuolar H^+-ATPase
Vps	vacuolar protein sorting

List of Published Works

2014

Weber, S., Stirnimann, C. U., Wieser, M., Frey, D., Meier, R., Engelhardt, S., Li, X., Capitani, G., Kammerer, R. A., Hilbi, H. A type IV-translocated *Legionella* cysteine phytase counteracts intracellular growth restriction by phytate. *J. Biol. Chem., 289*(49), 34175-34188.

Weber, S., Wagner, M., Hilbi, H. Live-cell imaging of phosphoinositide dynamics and membrane architecture during *Legionella* infection. *mBio*, *5*(1), e00839-13.

Weber, S. and Hilbi, H. Live cell imaging of phosphoinositide dynamics during *Legionella* infection. In *In Meth. Mol. Biol., Pathogen-host interactions: methods and protocols* (pp. 153-167). *Vergunst, A.C. & O'Callaghan, D. (eds.), Springer Press.*

2013

Weber, S., Dolinsky, S., Hilbi, H. Interactions of *Legionella* effector proteins with host phosphoinositide lipids. In *Legionella* (pp. 367-380). Humana Press.

Finsel, I., Ragaz, C., Hoffmann, C., Harrison, C. F., **Weber, S.**, van Rahden, V. A., Johannes, L., Hilbi, H. The *Legionella* effector RidL inhibits retrograde trafficking to promote intracellular replication. *Cell host & microbe*, *14*(1), 38-50.

2011

Hilbi, H., **Weber, S.**, Finsel, I. Anchors for effectors: subversion of phosphoinositide lipids by *Legionella*. *Frontiers in microbiology*, *2*.

Summary

The causative agent of Legionnaires' disease, *Legionella pneumophila*, colonizes diverse environmental niches including biofilms, plant material and protozoa. *Legionella*-containing vacuole (LCV) formation is governed by the bacterial Icm/Dot type IV secretion system that translocates ~300 different "effector" proteins into host cells. Several translocated effectors anchor to the LCV cytosolic membrane through phosphoinositide (PI) lipids. The spatiotemporal LCV PI pattern remains unknown. In the course of this dissertation, the soil amoeba *Dictyostelium discoideum* producing fluorescent probes for specific PI lipids was used to characterize the LCV PI dynamics by live cell imaging.

Upon uptake of wild-type or Icm/Dot-deficient (avirulent Δ*icmT* mutant) *L. pneumophila*, PtdIns(3,4,5)P_3 transiently accumulated for an average of 40 s on these early phagosomes, which acquired PtdIns(3)*P* within 1 min after uptake. While phagosomes containing Δ*icmT* mutant bacteria remained positive for PtdIns(3)*P*, more than 80% of wild-type LCVs gradually lost this PI within 2 h. This process was accompanied by a major rearrangement of PtdIns(3)*P*-positive membranes, which were condensed and segregated from the replication-permissive compartments. PtdIns(4)*P* transiently localized to early phagosomes harboring wild-type or Δ*icmT L. pneumophila* and was cleared within minutes after uptake. During the following 2 h, PtdIns(4)*P* steadily accumulated again only on wild-type LCVs, which maintained a discrete PtdIns(4)*P* identity spatially separated from the tightly surrounding endoplasmic reticulum (ER) for at least 8 h. The separation of PtdIns(4)*P*-positive and ER membranes was even more pronounced for LCVs harboring Δ*sidC-sdcA* mutant bacteria defective for ER recruitment. This feature demonstrated the sequential assembly of the LCV, in which PtdIns(4)*P* is generated on the LCV membrane, then subsequently used as an anchor by SidC which recruits the ER membrane into close surrounding.

In habitats naturally colonized by *L. pneumophila*, *myo*-inositol-hexakisphosphate (phytate) is prevalent and used as a phosphate storage compound or as a siderophore. The *L. pneumophila* protein LppA was identified as an Icm/Dot substrate and cysteine-phytase. Phytate could reversibly abolish growth of *L. pneumophila* in broth, an inhibition which could be relieved by LppA overproduction or by metal ion titration. *L. pneumophila* lacking *lppA* replicated less efficiently in amoebae under phytate load.

These findings elucidate the temporal and spatial dynamics of PI lipids implicated in LCV formation and provide insight into LCV membrane and effector protein interactions. The chelator phytate was also identified as an intracellular bacteriostatic agent and revealed a T4SS-translocated *L. pneumophila* phytase that counteracts intracellular bacterial growth restriction by phytate.

Zusammenfassung

Legionella pneumophila, der Erreger der Legionärskrankheit, kolonisiert diverse ökologische Nischen einschließlich komplexer Biofilme, pflanzlichen Materials und freilebender Protozoen. Die Bildung der sogenannten *Legionellen*-enthaltenden Vakuole (LCV) ist vom Icm/Dot Typ IV Sekretionssystem (T4SS) abhängig, welches schätzungsweise 300 verschiedene "Effektor"-Proteine in die Wirtszelle translozíert. Einige dieser Effektoren können an Phosphoinositide (PI) auf der zytoplasmatischen Seite der LCV-Membran binden. Die räumlich-zeitliche PI Dynamik auf der LCV war weitgehend unbekannt. Im Rahmen dieser Dissertation wurden PI-spezifische fluoreszierende Sonden in der Amöbe *Dictyostelium discoideum* produziert, um das LCV PI-Muster mittels Echtzeitmikroskopie zu charakterisieren.

Im Verlauf der Aufnahme von Wildtyp *L. pneumophila* oder einer avirulenten Mutante (Δ*icmT*) akkumulierte das Lipid PtdIns(3,4,5)P_3 für durchschnittlich 40 s auf dem Phagosom, welches innerhalb der ersten Minute auch PtdIns(3)*P* aufgenommen hatte. Während Phagosomen, welche die Δ*icmT* Mutante enthalten, PtdIns(3)*P* behielten, verloren über 80% der Wildtyp-enthaltenden LCV das Lipid innerhalb von 2 h. Dieser Verlust erfolgte im Zusammenhang mit einer Umgestaltung von zellulären PtdIns(3)*P*-Membranen, die verdichtet und von der LCV isoliert wurden. PtdIns(4)*P* akkumulierte direkt nach der Aufnahme von Bakterien auf Phagosomen, die Wildtyp *L. pneumophila* oder Δ*icmT* Mutante enthielten und verschwand in den ersten Minuten wieder. Über die nächsten 2 h akkumulierte neuerlich PtdIns(4)*P* exklusiv an der Wildtyp LCV, auf der PtdIns(4)*P* für mindestens 8 h getrennt von dem eng ummantelnden Endoplasmatischen Reticulum (ER) zu erkennen war. Die Trennung zwischen LCV Membran und ER war umso deutlicher in Wirtszellen erkennbar, die mit einer *L. pneumophila* Mutante (Δ*sidC-sdcA*) infiziert wurden, die Defekte in der Rekrutierung von ER zeigt. Diese Beobachtungen illustrieren einen sequenziellen Ablauf des LCV Aufbaus, wobei erst PtdIns(4)*P* auf der LCV Membran produziert wird, das als Anbindestelle für den Effektor SidC dient, welcher anschließend das ER in unmittelbare Nähe bringt.

In den von *L. pneumophila* kolonisierten Lebensräumen ist *myo*-Inositol-Hexakisphosphat (Phytat) sehr häufig und wird als Phosphatspeicher oder Siderophor verwendet. Das Legionellen-Protein LppA wurde als Cystein-Phytase und Effektor des Icm/Dot T4SS identifiziert. Phytat hemmte das Wachstum von *L. pneumophila* in Flüssigkultur reversibel und wirkte somit bakteriostatisch, nicht bakteriozid. Diese Inhibition des Wachstums wurde durch die Überproduktion von LppA oder die Zufuhr von Mikronährstoffen überwunden. Verglichen mit Wildtyp *L. pneumophila* multiplizierte ein Stamm, dem das *lppA* Gen fehlte, schlechter unter Phytat Stress in Amöben.

Insgesamt vermitteln diese Ergebnisse ein detailliertes Bild der räumlich-zeitlichen Dynamik der PI Lipide, die an der Bildung der LCV beteiligt sind und geben einen vertieften Einblick in die LCV-Membranarchitektur und Wechselwirkung mit Effektorproteinen. Das Molekül Phytat wurde in dieser Arbeit als bakterienhemmendes Mittel von Amöben identifiziert. Des Weiteren wurde eine neue, translozierte *L. pneumophila* Phytase charakterisiert, die der bakteriostatischen Wirkung von Phytat in Amöben entgegenwirkt.

1 Introduction

1.1 *Legionella pneumophila* Ecology and Pathogenesis

1.1.1 Discovery and Ecology

Legionnaire's disease first gained attention as an epidemiological problem at a 1976 convention of the American Legion, at which 29 of the 182 infected succumbed to the illness. The etiological agent was soon after identified as a Gram-negative bacterium, *Legionella pneumophila* acquired through airborne transmission (Fraser *et al.*, 1977; McDade *et al.*, 1977; Muder *et al.*, 1986). There was no indication that *L. pneumophila* could be transmitted from person to person (Victor *et al.*, 1983), meaning that humans are an accidental host representing an evolutionary dead end for the pathogen. *L. pneumophila* is a non-capsulated, flagellated, rod-shaped obligate aerobe. It belongs to the class γ-proteobacteria of the family Legionellaceae (Brenner *et al.*, 1979). *L. pneumophila* is the most extensively studied of the species, as two of its multiple strains, "Philadelphia 1" and "Paris", are responsible for the overwhelming majority of cases (Victor *et al.*, 2002). Progression of the disease involves severe pneumonia accompanied by fever, malaise, nonproductive cough and in some cases, renal failure (Tsai *et al.*, 1979). Legionnaire's disease has a relatively high rate of mortality as instanced by an outbreak from a water-cooling tower with 21% fatality (Nguyen *et al.*, 2006). Infections that are not fatal but result in flu-like symptoms are termed Pontiac fever (Glick *et al.*, 1978).

Numerous outbreaks of Legionnaire's disease have occurred since the discovery of the bacterium, which in the grand scheme of known infectious agents, was relatively recent. This late emergence can be attributed to increased urbanization and development and use of anthropogenic water systems, as witnessed by outbreaks from water towers and presence of the bacteria in household water systems and air conditioners (Nguyen *et al.*, 2006; Bollin *et al.*, 1985; Dondero *et al.*, 1980). Of particular hazard are ventilation and cooling systems in hospitals, which put already immunocompromised patients at high risk of infection by *L. pneumophila* (Sabria and Yu, 2002). Nearly all cases arise from artificial water sources, as the bacteria are generally incapable of replicating independently of a host in natural water sources (Declerck, 2010).

In its freshwater environment, the bulk of *L. pneumophila* colonizes pre-existing biofilms (Murga *et al.*, 2001; Mampel *et al.*, 2006; Declerck, 2010), where the bacteria cycle between replicative and infections phases (Molofsky and Swanson, 2004). This biphasic lifestyle is reflected by major changes in gene expression (Brüggemann *et al.*, 2006). The natural host for *L. pneumophila* is the free-living and soil dwelling *Acanthamoeba castellanii* (Rowbotham, 1989; Holden *et al.*,

1984). *L. pneumophila* viability is not limited to *A. castellanii*, but extends to a variety of amoebae or protozoa including *Hartmannella vermiformis* (Fields *et al.*, 1993), *Dictyostelium discoideum* (Hagele *et al.*, 2000; Solomon *et al.*, 2000), *Tetrahymena pyriformis* (Fields *et al.*, 1984), and *Naegleria fowleri* (Newsome *et al.*, 1985) among others. Multiple mammalian cell lines can also support replication (Fields, 1996). In spite of *L. pneumophila*'s broad host range for intracellular replication, extracellular growth in the laboratory is only supported with special media (Feeley *et al.*, 1979).

It was proposed that *L. pneumophila* co-evolved with its natural host resulting in a selection of virulence factors which can also support infection in other organisms (Greub and Raoult, 2004; Brüggemann *et al.*, 2006). Namely, human alveolar macrophages bear significant resemblance to *A. castellanii*, and as such are the target of *L. pneumophila* infection in humans (Rowbotham, 1980; Nash *et al.*, 1984). *L. pneumophila* has a very plastic survival mechanism, employing several strategies to evade host defences and exploit host factors to create a replication-permissive niche in a vacuole derived from the host's plasma membrane (PM) (Brüggeman *et al.*, 2006; Hubber and Roy, 2010). Upon uptake, *L. pneumophila* avoids the endocytic pathway (Horwitz and Maxfield, 1984; Andrews *et al.*, 1998), acquires several host proteins, and ultimately takes on the identity of an ER-like compartment (Swanson and Isberg, 1995; Kagan and Roy, 2002). This compartment, termed the *Legionella*-Containing Vacuole (LCV), supports replication of the bacteria until their release as highly virulent and motile rods. *L. pneumophila* presents itself as an interesting candidate for study, not only for its wealth of virulence factors, but also for the array of host processes it manipulates.

1.1.2 Virulence through a Type-IV Secretion System

Several pathogenic bacteria employ secretion systems as part of their invasive strategy. In particular, the type III secretion system (T3SS) used by *Salmonella enterica*, *Shigella flexneri*, enteropathogenic *Escherichia coli*, and *Yersinia sp.* among others has been extensively characterized (Cornelius *et al.*, 2000). Similarly, *L. pneumophila*, *Coxiella burnetii*, *Bordetella pertussis*, *Helicobacter pylori*, and *Brucella sp.* among others employ a type IV secretion system (T4SS), functionally homologous to the T3SS (Segal *et al.*, 2005). Compared to the T3SS, the T4SS is optimized to accommodate larger substrates, and as such used by bacteria to translocate proteins and nucleoprotein complexes into cells (Christie and Vogel, 2000).

L. pneumophila and *C. burnetii* assemble a type IVB secretion system (Segal *et al.*, 2005). The type IVB secretion system assembled by *L. pneumophila* has twice as many proteins as the type IVA, with very little homology (Segal *et al.*, 2005). The essential mediator of the *L. pneumophila* infection is the Icm/Dot (intracellular multiplication/defective organelle trafficking) T4SS. This translocation apparatus takes early origin as an apparatus for bacterial conjugation (Christie, 2001). It

is still capable of conjugation but serves another function in translocating “effector proteins”, the virulence factors of *L. pneumophila*, into the host cell (Burns, 2003; Vogel *et al.*, 1998).

The T4SS in *L. pneumophila* is an assembly of twenty-six proteins encoded from genes organized on two separate regions of the genome (Vincent *et al.*, 2012, Segal *et al.*, 2005). From a selection of these proteins, two subcomplexes are formed, consisting of five proteins each. The subassembly comprising the core of the secretion system and spanning both bacterial membranes comprises of DotC, DotD, DotF, DotG, and DotH proteins (Vincent *et al.*, 2006). Protein dimer pairs of DotF and DotG mediating the transmembrane connection can independently associate with DotH, DotC, and DotD in the outer membrane (Vincent *et al.*, 2006). The pore forming protein DotH requires DotC and DotD lipoproteins for its insertion into the outer membrane (Vincent *et al.*, 2006; Nakano *et al.*, 2010). The second subassembly complex consists of coupling protein DotL, apparatus proteins DotM and DotN, and secretion adaptor proteins IcmS and IcmW which serve as chaperones for effector proteins (Vincent *et al.*, 2012; Cambronne and Roy, 2007). DotL directly binds DotM, serving as an inner membrane receptor linking substrates to secretion where catalyzed ATP hydrolysis provides energy for translocation (Vincent *et al.*, 2012; Tato *et al.*, 2005).

Additional T4SSs were described in *L. pneumophila*. The *Legionella* virulence homologue (*lvh*) is homologous to the type IVA and the *tra* system is homologous to Tra proteins of *E. coli* plasmid F (Segal *et al.*, 1999; Brassinga *et al.*, 2003). The *lvh* is not essential for intracellular replication of *L. pneumophila*, but some Icm/Dot and *lvh* components can interact and substitute one another (Segal *et al.*, 1999). The approximately 65 kb *tra* pathogenicity island is only found in Philadelphia 1 strains, but is absent from the JR32 strains used in this work (Brassinga *et al.*, 2003).

To date, around 300 effector proteins have been discovered in *L. pneumophila*. Contrary to the T3SS which translocates substrates via an N-terminal secretion signal, all substrates of the T4SS possess a C-terminal secretion signal. RalF was the original effector for which the C-terminal translocation signal was identified (Nagai *et al.*, 2005). Since then, diverse screening methods were designed to identify potential effectors of the Icm/Dot T4SS. Substrates have been identified based on their interaction with the chaperone complex of IcmS and IcmW (Ninio *et al.*, 2005). Systematic screening has been used, involving *in silico* pre-filtering of candidates based on similarity of translocation signals to known Icm/Dot substrates followed by confirmation by adenylate cyclase translocation assays (Kubori *et al.*, 2008). Approaches also examined the presence of conserved promoter elements, bound by CpxR or PmrA, which serve as regulators of the T4SS and effectors (Altman and Segal, 2008; Zusman *et al.*, 2007). Genetic screens in yeast led to discovery of several effectors which interfere with membrane or vesicle trafficking (Heidtman *et al.*, 2009; De Felipe, 2008; Shohdy *et al.*, 2005). Upregulation of genes in *L. pneumophila* during infection was also used as a cue for identifying genes encoding proteins which exploit host cell function (Brüggemann *et al.*,

2006; De Felipe *et al.*, 2005; Cazalet 2004). Finally, sophisticated computer learning and bioinformatics approaches have provided long lists of probable Icm/Dot substrates based on sequence homology with both known effectors and non-secreted proteins. (Burnstein *et al.*, 2009)

1.1.3 Uptake of *L. pneumophila* into a Host Cell

L. pneumophila can invade a wide range of hosts between amoeboid and mammalian cells (see **1.1.1**). In its natural environment, *L. pneumophila* encounters exclusively phagocytic predators. Nonetheless, it can also invade non-phagocytic cells with varying efficiency (Dreyfus, 1987; Fields, 1996). The role of the T4SS is a central point of focus in investigating internalization of the bacteria. It was determined that the T4SS accounted for a 10-fold more efficient uptake of wild-type *L. pneumophila* over Icm/Dot defective mutants into *A. castellanii*, by a process independent of bacterial adherence to a receptor (Hilbi *et al.*, 2001). Stressing bacterial cultures by overnight incubation in phosphate-buffered saline suppressed the defect in entry observed for dotA and dotB mutants into the host cell. These bacteria also showed an enhanced resistance to oxidative stress (Bandyopadhyay *et al.*, 2004). Similarly, it was reported that the Icm/Dot T4SS promotes macropinocytic uptake of *L. pneumophila* into murine macrophages (Watarai *et al.*, 2001). Furthermore, the phosphatidylinositol-3 kinase (PI3K) inhibitor wortmannin blocked uptake of avirulent *L. pneumophila* without affecting acting polymerization (Khelef *et al.*, 2001). Different entry strategies were proposed for wild-type and Icm/Dot mutants and that wild-type bacteria may inactivate or circumvent the PI3K on the way to establishing its replicative niche (Khelef *et al.*, 2001). In agreement, PI3K was shown to be dispensable for wild-type *L. pneumophila* in infection of *D. discoideum* (Weber *et al.*, 2006). In contrast to the previous studies on uptake, it was proposed that *L. pneumophila* is taken up by macropinocytosis, as opposed to phagocytosis, requiring PI3K and PTEN unlike *E. coli* (Peracino *et al.*, 2010). Macropinocytosis, by comparison to phagocytosis, does not necessitate bacterial adhesion to the cell.

The necessity of PtdIns(3,4,5)P_3 in uptake of *L. pneumophila* is not surprising given its role in directing assembly of actin into dendritic structures (Gerisch, 2010). Actin depolymerisation coincides with clearance of PtdIns(4,5)P_2. This clearance is even necessary for closure of the macropinosome, which in itself entails an extensive rearrangement of the actin cortex (Peracino *et al.*, 2010; Hacker *et al.*, 1997). Uptake of *L. pneumophila* into *D. discoideum* shows coronin enrichment around entry sites and is blocked by latrunculin A, similar to the host's uptake of inert particles (Lu and Clarke, 2005). It was also proposed that the ER membrane contributed to phagosome formation and protection of *L. pneumophila* phagosomes from fusion with lysosomes (Gagnon *et al.*, 2002; Desjardins, 2003), more so since the LCV acquired an ER label shortly after internalization (Fajardo *et al.*, 2004). However,

live cell imaging of *D. discoideum* expressing a *gfp*-fusion to the resident ER marker calnexin showed that ER membranes were in close proximity to the internalized phagosome, but did not interact with it (Lu and Clarke, 2005).

Research has also focused on factors determining internalization of *L. pneumophila* independently of the Icm/Dot T4SS. The protein LpnE was attributed to efficient entry of *L. pneumophila* into THP and A549 cells, presumably through tetratricopeptide repeats which may be important for LpnE-mediated interaction of *L. pneumophila* with host cells (Newton *et al.*, 2006). Albeit, the cells tested were not professional phagocytes and LpnE may be less crucial to infection of amoebae. The *Legionella* quorum-sensing cluster was also identified as a determinant of efficient *L. pneumophila* uptake into a host. Deletions of the cluster regulator *lqsR*, sensor kinases *lqsS* or *lqsT*, or the entire cluster caused dramatic decreases in uptake efficiency of the bacteria (Kessler *et al.*, 2013). Overexpression of the autoinducer, LqsA (Tiaden et al., 2010), could however revert a single *lqsS* or *lqsT* defect.

1.1.4 Evasion of the Endocytic Pathway

Upon entry into the host cell in a phagosome (macropinosome), *L. pneumophila* is confronted with the classical endocytic pathway, which typically results in acidification of a phagosome by fusion with lysosomes. However, *L. pneumophila* has evolved an Icm/Dot-coordinated strategy to avoid lysosomal fusion (Roy *et al.*, 1998). Accordingly, wild-type *L. pneumophila* does not acquire VatM, the transmembrane subunit of the acidifying V-ATPase complex. Internalized phagosomes as well as maturing LCVs are void of the marker (Chen *et al.*, 2004; Lu and Clarke, 2005). In *D. discoideum*, macropinosomes containing inert particles acquire VatM within minutes of internalization, meaning that *L. pneumophila* already interferes with endocytic trafficking just following internalization (Clarke *et al.*, 2002). *L. pneumophila* is able to maintain a neutral pH in its phagosome and LCV, and doing so is necessary for its viability. In addition to VatM being excluded from the phagosome, a secreted effector SidK interacts with the VatA subunit of the V-ATPase, thereby inhibiting proton translocation to and acidification of the vacuole (Xu *et al.*, 2010).

L. pneumophila wild-type-containing vacuoles do not associate with Rab5 and the majority remain devoid of Rab7 and Lamp1, while avirulent strains acquire these markers (Roy *et al.*, 1998; Clemens *et al.*, 2000). The Icm/Dot effector VipD interferes with endosomal trafficking through interaction with Rab5 and Rab22, obstructing interaction of these Rabs with their downstream partners (Ku *et al.*, 2012). Presence of Rab7 and additional endosomal marker Rab14 on the LCV membrane indicates that the LCV nonetheless communicates with the endocytic pathway (Urwyler *et al.*, 2009). The effector AnkX interferes with microtubule-dependent vesicle trafficking, obstructing

LCV fusion with late endosomes (Pan *et al.*, 2008). AnkX acts through phosphocholination of Rab1 and the endocytic pathway regulator Rab35 (Mukherjee *et al.*, 2011). Another effector LegC3 indirectly blocks formation of trans-SNARE complexes during vacuole fusion, disrupting endocytic transport (Bennett *et al.*, 2013; De Felipe *et al.*, 2008). Finally, independently of secreted effectors, developmentally-regulated changes to the surface lipopolysaccharide composition on *L. pneumophila* itself were shown to hinder late endosome fusion with lysosomes (Fernandez-Moreira *et al.*, 2006).

1.1.5 Formation of the Replication-Permissive ER-Like Compartment

Evasion of lysosomal degradation by *L. pneumophila* is accompanied by modifications to the phagosome (macropinosome) which see the transition of the internalized vacuole into the replication-permissive LCV. The multifaceted LCV assembly takes place over several hours in a well orchestrated series of spatiotemporally coordinated events. The ultimate result is *L. pneumophila* doubling roughly every 2 h in a compartment resembling the ER (Horwitz, 1983; Tilney *et al.*, 2001). The acquired ER identity is the most obvious feature of the LCV, and one of the most extensively studied (**Figure 1.1**). ER-derived vesicles and mitochondria are found in close association to the *Legionella* phagosome within minutes after uptake (Kagan and Roy, 2002; Horwitz, 1983). Initially observed are the smooth ER exit site (ERES) vesicles, whose presence gives way to the appearance of ribosomes within a few hours (Swanson and Isberg, 1995). The appearance of ribosomes on the LCV also coincides with the intrinsic ER chaperone calnexin, or glucose 6-phosphatase in the LCV lumen (Kagan and Roy, 2002; Robinson and Roy, 2006), implying that the ribosomes are of ER origin. Presence of glucose 6-phosphatase in the lumen pointed at delivery of soluble ER components into the LCV. As such, it was reported that the ER fused with the LCV membrane (Robinson and Roy, 2006). On a more macroscopic scale, the process of ER acquisition to the *Legionella* vacuole was characterized in *D. discoideum* expressing fluorescent fusions of ER proteins (Lu and Clarke, 2005). ER exit vesicles were observed to associate with the LCV 15 minutes after infection. This association correlated with a reduction in phagosome motion. After about 50 min post infection, the intrinsic ER marker calnexin was observed to surround the LCV. At this point, LCV motion came to a halt, as if to indicate that the LCV had made a connection to the ER network.

Rab1 mediates ER-Golgi transport and fusion and is detected on the internalized *Legionella* wild-type phagosome minutes after uptake (Kagan *et al.*, 2004). Rab1 is a small GTPase recruited to the LCV, where it is activated through guanine exchange factor (GEF) activity of the PtdIns(4)*P*-binding effector SidM (Machner and Isberg, 2006; Murata *et al.*, 2006; Brombacher *et al.*, 2009; Schoebel *et al.*, 2009). SidM can prolong its interaction by ampylation of Rab1, thereby preventing deactivation of its target by the GTPase-activating protein (GAP) LepB (Ingmundson *et al.*, 2007;

Müller *et al.*, 2010). The effector SidD serves as a de-ampylase, allowing LepB to activate the GTPase activity of Rab1, causing it to dissociate from the LCV membrane (Neunuebel *et al.*, 2011; Gazdag *et al.*, 2013). Additionally, the effector LidA binds to the LCV via PtdIns(3)*P* where it preserves Rab1 in its active state (Machner and Isberg, 2006; Brombacher *et al.*, 2009; Neunuebel *et al.*, 2012).

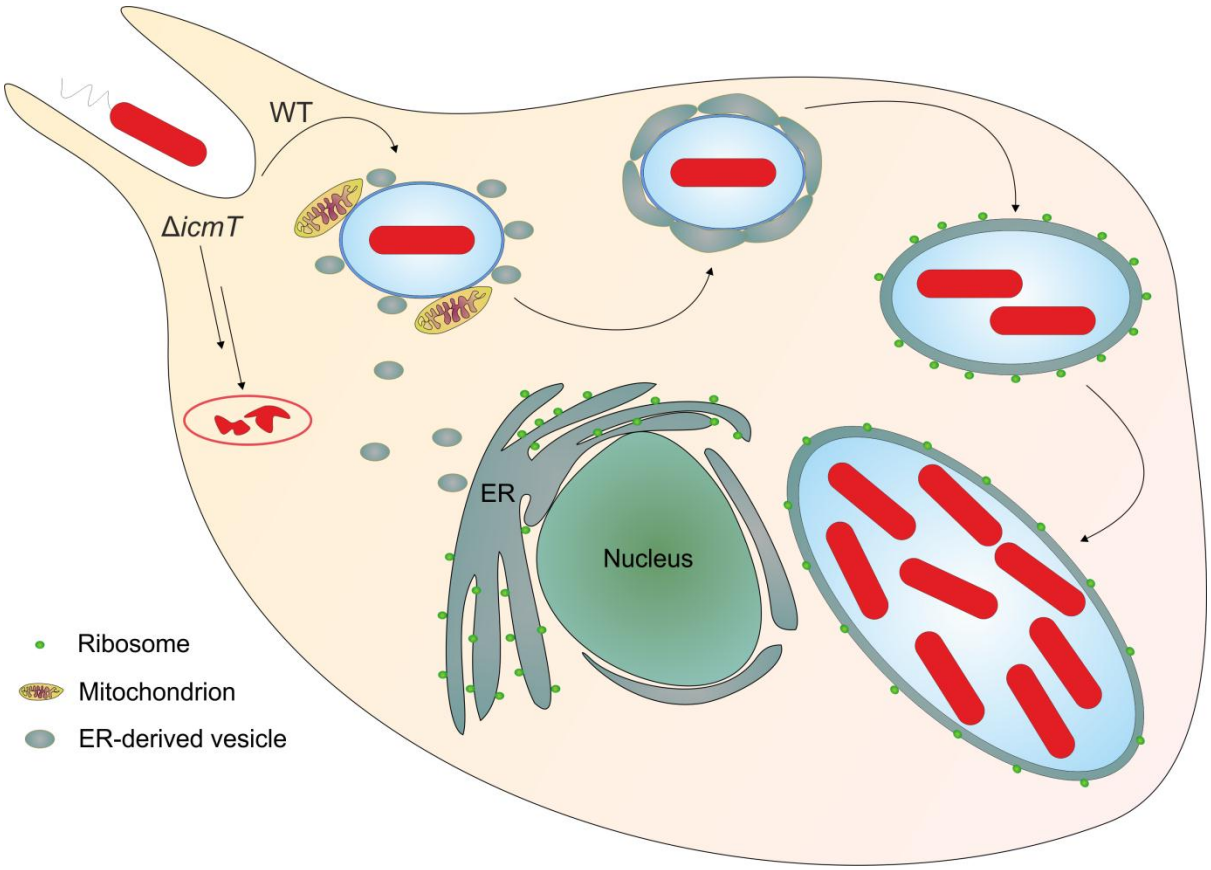

Figure 1.1 Standard model for acquisition of an ER-like identity by the internalized *Legionella*-containing phagosome. The internalized *Legionella* phagosome evades lysosomal degradation and associates with mitochondria and ER-derived vesicles. It then fuses with the recruited ER vesicles. Following steps involve reported fusion of the LCV with ER membranes and transition of the LCV into a compartment resembling the rough ER. Avirulent Δ*icmT L. pneumophila* do not intercept vesicles from the ER and are degraded over the following hours. ER, endoplasmic reticulum.

A widely accepted model of LCV ER recruitment has a central role for Rab1. Activated Rab1 drives membrane fusion by tethering of ER-derived vesicles to the LCV. The SNARE protein Sec22b present on vesicles of ER origin typically partners with SNARES on the Golgi complex (Xu *et al.*, 2000). Sec22b was identified on the LCV, but in absence of the Golgi SNARE complex (Derre and Isberg, 2004; Kagan *et al.*, 2004). Rather, Sec22b can form "illegitimate" complexes with PM syntaxins which are present on the phagosome derived from the PM upon uptake of *L. pneumophila* (Arasaki and Roy, 2010). A few Icm/Dot effectors were identified to play a role in ER recruitment to

the LCV. It was reported that Δ*sidJ* mutants showed a growth defect inferred from the delayed acquisition of ER proteins to the LCV (Liu and Luo, 2007). Double mutants lacking *sidC* and its paralogue *sdcA* also show impaired acquisition of ER, but however do not demonstrate a growth defect (Ragaz *et al.*, 2008). Thus, the requirement for ER recruitment and potentially for ER fusion with the LCV is unclear.

1.1.6 Phosphoinositide Anchors on the *Legionella*-Containing Vacuole

Phosphoinositide (PI) lipids on the cytosolic face of the LCV serve as molecular anchors for multiple *L. pneumophila* effector proteins. In the cell, norperipheral membrane proteins bind to the unique PI head groups through specific recognition folds, such as the PH, PX, FYVE, ENTH/ANTH or FERM domains (Downes *et al.*, 2005; Lemmon, 2008), where they exert their function in vesicle trafficking routes within eukaryotic cells (De Matteis and Godi, 2004; Behnia and Munro, 2005; Di Paolo and De Camilli, 2006). The PI composition of the LCV is poorly characterized, but it has been shown that PtdIns(4)*P* accumulates dependent on the Icm/Dot T4SS and that *L. pneumophila* secretes effectors that bind to both PtdIns(3)*P* and PtdIns(4)*P* (Weber *et al.*, 2006; 2009). As discussed in the previous section (**1.1.5**), SidM and LidA bind to LCV PtdIns(4)*P* and PtdIns(3)*P* respectively to support activated Rab1 function (Brombacher *et al.*, 2009). SidC, which also binds to PtdIns(4)*P* through its 20 kDa $P4C_{SidC}$ domain, recruits ER vesicles to the LCV (Ragaz *et al.*, 2008). The Icm/Dot substrate RalF is an ADP ribosylation factor (ARF) GEF which activates members of the ARF family and is required for Arf1 localization to the *Legionella* phagosome (Nagai *et al.*, 2002). RalF itself localizes to the LCV independently of PI lipids, but potentially indirectly recruits PI4KIIIβ through its interaction with Arf1 (Nagai *et al.*, 2002; Hilbi *et al.*, 2011; Godi *et al.*, 1999).

LpnE is likely not a substrate of the Icm/Dot T4SS but nonetheless selectively binds to PtdIns(3)*P* on the LCV (Weber *et al.*, 2009). It interacts with the host PI phosphatase OCRL1 in mammalian cells, or its homologue Dd5P4 in *D. discoideum*. OCRL1 localizes to and accumulates on LCVs (Weber *et al.*, 2009). In absence of the PI phosphatase, less SidC binding was observed on the LCV, indicative of reduced PtdIns(4)*P* production, yet bacterial replication was significantly increased (Weber *et al.*, 2009).

Some effectors are not implicated in shaping the LCV PI pattern, but specifically bind PtdIns(3)*P*. The glucosyltransferase SetA is recruited to the LCV by its C-terminal PtdIns(3)*P*-binding domain (Jank *et al.*, 2012). The Effector LtpD, which localizes to the LCV and endosomes, was proposed to potentially interfere with endosomal vesicle trafficking (Harding *et al.*, 2013). RidL works to inhibit retrograde trafficking, presumably inhibiting retromer function, thereby promoting

intracellular replication (Finsel *et al.*, 2013). As RidL could be detected on the LCV at 1 h after infection, PtdIns(3)*P* could be indirectly inferred as an LCV lipid component at that time.

1.1.7 Exit of *L. pneumophila* from the Host Cell and Propagation of Infection

Upon reaching critical density, the sedentary replicating rods of *L. pneumophila* become animated with flagella as they transition to an infectious state. Before further infection can proceed, they must escape the bounds of their current host cell. To this end, a few strategies might be at play. The role of an egress pore in cell lysis was put forth although no candidate protein could be associated with this activity (Molmeret and Kwaik, 2002; Molmeret *et al.*, 2002). Also unclear is how SNARE-like *L. pneumophila* effectors LepA and LepB might participate in non-lytic fusion of the LCV with the host cell PM causing release of the bacteria (Chen *et al.*, 2004). Alternatively, *L. pneumophila* might disrupt the LCV membrane to become cytosolic prior to its release (Molmeret *et al.*, 2004). In any case, *L. pneumophila* exiting its natural host *A. castellanii* displays enhanced virulence for further infection (Cirillo *et al.*, 1999).

1.2 Phosphoinositide Metabolism and Modulation by *L. pneumophila*

1.2.1 Phosphatidylinositol and the Seven Naturally Occurring Phosphoinositides

myo-inositol (Ins) is linked at position 1 via a phosphodiester moiety to the sn-3 position of diacylglycerol (DAG) to form phosphatidylinositol (PtdIns). PtdIns is synthesized in the ER from CDP-DAG and Ins by phosphatidylinositol synthase (Agranoff *et al.*, 1958). In prior steps, DAG is converted to phosphatidic acid by a diacylglycerol kinase. Phosphatidic acid and CTP are then converted to CDP-DAG by GDP-diacylglycerol synthase. Most mono-phosphorylations of PtdIns occur by PI4Ks and class III PI3Ks in endomembranes (see **1.2.2**), namely of endosomes and the Golgi (Balla, 2013).

PtdIns can be reversibly phosphorylated at its D3, D4, and D5 positions to give seven naturally occurring PI lipids, PtdIns(3)*P*, PtdIns(4)*P*, PtdIns(5)*P*, PtdIns(3,4)P_2, PtdIns(3,5)P_2, PtdIns(4,5)P_2, and PtdIns(3,4,5)P_3 (**Figure 1.2**). PI lipids anchor into membranes with their fatty acid tails, presenting their head group on the membrane surface. They account for roughly 5% of phospholipids and 1% of cellular lipids (Nasuhoglu *et al.*, 2002). At the membrane surface, PIs can regulate protein function and define subcellular localization of peripheral proteins through reversible non-covalent binding (Balla, 2013). Their localization exclusively to the cytosolic face of a membrane makes them available for inter-conversion by phosphatases and kinase. PIs control protein function

through conformational change to the protein which occurs upon association or by promoting interaction of membrane-bound proteins (Cho and Stahelin, 2005).

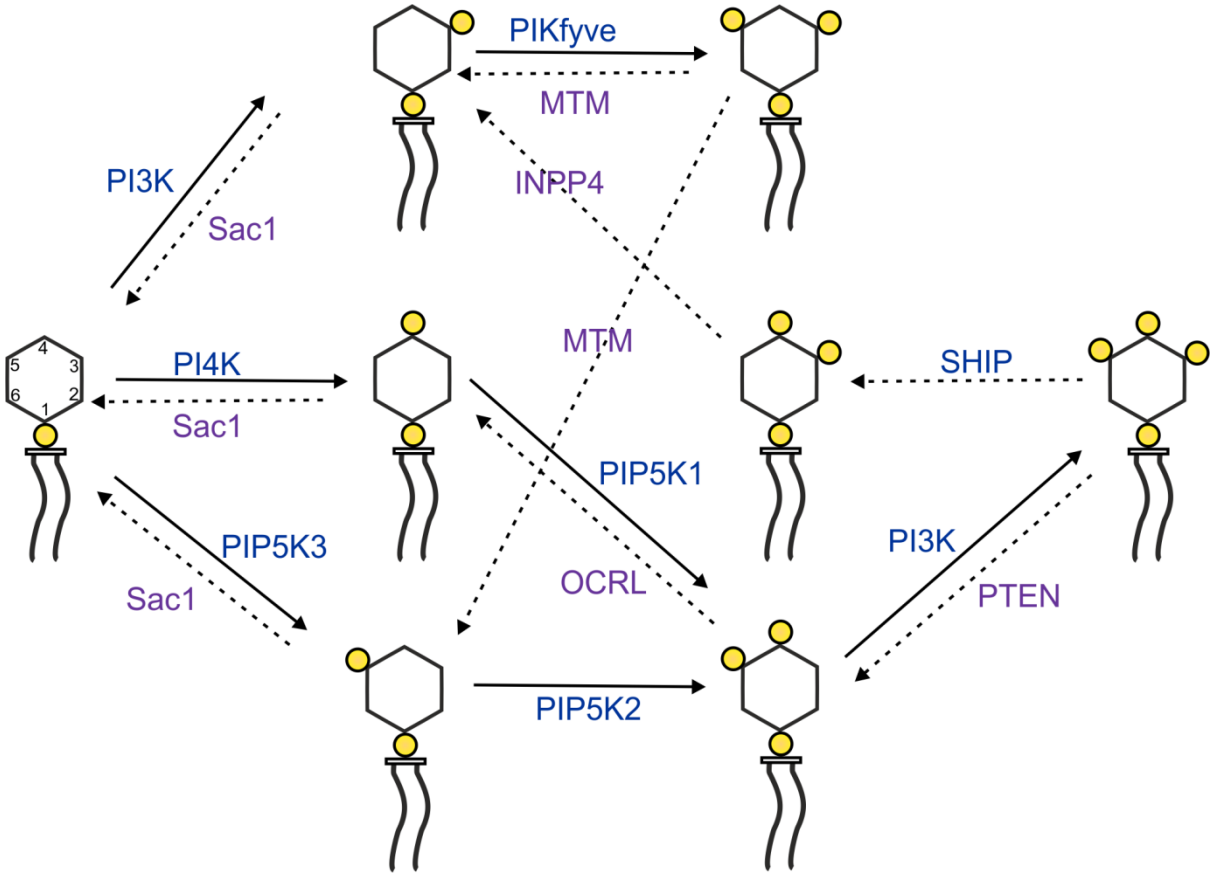

Figure 1.2 Synthesis, metabolism, and inter-conversion of the seven naturally occurring phosphoinositide lipids. PI lipids can be synthesised from PtdIns or through metabolism of other higher order PI lipids. PI lipid synthesis is highly spatially and temporally regulated. The indicated PI kinases (blue) and PI phosphatases (purple) are described in section **1.2.2**.

PIs are subject to a strict subcellular localization as well as spatial and temporal control. PtdIns(4,5)P_2 and PtdIns(4)*P* account for the majority of PI lipids in the cell. PtdIns(3,4,5)P_3 and PtdIns(3,4)P_2 are only transiently observed in the dynamic cell. These four lipids occur on the PM. PtdIns(4,5)P_2 mediates adhesion of the cytoskeleton to the PM and also serves as a precursor to second messengers (Raucher *et al.*, 2000). PtdIns(4)*P* also makes up the identity of the Golgi apparatus and secretory vesicles (De Matteis *et al.*, 2005), and to a lesser extent is found at ER exit sites where it regulates ER export (Blumental-Perry *et al.*, 2006). Early endosomes (EE) and multivesicular bodies (MVB) are characterized by PtdIns(3)*P*, while late endosomes (LE) and MVB transiently acquire PtdIns(3,5)P_2, which is important for recycling membranes (Gary *et al.*, 1998). PtdIns(5)*P* is present at the nuclear membrane where it is held in a balance with PtdIns(4,5)P_2 and linked to stress-induced nuclear signalling and apoptosis (Jones *et al.*, 2006). As the lipid composition

of a membrane is tightly regulated, intrinsic lipid specificities can direct proteins to distinct lipid targets at a specific location in the cell (Sprong *et al.*, 2001). For example, the protein Akt binds to PtdIns(3,4,5)P_3 at the PM, where it is activated by phosphorylation to regulate many downstream processes critical to cell survival and apoptosis (Stokoe *et al.*, 1997). PtdIns transfer proteins (PITP) can transfer PtdIns between membranes but it is not entirely understood how they function in the cell (Balla, 2013). PITPs were originally thought to transfer PtdIns from the ER to the PM, but the mode of action is more involved, with the notion that PITPs equally importantly present PtdIns to enzymes as a type of catalytic chaperone (Cockcroft and Garner, 2011; Kular *et al.*, 2002; Ile *et al.*, 2006).

1.2.2 Phosphoinositide Phosphatases and Kinases

A series of PI kinases and phosphatases serve to synthesise, clear, or interconvert PI lipids along strictly specific and regulated pathways. Distinct enzymes exist to act on specific phosphorylation states of each lipid. Enzymes with overlapping or multiple activities *in vitro* may also be limited to a specific substrate in the cell, based on their subcellular localization (Wen *et al.*, 2008).

The inositol-5-phosphatase SHIP (SRC Homology 2 Domain-containing Inositol-5-Phosphatase) is activated by its recruitment from the cytosol to membranes via its protein-protein interaction domains (Balla, 2013). The classical function of SHIP is to hydrolyze PtdIns(3,4,5)P_3 to PtdIns(3,4)P_2 at the plasma membrane (Wisniewski *et al.*, 1999), a key role in controlling PI3K products (Batty *et al.*, 2007). SHIP has more recently been shown to hydrolyze PtdIns(4,5)P_2 in clathrin-mediated endocytosis (Nakatsu *et al.*, 2010), where it negatively regulates phagocytosis upon its recruitment to the phagocytic cup (Cox *et al.*, 2001).

OCRL1 is expressed in a wide range of tissues and subcellularly localizes to the trans-Golgi network (TGN) and endosomes, promoting retrograde trafficking between the two compartments (Dressman *et al.*, 2000; Suchy *et al.*, 1995; Ungewickell *et al.*, 2004; Choudhury *et al.*, 2005). It preferentially dephosphorylates PtdIns(4,5)P_2 yielding PtdIns(4)*P*. Dd5P4 is a close homologue to OCRL1, the latter of which can mostly restore function in a *Dd5P4* mutant of *D. discoideum* (Loovers *et al.*, 2007). These mutants are severely deficient in bacterial uptake. PtdIns(3,4,5)P_3 is produced normally in the phagocytic cup, but the phagosome doesn't close, suggesting that its conversion by the PI phosphatase is a necessary step in endocytosis (Loovers *et al.*, 2007). Mutations in the OCRL gene cause the X-linked human disease oculocerebrorenal syndrome of Lowe which manifests as congenital cataract, renal tubular acidosis, and mental retardation (Attree *et al.*, 1992; Lowe *et al.*, 1952). Although inositol phosphates (Ins*P*) can compete for binding, PtdIns(4,5)P_2 is the preferred substrate (Zhang *et al.*, 1995). Another PI 5-phosphatase is INPP5B which localizes to the Golgi network and hydrolyzes PtdIns(4,5)P_2, PtdIns(3,5)P_2, and PtdIns(3,4,5)P_3 (Kong *et al.*, 2000). It is

recruited to the phagocytic cup where it converts PtdIns(3,4,5)P_3 to PtdIns(3,4)P_2 (Kamen *et al.*, 2007). Finally, INPP4PA/B hydrolyzes PtdIns(3,4)P_2 to PtdIns(3)*P* and TMEM55A/B hydrolyzes PtdIns(4,5)P_2 to PtdIns(5)*P* (Balla, 2013).

The PI 3-phosphatase PTEN (Phosphatase and Tensin homolog located on chromosome TEN) is one of the critical enzymes antagonizing PtdIns(3,4,5)P_3, converting it to PtdIns(4,5)P_2 at the PM (Li *et al.*, 1997; McConnachie *et al.*, 2003). The N-terminus of PTEN accounts for membrane binding and localization (Redfern *et al.*, 2008), while C-terminal phosphorylation renders the enzyme inactive (Odriozola *et al.*, 2007). PTEN is a major tumor suppressor, as PtdIns(3,4,5)P_3 can stimulate cell proliferation and increases a cell's ability to migrate and resist apoptosis (Yamada and Araki, 2001). Additional 3-phosphatases are the myotubularins (MTM), capable of converting PtdIns(3)*P* and PtdIns(3,5)P_2 to PtdIns and PtdIns(5)*P*, respectively (Laporte *et al.*, 2003).

Phospholipase C (PLC) does not belong to the PI phosphatases, but is critical in regulating PtdIns(4,5)P_2 levels and resulting second messenger molecules. PLC hydrolyzes the phosphodiester bond between the D1 position of the phosphoinositol and the sn-3 position of DAG. PLC is active at the PM where the physicochemical environment is important for its localization, suggesting a possible regulation of PLC through presence of its substrate (Irvine *et al.*, 1984). PLC cycles between the cytosol and the PM, where it anchors to PtdIns(4,5)P_2 through its PH domain (Yamaga *et al.*, 1999). PtdIns(4,5)P_2 is the best known substrate, which yields DAG and Ins(1,4,5)P_3, two important second messengers (Berridge, 1984). The generated Ins(1,4,5)P_3 can in turn compete for the PH domain of PLC, thereby displacing it from the membrane and regulating its activity (Lomasney *et al.*, 1996). Ins(3,4,5)P_3 binds to a ligand-gated calcium-release channel, primarily on the ER, causing direct release of Ca^{2+} by gradient diffusion (Berridge, 1993; Ross *et al.*, 1989).

Multiple PI kinases also exist to antagonise PI phosphatase function. The phosphatidylinositol 3-kinases (PI3K) are divided into three classes. The class I PI3K make PtdIns(3,4,5)P_3 from PtdIns(4,5)P_2 at the PM. Class II PI3K can phosphorylate the D3 position of PtdIns and PtdIns(4)*P*, but not PtdIns(4,5)P_2 *in vitro*, but most likely produce PtdIns(3)*P* as their signalling molecule (Wen *et al.*, 2008). The class III PI3K is represented by a single Vps34 homologue which exclusively phosphorylates PtdIns to PtdIns(3)*P* (Vieira *et al.*, 2001).

PI4Ks are classified as either type II or III. The originally identified class I was later discovered to be a PI3K (Balla, 2013). The PI4Ks can only phosphorylate PtdIns, yielding PtdIns(4)*P*, a major precursor to PtdIns(4,5)*P* (De Matteis *et al.*, 2005). PI4K IIα is membrane-associated while PI4K IIβ is cytosolic, and both PI4K II probably only produce a minor fraction of the cellular PtdIns(4)*P* (De Matteis *et al.*, 2005; Balla, 2013). PI4K IIIα is associated with the ER and PM. PI4K IIIβ shows nuclear and Golgi association. PI4K IIIβ Is regulated by Arf1 and plays an important role in regulating traffic in the late secretory pathway (Godi *et al.*, 1999; Walch-Solimena and Novick,

1999). Inhibition of Arf1's GDP/GTP exchange function by brefeldin A (BFA) causes a rapid dissociation of the PtdIns(4)*P*-specific probes FAPP1 and OSBP from the Golgi (Balla *et al.*, 2005). OSBP and FAPP1 probes both label PtdIns(4)*P* in the Golgi and on small cytoplasmic vesicles, but OSBP additionally labels PtdIns(4)*P* at the PM (Balla *et al.*, 2005). Moreover, $P4C_{SidC}$ strongly labels PtdIns(4)*P* at the PM along with small cytoplasmic vesicles (Ragaz *et al.*, 2008). As such, different PI4Ks are capable of producing distinct pools of PtdIns(4)*P*.

The type III phosphatidylinositol phosphate 5-kinase (PIP5K), known as PIKfyve in mammals (Ikonomov *et al.*, 2002), converts PtdIns(3)*P* to PtdIns(3,5)P_2. It localizes through its FYVE domain to endosomes and MVBs, where it plays an important role in sorting pathways (Dove *et al.*, 2002). Inhibition of this kinase results in swollen endocytic compartments and defects in endocytosis (Ikonomov *et al.*, 2003), as well as disruption of retrograde traffic from the endosomes to the TGN (Rutherford *et al.*, 2006). In addition, cells no longer properly acidify their endocytic compartments, but the role of PtdIns(3,5)P_2 in V-ATPase activity is unclear (Jefferies *et al.*, 2008). The phosphatase Sac3 converts PtdIns(3,5)P_2 back to PtdIns(3)*P* (Ikonomov *et al.*, 2009). Sac1 is capable of returning all mono-phosphorylated PIs to PtdIns (Hughes *et al.*, 2000).

1.2.3 Bacterial PI Phosphatases in Invasion and Evasion of Host Defence

Multiple intracellularly replicating bacteria make use of a secreted PI phosphatase to facilitate their own uptake, evade endocytic trafficking, or modify their vacuole into a replication-permissive compartment. *Shigella flexneri* injects its type III-secreted PI phosphatase IpgD into its target cell from the exterior. This PI 4-phosphatase converts PM PtdIns(4,5)P_2 to PtdIns(5)*P*, causing cytoskeletal remodelling and detachment of the cell from the surrounding matrix (Niebuhr *et al.*, 2002). This remodelling results in membrane ruffling which facilitates uptake of the bacteria. PtdIns(5)*P* also serves to activate the PI3K/Akt survival pathway, hindering apoptosis of the host cell (Pendaries *et al.*, 2006). IpgD does not appear to mediate changes to the bacterial phagosome, as the bacterium escapes this compartment shortly after uptake.

Like IpgD, the type III-secreted SopB (SigD) in *Salmonella enterica* promotes uptake of the bacteria. SopB causes rapid clearance of PtdIns(4,5)P_2 from *Salmonella* entry sites, disrupting PM integrity (Terebiznik *et al.*, 2002). Unlike IpgD, SopB is critical for further modifications to the pathogen vacuole. It is required for generation of PtdIns(3)*P* on the *Salmonella*-containing vacuole (SCV) (Hernandez *et al.*, 2004). PtdIns(3)*P* however is produced by an indirect mechanism. The PtdIns(3)*P* is synthesized from PtdIns by Vps34 which is recruited to the SCV through its association with Rab5 (Mallo *et al.*, 2008). SopB serves to reduce the overall negative charge on the SCV by

clearing PtdIns(4,5)P_2 and indirectly phosphatidylserine, resulting in dissociation of many host endocytic trafficking proteins and inhibiting SCV-lysosome fusion (Bakowski *et al.*, 2010).

In contrast to the previously described pathogens which force entry into non-phagocytic cells, *Mycobacterium tuberculosis* and *L. pneumophila* are taken up by professional phagocytes and do not secrete known PI phosphatases for efficient entry. In the case of *Mycobacterium*, two secreted PI 3-phosphatases, SapM and MptpB, modify the *Mycobacterium*-containing vacuole (MCV) to clear PtdIns(3)*P* to PtdIns, thereby inhibiting endocytic phagosome maturation (Vergne *et al.*, 2005; Beresford *et al.*, 2007). A PI 3-phosphatase, the Icm/Dot effector SidP, was also reported in *L. pneumophila*. *In vitro*, this PI phosphatase could convert PtdIns(3,5)P_2 to PtdIns(5)*P* and PtdIns(3)*P* to PtdIns (Toulabi *et al.*, 2013). SidP was able to complement an absent PI phosphatase function in yeast, but no intracellular growth or PI phenotype was reported in infected cells. Another secreted effector, SidF, was similarly reported as a PI 3-phosphatase, resulting in the *in vitro* production of PtdIns(4)*P* directly from PtdIns(3,4)P_2 or from PtdIns(3,4,5)P_3 in combination with OCRL (Hsu *et al.*, 2012). It was also reported that *sidF* deletion strains accumulated less SidC on the LCV compared to wild-type strains, as an indirect readout for PtdIns(4)*P*. Nonetheless, intracellular replication was not affected by this deletion.

1.2.4 The Amoeba *Dictyostelium discoideum* as a Model for Observing PI Lipids

The social soil amoeba *Dictyostelium discoideum* is a powerful model for investigation of cell biological and developmental processes (Müller-Taubenberger *et al.*, 2012). More pertinent is its value in studying host-pathogen interactions (Hilbi *et al.*, 2007; Clarke, 2010). Genetic manipulation of the haploid chromosome is straightforward and a multitude of genetic tools are available for the amoeba, including the genome sequence, DNA microarrays, plasmids allowing constitutive or inducible gene expression, targeted deletions of (multiple) genes, and random mutants obtained by “restriction enzyme-mediated integration” (REMI) mutagenesis (Kuspa and Loomis, 1992). Expression vectors have been optimized for N- or C-terminal fusions of desired proteins with green or red fluorescent proteins (Fischer *et al.*, 2004), either as extra-chromosomal (Levi *et al.*, 2000) or integrating plasmids (Faix *et al.*, 1992; Manstein *et al.*, 1995).

1.3 Phytate, Phytases and Inositol Phosphates

1.3.1 Distribution of Phytate and Bacterial Phytases

Phytate, also known as *myo*-inositol (1,2,3,4,5,6)hexakisphosphate (InsP_6), is the most abundant form of organic phosphate in the environment (Turner *et al.*, 2002). Organic phosphate, from for example microbial macromolecules, is rapidly mineralized in soil (Macklon *et al.*, 1997). Some compounds on the other hand are resistant to mineralization. Phytate is the most notable, accounting for upwards of 80% of organic phosphate in soil (Turner *et al.*, 2002). Similarly, phytate can account for 65 – 80% of total phosphorous in grains (Lott *et al.*, 2000), and up to 80% of phosphorous in the manure of monogastric animals (Barnett, 1994). Owing to its high negative charge from six phosphate groups, phytate is tightly complexed to a variety of soil components upon its liberation from plant matter and animal waste (Lung and Lim, 2006). The accumulation of phytate in soil has been attributed to its extreme resistance to enzymatic hydrolysis (Tang *et al.*, 2006). Phytate from terrestrial runoff is deemed to be the major source of organic phosphate delivery to aquatic systems, where it is rapidly mineralized (Suzumura and Kamatani, 1995), possibly due to the enhanced solubility (Lim *et al.*, 2007). In these aquatic systems where as much as half of the inert phosphate is exclusively mineralized by phytases (Herbes *et al.*, 1975), the crucial role of these enzymes in recycling organic phosphate is evident. In sediment, phytases were reported to mineralize 34% of organic phosphate compared to the under 5% by alkaline phosphatases (De Groot and Golterman, 1993).

The four known classes of phytases include the histidine acid phosphatase (HAP), cysteine phytase (CPhy) (Chu *et al.*, 2004), purple acid phosphatase (PAP), and β-propeller phytase (BPP) (Mullaney and Ullah, 2003). The biochemical properties of these bacterial phytases were well characterized, but their occurrence and distribution was poorly established. In 2007, a bioinformatics approach examined all known bacterial genome sequences for the presence of conserved phytase motifs (Lim *et al.*, 2007). The results indicated that BPPs were the only phytases found in aquatic environs, but also found in soil and plant-living bacteria. HAPs occurred mainly in plant pathogens and enteric bacteria. CPhys were also found in plant pathogens, enteric bacteria, and additionally some free-living bacteria. Among these free-living bacteria, *L. pneumophila* was identified as having a potential CPhy carrying the conserved catalytic sequence HCXXGXXR(T/S) (Chu *et al.*, 2004).

1.3.2 Synthesis of Phytate and Inositol Phosphates by Amoebae

Phytate serves as a store for phosphorous, micro-nutrients, and inositol in plant cells (Raboy, 2003), and as an anti-stress compound and source for other inositol phosphates in *Dictyostelium*. *D.*

discoideum can grow on media that do not contain inositol (Franke and Kessin, 1977), and ^{31}P-NMR revealed that these amoebae grown axenically were capable of synthesizing 0.7 mM phytate (Martin *et al.*, 1987). The *myo*-Ins isomer serves as a building block for phytate, all inositol phosphates, and PI lipids. Ins is utilized by only a few bacteria but all eukaryotes. In *Dictyostelium*, as is universal to eukaryotes, archaea, and eubacteria, Ins can be synthesized *de novo* through the conversion of D-glucose-6-P to Ins(3)*P*, and subsequent dephosphorylation to Ins (Loewus and Murthy, 2000; Stephens and Irvine, 1990; Majumder *et al.*, 1997). Environmental Ins or Ins(3)*P* can be used directly for InsP_6 synthesis, though the contribution that the inositol 3-phosphate synthase makes to the flux of Ins(3)*P* is unclear (Stephens and Irvine, 1990). On the path to InsP_6 synthesis, *D. discoideum* converts Ins(3)*P* to Ins(3,6)P_2, Ins(3,4,6)P_3, Ins(1,3,4,6)P_4, and Ins(1,3,4,5,6)P_5 before the final product is reached (**Figure 1.3**).

The absence of an Ins(1,4,5)P_3-3-kinase in *D. discoideum* means that InsP_6 synthesis can proceed regulated independently of Ins(1,4,5)P_3 and PI lipids (Stephens and Irvine, 1990). Instead, the InsP_3 produced in InsP_6 synthesis is Ins(3,4,6)P_3. Ins(1,4,5)P_3 however is dephosphorylated to Ins (Van Haastert and Van Dijken, 1997). In the nucleus only, InsP_6 synthesis can start from Ins(1,4,5)P_3, but it is not clear how the precursor would enter the nucleus or if the process actually occurs physiologically (Van der Kaay *et al.*, 1995). As deletion of the only *D. discoideum* PLC did not noticeably affect Ins(1,4,5)P_3 levels, another route was discovered in which Ins(1,3,4,5,6)P_5 was dephosphorylated to Ins(1,4,5)P_3, (Bominaar *et al.*, 1991). Accordingly, Ins(1,3,4,5,6)P_5 is the only inositol phosphate present in reduced levels in PLC null cells (Bominaar *et al.*, 1991).

A few years after characterization of InsP_6 synthesis in *D. discoideum*, Ins pyrophosphates were discovered simultaneously in *Dictyostelium* and in mammalian cells (Stephens *et al.*, 1993; Menniti *et al.*, 1993). Ins pyrophosphates were found to exist as 5PP-InsP_5 and 6PP-InsP_5 (InsP_7) and 5,6(PP)$_2$-InsP_4 (InsP_8) (Laussmann *et al.*, 1997). These high energy pyrophosphates are rapidly turned over by phosphatases and kinases, where 30-50 % of cellular phytate is estimated to be cycled through pyrophosphate derivatives every hour (Stephens *et al.*, 1993). Revised methods employing a gel electrophoresis technology to characterize pyrophosphate metabolism in *D. discoideum* estimated concentrations of InsP_7 and InsP_8 as 0.06 mM and 0.18 mM respectively (Pisani *et al.*, 2014), indicating that they were several times higher than previously reported (Laussmann *et al.*, 2000, Luo *et al.*, 2003).

Though the functions of Ins pyrophosphates in *D. discoideum* remain to be explored, InsP_7 was found to physiologically regulate chemotaxis (Luo *et al.*, 2003). InsP_7 physiologically competes with PtdIns(3,4,5)P_3 for PH domain binding, regulating chemotactic response. Deletion of the InsP_6 kinase eliminates production of Ins pyrophosphates which results in elevated PH domain translocation to the PM and enhanced sensitivity of the cells to the chemotactic second messenger cAMP (Luo *et*

al., 2003). Normally, levels of InsP_7 and InsP_8 are rapidly increased by cAMP via a G protein-coupled cAMP receptor, which thus presents Ins pyrophosphates as negative regulators of chemotaxis, quite likely through maintenance of an InsP_7-PtdIns(3,4,5)P_3 balance (Luo *et al.*, 2003).

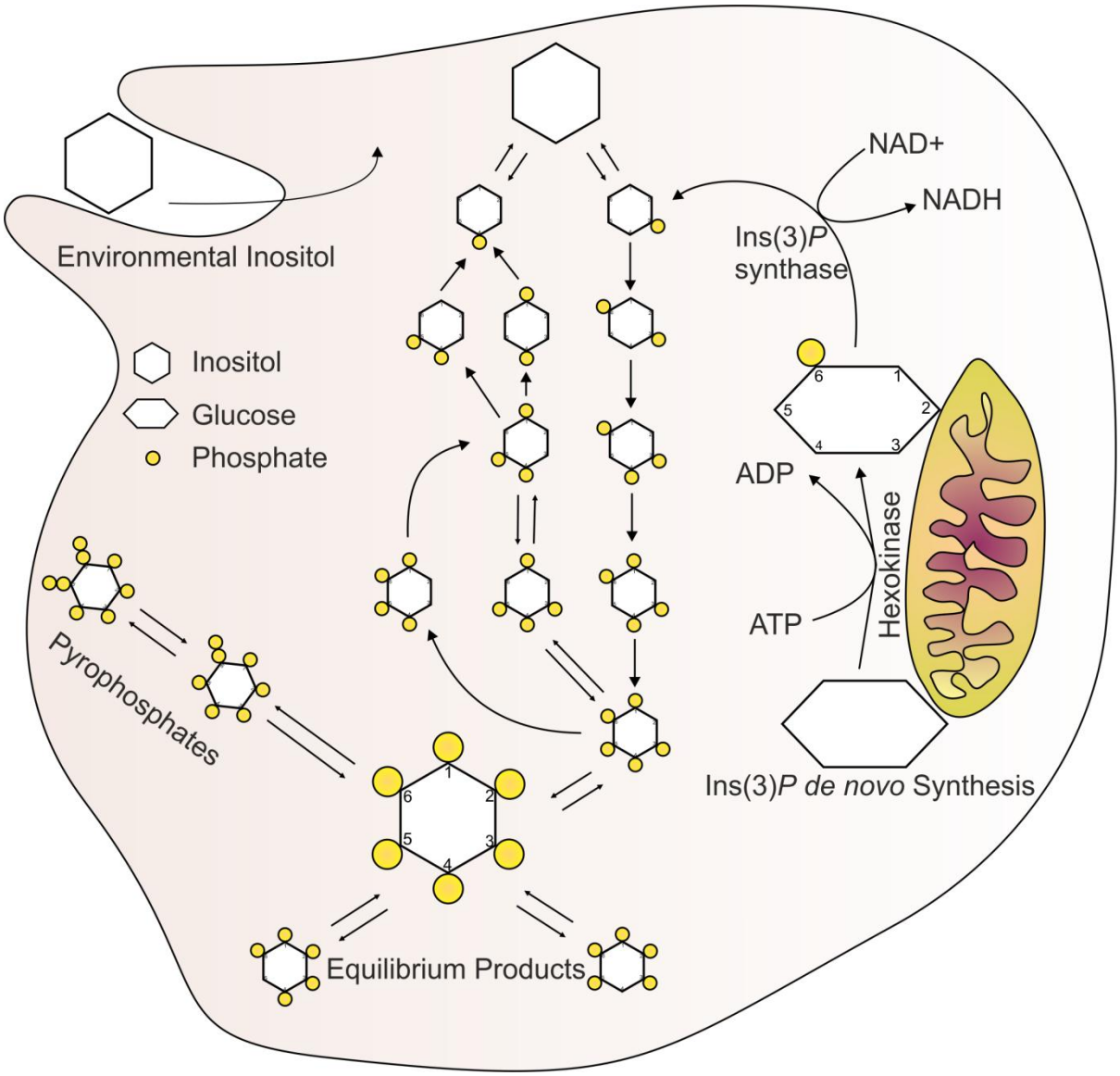

Figure 1.3 Stepwise phytate synthesis by *D. discoideum*. Environmental inositol can be used as a starting substrate for synthesis of InsP_6. Synthesis can also be initiated from Ins(3)*P* which can be synthesized *de novo* from glucose-6-phosphate. With the exception of the conversion of glucose to glucose-6-phosphate by hexokinase at the mitochondrial membrane, all synthesis takes place in the cytoplasm. InsP_6 can be further phosphorylated to inositol pyrophosphates.

1.4 Aim of the Thesis

Phosphoinositide lipids are at the centre of study with much vested interest in their role on the LCV in *L. pneumophila* infection. PI lipids serve as anchors for secreted effectors which remodel a compartment destined for degradation into a replication-permissive niche protected from host cell defenses and supporting propagation of the species. To date, numerous publications have speculated on the temporal association of specific PI lipids on the LCV (Peracino *et al.*, 2010; Hilbi *et al.*, 2011; Toulabi *et al.*, 2013). Conceptual models have also been generated based on assumptions about the LCV PI pattern (Hsu *et al.*, 2012). In spite of all the interest surrounding PI lipids, effectors that bind to them, and their modulation of downstream processes, a spatiotemporal characterization of these lipids on the LCV is absent. This thesis provides a thorough characterization of the dynamic LCV PI pattern and establishes a clear frame of reference for understanding the maturation of the LCV and processes involved in shaping the PI pattern.

In the course of the LCV PI lipid characterization, *L. pneumophila* PI phosphatases were sought which could potentially modulate these lipids. Gene lpg2819 (LppA) was identified as a candidate, having satisfied all conditions of a PI phosphatase *in vitro*. The following cellular experiments showed that LppA was instead a novel secreted phytase. It was therefore demonstrated that this phytase could assist the bacteria during intracellular replication under phytate load.

2 Materials and Methods

2.1 Materials

2.1.1 Components of Media, Buffers, Reagents, and Disposables

Component	Supplier
1 Kb Plus DNA Ladder	Life Technologies (Grand Island)
384-well plates	Greiner (Frickenhausen)
ACES	AppliChem (Darmstadt)
Acrylamide/Bisacrylamide	Serva (Heidelberg)
Activated charcoal powder	Fluka (Buchs)
Agar	BD Biosciences (Franklin Lakes)
Agarose	Biozym (Hessisch Oldendorf)
Bacteriological Peptone	Oxoid (Wesel)
Bacto Proteose Peptone	BD Biosciences (Franklin Lakes)
Bacto Yeast Extract	BD Biosciences (Franklin Lakes)
BBL Yeast Extract	BD Biosciences (Franklin Lakes)
β-mercaptoethanol	AppliChem (Darmstadt)
$CaCl_2$ x 2 H_20	Roth (Karlsruhe)
cAMP Direct Biotrak EIA	GE Healthcare (Chalfont St Giles)
Cell culture flasks	TPP (Trasadingen)
cOmplete, Mini Protease Inhibitor	Roche (Basel)
Cryogenic freezing tubes	Thermo (Waltham)
D(+)-Glucose-Monohydrate	Fluka (Buchs)
DMSO	Merck (Darmstadt)
DNA purifcation kit	Qiagen (Germantown)
DNA purification kit	Macherey-Nagel (Dueren)
DNase	Roche (Basel)
dNTP mix	Thermo (Waltham)
DreamTaq Green PCR Master Mix (2x)	Thermo (Waltham)

ECL detection kit	GE Healthcare (Chalfont St Giles)
EDTA (disodium salt)	Sigma-Aldridge (St. Louis)
Electroporation cuvette (2 – 4 mm gap)	Bio-Rad (Munich)
Ethanol	Roth (Karlsruhe)
FCS	Life Technologies (Grand Island)
FeN_3O_9 x 9 H_2O	Sigma-Aldridge (St. Louis)
Glutathione Sepharose 4B	GE Healthcare (Chalfont St Giles)
Glucose	Roth (Karlsruhe)
Glycerol	Roth (Karlsruhe)
Glycine	MP Biomedicals (Eschwege)
HCl	Roth (Karlsruhe)
Inositol	Sigma-Aldridge (St. Louis)
Inositol phosphates	Echelon Biosciences (Salt Lake City)
Isopropanol	Roth (Karlsruhe)
K_2HPO_4	Merck (Darmstadt)
KH_2PO_4	Fluka (Buchs)
Latrunculin B	Sigma-Aldridge (St. Louis)
LB Agar	Life Technologies (Grand Island)
LB Broth Base	Life Technologies (Grand Island)
L-cysteine	Sigma-Aldridge (St. Louis)
L-glutamine	Life Technologies (Grand Island)
LoFlo	ForMedium (Norfolk)
Methanol	Roth (Karlsruhe)
µ-slide 8 well	ibidi (Martinsried)
µ-dish 35 mm	ibidi (Martinsried)
$MgCl_2$ x 6 H_20	Roth (Karlsruhe)
$MgSO_4$ x 7 H_20	Merck (Darmstadt)
NaCl	Roth (Karlsruhe)
NaOH	Roth (Karlsruhe)
PageRuler Prestained Protein Ladder 10-170K	Thermo (Waltham)

PFA	Sigma-Aldridge (St. Louis)
Phosphatidylinositol phosphates Di-C8	Echelon Biosciences (Salt Lake City)
Phusion polymerase	Thermo (Waltham)
Phytic acid sodium salt	Sigma-Aldridge (St. Louis)
PIP strips	Echelon Biosciences (Salt Lake City)
PTP assay kit	Sigma-Aldridge (St. Louis)
Restriction enzymes	Thermo (Waltham)
RPMI 1640	Life Technologies (Grand Island)
T4 DNA-Ligase	New England Biolabs (Ipswich)
TEMED	Biomol Feinchemikalien (Hamburg)
TRIS-HCl	MP Biomedicals (Santa Ana)
Tryptone / Peptone from Casein	Roth (Karlsruhe)
Tween® 20	Roth (Karlsruhe)
Yeast extract	BD Biosciences (Franklin Lakes)
Wortmannin	Sigma-Aldridge (St. Louis)
$ZnCl_2$	Sigma-Aldridge (St. Louis)

Standard laboratory materials and reagents were used in addition to the listed items.

2.1.2 Laboratory Equipment

Item	**Model**	**Manufacturer**
Autoclave	Varioklav classic	H+P (Oberschleissheim)
Benchtop centrifuge	5417R	Eppendorf (Hamburg)
CCD camera	Orca ER	Hamamatsu Photonics (Hamamatsu)
Centrifuge	3-30K	Sigma-Aldridge (St. Louis)
Centrifuge	5810	Eppendorf (Hamburg)
Centrifuge	Megafuge 1.0R	Thermo (Waltham)
CMOS camera	Orca Flash 4.0	Hamamatsu Photonics (Hamamatsu)

CO_2 incubator	Heraeus HeraCell 240	Thermo (Waltham)
Colony counter	Countermat flash	IUL (Barcelona)
Confocal microscope (scanning)	Leica TCS SP5	Leica (Mannheim)
Confocal microscope (spinning disk)	TE 300 eclipse	Nikon Instruments (Düsseldorf)
Cryogenic freezer box	Cryo 1° freezing container	Thermo (Waltham)
Culture microscope	Primo Vert	Zeiss (Oberkochen)
Diaphragm vacuum pump	MZ 2C	MZ 2C Vacuubrand (Wertheim)
Electrophoresis chamber	Mini-Protean 3	Bio-Rad (Munich)
Electrophoresis chamber	Mini-Subcell GT	Bio-Rad (Munich)
Electroporation device	GenePulser Xcell	Bio-Rad (Munich)
French press	SIM AMINCO	Spectronic (New York)
Gel imaging system	ChemiDoc MP System	Bio-Rad (Munich)
Gel imaging system	GelDoc EQ	Bio-Rad (Munich)
Hot plate magnetic stirrer	RCT basic	IKA (Staufen)
Ice machine	AF30	Scotsman (Vernon Hills)
Incubation cabinet	Certomat BS-1	Sartorius (Goettingen)
Incubation cabinet	Oribital shaker, Forma	Thermo (Waltham)
Incubator	Heraeus BR6000	Thermo (Waltham)
Incubator	Heraeus Function Line	Thermo (Waltham)
Incubator	IPP500	Memmert (Schwabach)
Medical film developer	FPM-100A	Fuijilm EU (Düsseldorf)
Mixer	Vortex-Genie 2	IKA (Staufen)
PCR machine	T3	Biometra (Goettingen)
pH-meter	Level 1	inoLab (Weilheim)
Pipettes	Pipetman	Gilson (Middleton)
Pipettor	Pipetus	Hirschmann (Eberstadt)

Power supply	PAC100	Bio-Rad (Munich)
Precision balance	BP61-S	Sartorius (Goettingen)
Precision balance	PG2002-S	Mettler-Toledo (Greifensee)
Protein transfer device	MAXI-Semi-Dry-Blotter	Roth (Karlsruhe)
Rocking platform shaker	Duomax 1030	Heidolph (Schwabach)
Rolling mixer	RM5-35s 1732	Fröbel (Lindau)
Spectrophotometer	Helios Epsilon	Thermo (Waltham)
Spectrophotometer	NanoDrop ND-1000	PeqLab (Erlangen)
Spinning disk software	Velocity 6.1	Perkin-Elmer (Cambridge)
Spinning disk system	UltraVIEW	Perkin-Elmer (Cambridge)
Suspension mixer	CMV	Fröbel (Lindau)
Thermal mixer	Thermomixer comfort	Eppendorf (Hamburg)
UV-transilluminator		Bachofer (Reutlingen)
Water bath	Wasserbad 1005	GFL (Burgwedel)

Standard laboratory equipment was used in addition to the listed items.

2.1.3 Buffers and Media

2.1.3.1 *Legionella pneumophila*

Charcoal Yeast Extract (CYE) Agar (Feeley *et al.*, 1979)

Component	Amount/Litre	Supplier
ACES	10 g	AppliChem
Bacto Yeast Extract	10 g	BD Biosciences
Activated Charcoal Powder p.a. puriss	2 g	Fluka
Agar	15 g	BD Biosciences
L-cysteine	0.4 g in 10 ml H_2O	Sigma
FeN_3O_9 x 9 H_2O	0.25 g in 10 ml H_2O	Sigma
Antibiotic		
Chloramphenicol	5 mg	Roth
Gentamicin	10 mg	Roth
Kanamycin	50 mg	Roth

Dissolve ACES and Yeast Extract in H_2O and adjust pH to 6.9 with 10 M KOH. H_2O is added up to the desired final volume. Add charcoal, agar, and a stirbar to each flask. Autoclave and allow to cool to 50°C. Add sterile filtered cysteine and iron solutions (10 ml per 1 L agar). Add antibiotic solutions as required. Distribute the well-homogenized mixture into standard petri dishes. Let the plates dry for 1-2 days at RT. Store at 4°C.

ACES Yeast Extract (AYE) Medium (Horwitz, 1983)

Component	Amount/Litre	Supplier
ACES	10 g	AppliChem
Bacto Yeast Extract	10 g	BD Biosciences
L-cysteine	0.4 g in 10 ml H_2O	Sigma
FeN_3O_9 x 9 H_2O	0.25 g in 10 ml H_2O	Sigma
Antibiotic		
Chloramphenicol	5 mg	Roth
Gentamicin	10 mg	Roth
Kanamycin	30 mg	Roth

Add ACES and Yeast Extract to 900 mL H_2O. Dissolve cysteine and iron in 10-20 mL H_2O each separately. Add cysteine solution slowly while stirring, followed by the iron solution. Adjust pH to 6.9 with 10 M KOH, then add H_2O to up to final volume. Filter the mixture through a glass fiber filter 6-8 times. Sterile filter the media. Refrigerate in the dark.

2.1.3.2 *Escherichia coli*

Luria-Bertani (LB) Agar

Component	Amount/Litre	Supplier
LB agar	32 g	Life Technologies
Antibiotic		
Ampicillin	100 mg	Roth
Chloramphenicol	30 mg	Roth
Kanamycin	30 mg	Roth

LB agar was dissolved in H_2O. The solution was autoclaved and cooled to 50°C before plating. Antibiotics were added as required. Plates were stored at 4°C.

Luria-Bertani Medium

Component	Amount/Litre	Supplier
Luria Bertani broth base	20 g	AppliChem

LB broth base was dissolved in H_2O. The solution was autoclaved and cooled to 50°C. Antibiotics were added as required as for LB agar. Plates were stored at 4°C.

Transformation Buffer 1 (TFB1)

Component	Amount/Litre	Supplier
Potassium acetate	2.82 g (30 mM)	Roth
KCl	7.46 g (100 mM)	Roth
$CaCl_2$ x 2 H_2O	1.48 g (10mM)	Roth
MnCl	6.3 g (50 mM)	Roth
Glycerol	150 ml (15%)	Roth

Adjust pH to 6.5 with KOH and add H_2O to final volume. Store sterile filtered aliquots at -20°C.

Transformation Buffer 2 (TFB2)

Component	Amount/Litre	Supplier
MOPS	0.42 g (10 mM).	Roth
$CaCl_2$ x 2 H_2O	1.11 g (75 mM)	Roth
KCl	0.074 g (10 mM)	Roth
Glycerol	15 mL (15%)	Roth

Adjust pH to 6.5 with KOH and add H_2O to reach final volume. Sterile filter and freeze 4 ml aliquots at -20°C.

2.1.3.3 *Dictyostelium discoideum*

HL5 medium (Watts and Ashworth, 1970)

Component	Amount/Litre	Supplier
D(+)-glucose monohydrate	11 g	Fluka
BBL yeast extract	5 g	BD Biosciences
Bacto proteose peptone	5 g	BD Biosciences
Bacteriological peptone	5 g	Oxoid
Na_2HPO_4	0.355 g (2.5 mM)	Fluka
KH_2PO_4	0.34 g (2.5 mM)	Fluka

Adjust pH with 1 M KOH or 1 M HCl to 6.5, autoclave and store at 4°C. Glucose is sterile filtered separately.

LoFlo Medium

Component	Amount/Litre	Supplier
LoFlo base	20 g	ForMedium (Norfolk)

Dissolve in water, autoclave and store at room temperature.

MB Medium (Solomon *et al.*, 2000)

Component	Amount/Litre	Supplier
Yeast Extract	7 g	Oxoid
Bacto Proteose Peptone	14 g	BD
MES buffer	4.26 g (20 mM)	AppliChem

Prepare day prior to use. The pH was adjusted to 6.9 with 1 M KOH. Medium was autoclaved and stored at 4°C.

SorC Buffer (Malchow *et al.*, 1972)

Component	Amount/Litre	Supplier
$NaHPO_4$	0.28 g (2 mM)	Fluka
KH_2PO_4	2.04 g (15 mM)	Fluka
$CaCl_2$ x 2 H_2O	7.35 mg (50 mM)	Roth

The pH was adjusted to 6.0 with KOH, Medium was autoclaved and stored at 4°C.

2.1.3.4 *Acanthamoeba castellanii*

PYG Medium (Moffat and Tompkins, 1992)

Component	Amount/Litre	Supplier
Bacto proteose peptone	20 g	BD BioSciences
BBL yeast extract	1 g	BD BioSciences
$MgSO_4$ x 7 H_2O	10 ml (4 mM)	Roth
Sodium citrate x 2 H_2O	3.4 ml (1 M)	Roth
$Fe(NH_4)_2$ x 7 H_2O	10 ml (0.25 M)	Roth
Na_2HPO_4	10 ml (0.25 M)	Roth
KH_2PO_4	2.5 mg (2.5 mM)	Fluka
D(+)-glucose monohydrate	19.8 g	Fluka

pH was adjusted to 6.5 with 1 M KOH or 1 M HCl. After addition of 50 ml 2 M glucose, medium was sterile filtered using a flask-mounted filter cartridge and stored at 4°C.

Ac Buffer (Moffat and Tompkins, 1992)

Component	Amount/Litre	Supplier
$MgSO_4$ x 7 H_2O	985.9 mg (4 mM)	Oxoid
$CaCl_2$	44 mg (0.4 mM)	BD
Sodium citrate x 2 H_2O	999 mg (3.4 mM)	AppliChem
Na_2HPO_4 x 7 H_2O	86 mg (0.05 mM)	Fluka
KH_2PO_4	2.5 mg (2.5 mM)	Fluka
NH_4Cl	2.6 mg (0.05 mM)	Fluka
$FeSO_4$	7.55 mg (0.05 mM)	Merck

The pH was adjusted pH to 6.5 with 1 M HCl. Medium was autoclaved and stored at 4°C.

2.1.3.5 Protein Buffers

Phosphate-Buffered Saline (PBS)

Component	Amount/Litre	Supplier
$MgSO_4$ x 7 H_2O	80 g (136 mM)	AppliChem
$CaCl_2$	2 g (2.7 mM)	Fluka
Sodium citrate x 2 H_2O	14.2 g (10 mM)	Fluka
Na_2HPO_4 x 7 H_2O	2.4 g (1.5 mM)	Fluka

Adjust to pH 7.4 with NaOH. Autoclave and store at RT.

Tris-Buffered Saline (TBS)

Component	Amount/Litre	Supplier
NaCl	80 g	AppliChem
Tris	6.5 g	Biosolve

Adjust to pH 7.5 with NaOH. Autoclave and store at RT.

Cleavage Buffer (GST-tags)

Component	Amount/Litre	Supplier
Tris	6.057 g (50 mM)	Biosolve
NaCl	8.766 g (150 mM)	Roth
EDTA	0.372 g (1 mM)	Applichem
DTT	0.154 g (1 mM)	Applichem

Adjust to pH 7.0 with HCl. Autoclave and store at 4°C.

Assay Buffer (Phosphate Release)

Component	Amount/Litre	Supplier
Tris	12.11 g (100 mM)	Biosolve
NaCl	7.01 g (120 mM)	Roth

Adjust to pH 7.4 with HCl. Sterile filter and store at room temperature.

2.1.4 Strains, Plasmids, Oligonucleotides, and Antibodies

Strain/plasmid	Relevant properties[a]	Source
E. coli		
TOP10		Invitrogen
BL21		Novagen
L. pneumophila		
CR01	*L. pneumophila* JR32 *sidC-sdcA*::Kan^R (Δ*sidC-sdcA*)	(Ragaz *et al.*, 2008)
GS3011	*L. pneumophila* JR32 *icmT3011*::Kan^R (Δ*icmT*)	(Segal and Shuman, 1998)
JR32	Virulent *L. pneumophila* serogroup 1 strain Philadelphia	(Sadosky *et al.*, 1993)
RM01	*L. pneumophila* JR32 *lpg2819*::Kan^R (Δ*lppA*)	R. Meier
D. discoideum		
Ax3		Laboratory collection
Ax3/pPH$_{CRAC}$-GFP	PH$_{CRAC}$-GFP, G418^R	(Weber *et al.*, 2014)
Ax3/pRM6	2×FYVE-GFP, G418^R	(Weber *et al.*, 2014)
Ax3/pUS4	GFP-P4C$_{SidC}$ in pDXA, G418^R	(Ragaz *et al.*, 2008)
Ax3/pWS21	Calnexin-mRFPmars, Bls^R	(Weber *et al.*, 2014)
Ax3/pWS22	P4C$_{SidC}$-mRFPmars, Bls^R	(Weber *et al.*, 2014)
Ax3/pWS23	Arf1-mRFPmars, Bls^R	(Weber *et al.*, 2014)
Ax3/pWS27	LppA-GFP, G418^R	This work
Ax3/pCaln-GFP + pWS22	Calnexin-GFP and P4C$_{SidC}$-mRFPmars, G418^R Bls^R	(Weber *et al.*, 2014)
Ax3/pCaln-GFP + pWS23	Calnexin-GFP and Arf1-mRFPmars, G418^R Bls^R	(Weber *et al.*, 2014)
Ax3/pRM6 + pWS21	2×FYVE-GFP and Calnexin-mRFPmars, G418^R Bls^R	(Weber *et al.*, 2014)
Ax3/pRM6 + pWS22	2×FYVE-GFP and P4C$_{SidC}$-mRFPmars, G418^R Bls^R	(Weber *et al.*, 2014)
Ax3/pCaln-GFP + pWS22	Calnexin-GFP and P4C$_{SidC}$-mRFPmars, G418^R Bls^R	(Weber *et al.*, 2014)
Ax2	PH-PLCδ1-GFP	(Clarke *et al.*, 2010)
RAW 264.7	Murine macrophage cell line	ATCC TIB-71

Plasmids

pBsrH	P_{act15}, C-mRFPmars, Amp^R, Bls^R	(Fischer *et al.*, 2004)
pCaln-GFP	P_{act15}, *cnxA*-RSSSKLK-GFP (S65T), $G418^R$	(Müller-Taubenberger *et al.*, 2001)
pCR33	*Legionella* expression vector, Δ*mobA*, RBS, M45-$(Gly)_5$, Cam^R, (= pMMB207-C-RBS-M45)	(Weber *et al.*, 2006)
pCR56	pGEX-4T-1-$P4C_{SidC}$	(Ragaz *et al.*, 2008)
pCR76	pMMB207-C-P_{tac}-RBS-*gfp*-RBS-MCS	(Finsel *et al.*, 2013)
pDXA-HC	*Dictyostelium* expression vector, P_{act15}, Neo^R, Amp^R	Manstein *et al.*, 1995)
pGEX-6P-1	GST expression vector	GE Lifesciences
pGEX-4T-1	GST expression vector	GE Lifesciences
pMMB207C	*Legionella* expression vector, Δ*mobA*, - RBS, Cam^R	(Weber *et al.*, 2006)
pNT28	pMMB207C-RBS-*gfp* (constitutive *gfp*)	(Tiaden *et al.*, 2007)
pPH_{CRAC}-GFP	PH_{CRAC}-GFP (PH domain of protein CRAC), $G418^R$	(Parent *et al.*, 1998)
pPhyA	Synthetic construct of *S. ruminantium phyA* gene	This work
pRM1	pMMB207-C-RBS-M45-*lppA*	R. Meier
pRM6	2×FYVE-GFP (FYVE domain from EEA1), $G418^R$	(Weber *et al.*, 2014)
pRM9	pGEX-6P-1-$lppA_{\Delta 1\text{-}16}$	R. Meier
pSE7	pGEX-6P-1-$lppA_{\Delta 1\text{-}16}$, C215A	S. Engelhardt
pSE8	pGEX-6P-1-$lppA_{\Delta 1\text{-}16}$, K219A	S. Engelhardt
pSE9	pGEX-6P-1-$lppA_{\Delta 1\text{-}16}$, R221A	S. Engelhardt
pSE10	pGEX-6P-1-$lppA_{\Delta 1\text{-}16}$, G220D	S. Engelhardt
pSH97	pMMB207-C-RBS-*cyaA* (including polylinker)	(Finsel *et al.*, 2013)
pSH108	pMMB207-C-*cyaA*-*lppA*	S. Heiny
pSU4	GFP-$P4C_{SidC}$ in pDXA, $G418^R$	(Ragaz *et al.*, 2008)
pSW1	pMMB207-C, Δ$lacI^q$ (constitutive *dsred*)	(Mampel *et al.*, 2006)
pSW13	pGEX-4T-1-*lpnE*	(Weber *et al.*, 2009)
pTX-GFP	Extra-chromosomal *D. discoideum* vector, Neo^R, Amp^R	(Levi *et al.*, 2000)
pWS21	Calnexin-mRFPmars, Amp^R, Bls^R	(Weber *et al.*, 2014)
pWS22	$P4C_{SidC}$-mRFPmars (P4C domain of *L. pneumophila* SidC), Amp^R, Bls^R	(Weber *et al.*, 2014)
pWS23	Arf1-mRFPmars, Amp^R, Bls^R	(Weber *et al.*, 2014)
pWS25	pGEX-6P-1-*phyA*	This work
pWS27	LppA-GFP, Neo^R, Amp^R	This work
pWS31	pMMB207-C-RBS-*gfp*-RBS-*lppA*	This work

[a] Abbreviations: Amp, ampicillin; Bls, blasticidin-S; Cam, chloramphenicol; G418, geneticin; Kan, kanamycin; Neo, neomycin.

Oligo	Sequence (5' - 3') [a]	Comments
oRM5	AAAAACGCGGATCCATGAGCTTTAAAGGATTTAAAG	5’ of *lppA*, *Bam*HI
oRM6	AAAAACGCGTCGACCTAGATATTGAGCTTTTTCCATTC	3’ of *lppA*, *Sal*I
oWS53	AAATCAGATCCAAGC	Sequencing C-terminal GFP fusion in pTX-GFP
oWS54	CAACAAGAATTGGGAC	Sequencing C-terminal GFP fusion in pTX-GFP
oWS55	AAAAAAGGTACCATGCAAAGTTATGCCTCTAAATTGGC	5’ of *lppA*, *Kpn*I
oWS56	TTCTGACCAGGTACCTGAATATCCCATAAGGG	3’ of *lppA*, *KpnI*

[a] Restriction sites are underlined

Antibody	Host-Origin	Source
anti-GST	Mouse	Sigma (St. Louis)
anti-LppA	Rabbit	Affinity purified, GenScript (Piscataway)
anti-mouse IgG HRPO	Sheep	GE Healthcare (Chalfont St Giles)
anti-rabbit IgG FITC	Goat	Jackson ImmunoResearch (West Grove)
anti-rabbit IgG Rhodamine	Bovine	Santa Cruz (Dallas)
anti-rabbit IgG HRPO	Donkey	GE Healthcare (Chalfont St Giles)
anti-SidC	Rabbit	Affinity-purified (Weber *et al.*, 2006)

.

2.2 Methods

2.2.1 *Legionella pneumophila*

2.2.1.1 Cultivation of *L. pneumophila*

Legionella pneumophila strains were grown from glycerol stocks for 2-3 days on CYE agar. Liquid cultures were inoculated in AYE medium at an OD_{600} of 0.1 and grown at 37°C for 16-21 h to an OD_{600} of 3.0 – 3.4. Cultures were checked for fitness (namely motility and homogeneity of shape) with an inverted light microscope (40× objective).

2.2.1.2 *L. pneumophila* Glycerol Stocks

L. pneumophila liquid cultures grown approximately 18 h at 37°C were mixed 1:2 with sterile 50% glycerol and stored at -80°C.

2.2.1.3 Preparing Electrocompetent *L. pneumophila*

30 ml AYE were inoculated with 1 ml of a pre-stationary phase *L. pneumophila* culture. The culture was grown to an OD_{600} between 0.3 and 0.5 then washed 3 times on ice with sterile, 10% glycerol (10 ml, 2.5 ml, and 160 µl). Aliquots of 25 µl were shock frozen and stored at -80°C.

2.2.1.4 Transformation of *L. pneumophila* by Electroporation

100 ng of plasmid was added to electrocompetent *L. pneumophila* on ice. After 10 minutes, the mixture was transferred into a 2 mm gap electroporation cuvette. Electroporation (2.5 kV, 200 Ω, 25 µF), was followed by addition of 450 µl AYE. The bacteria were incubated for 5 h at 37°C under agitation then plated onto selective CYE agar.

2.2.2 *Escherichia coli*

2.2.2.1 Inoculation, Growth and Storage

E. coli cultures were inoculated from glycerol stocks onto plate or directly into 1 ml LB liquid cultures and grown overnight at 37°C. Glycerol stocks were made by combining sterile 50% glycerol in a ratio of 2:1 with a mature LB culture.

2.2.2.2 Preparation of $CaCl_2$ Competent Cells

A 5 ml LB culture was inoculated with the cell line to be prepared and incubated overnight at 37°C and 180 rpm. The pre-culture was decanted into a shake flask containing 100 ml LB and incubated to an OD_{600} of 0.5 – 0.7. The culture was centrifuged at 2100 x g for 10 min at 4°C and resuspended in 40 ml of ice cold TFB1. This centrifugation and resuspension step was repeated with subsequent addition of 4 ml TFB2. After 20 min incubation on ice, cells were centrifuged at 2100 x *g* for 10 min at 4°C. The resulting pellet was carefully resuspended in 3 – 5 ml ice cold TFB2, divided into 50 µl aliquots, and frozen at -80°C.

2.2.2.3 Transformation of $CaCl_2$ Competent Cells by Heat Shock

Frozen $CaCl_2$ competent cells were allowed to thaw on ice for 4 min, at which point 100 ng of plasmid was pipetted into the cell suspension and gently mixed. The mixture was incubated on ice for 10 min. Heat shock was administered for 1 min at 42°C in a heat block and cells were placed back onto ice for 2 min. 700 µl of LB was added under sterile conditions. Cells were regenerated in a 37°C water bath for 1 h then centrifuged for 3 min at 3000 rpm and 4°C. The supernatant was decanted and the pellet was plated on applicable antibiotic medium.

2.2.3 *Dictyostelium discoideum*

2.2.3.1 Culture Methods

Dictyostelium discoideum axenic strains were cultured in 10 mL HL5 medium at 23°C in 75 cm^2 area culture flasks. The amoebae were cultured to sub-confluence at which point 1-2 × 10^4 cells/ml were seeded to a new flask.

2.2.3.2 Transformation by Electroporation

Cell were grown to 70 – 80% confluence. Media was gently discarded and the cells adhered to the flask were washed with 10 ml electroporation buffer (EB). Cells were dislodged in a fresh 10 ml of EB. Cells were counted with a haemocytometer and EB was added to 25 ml. Cells were pelleted for 5 min at 500 × *g* at 4°C. Cells were resuspend cells in EB to give 10^6 cells/100 µl. 200 µl of cell mixture was added to each 2 mm gap cuvette along with 5-25 µl plasmid. Cells were transformed using the following settings: 850 V, 10 µF, 0.6 ms pulse length, 2 pulses spaced by a 5 second interval, 2 mm cuvette gap distance. Cuvettes were placed on ice for 3 min after which their contents were divided among 3 wells of a 6-well plate, each containing 3 ml HL5. The plate was incubated at 23°C. Antibiotic selection followed after 24 h with 10 µg/ml G418 or blasticidin-S.

2.2.3.3 Storage

Axenic cultures grown to 80% confluence were washed gently with HL5, resuspended in 4 ml freezing medium (80% HL5, 10% FCS, 10% DMSO), and distributed evenly to cryo-tubes. Tubes were placed in a 4°C pre-cooled cryogenic freezer box, and gradient frozen overnight at -80°C. They were subsequently transferred to cryogenic storage. Cells removed from cryogenic storage were thawed rapidly and immediately transferred to 9 ml HL5. After cells had adhered (approx. 30 min to 1 h), the medium was changed with a fresh 10 ml HL5. Antibiotic selection in the form of 10 µg/ml G418 or blasticidin-S was initiated accordingly.

2.2.4 *Acanthamoeba castellanii*

2.2.4.1 Culturing

Acanthamoeba castellanii was cultured in 10 mL PYG medium at 23°C in 75 cm^2 area culture flasks. The amoebae were cultured to sub-confluence at which point 1-2 × 10^4 cells/mL were seeded to a new flask.

2.2.4.2 Storage

A. castellanii were grown to 80% confluence were washed gently with HL5, resuspended in 4 ml freezing medium (80% PYG, 10% FCS, 10% DMSO), and distributed evenly to cryo-tubes. Tubes were placed in a 4°C pre-cooled cryogenic freezer box, and gradient frozen overnight at -80°C. They were subsequently transferred to cryogenic storage. Cells removed from cryogenic storage were thawed rapidly and immediately transferred to 9 ml PYG. After cells had adhered (approx. 30 min to 1 h), the medium was changed with a fresh 10 ml PYG.

2.2.5 RAW 264.7 Macrophages

2.2.5.1 Culturing

Murine RAW 264.7 macrophages were cultivated at 37°C and 5% CO_2 in RPMI 1640 medium supplemented with 10% FCS and 2 mM L-glutamine. Cells were grown to 90% confluence before splitting, during which they were washed once with PBS and scraped off using a cell scraper. Cells were diluted 1:5 in supplemented RPMI in a new flask.

2.2.5.2 Storage

Cultures grown to 80% confluence were washed with RPMI, resuspended in 4 ml freezing medium (70% RPMI, 20% FCS, 10% DMSO), and distributed evenly to cryo-tubes. Tubes were placed in a 4°C pre-cooled cryogenic freezer box, and gradient frozen overnight at -80°C. They were subsequently transferred to cryogenic storage. Cells removed from cryogenic storage were thawed rapidly and immediately transferred to 9 ml supplemented RPMI. After cells had adhered (approx. 1 h), the medium was changed for fresh 10 ml supplemented RPMI.

2.2.6 Molecular Cloning

DNA manipulations were performed according to standard protocols, and plasmids were isolated using kits from Qiagen or Macherey-Nagel. All PCR fragments were sequenced. To make pWS27, *lppA* was amplified by PCR from *lpg*2819 using oligonucleotides oWS55/oWS56. The fragments were cut with *Kpn*I and cloned into vector pTX-GFP after its treatment with alkaline phosphatase.

pWS31 was generated with the BamHI/SalI cloning of the *lppA* PCR product of oRM5/oRM6 into pCR76.

The *S. ruminantium* phytase gene *phyA* (Chu *et al.*, 2004) was synthesized by GenScript USA Inc. and delivered in commercial vector pUC57-Kan with flanking *Bam*HI and *Sal*I restriction sites. In the design, the intrinsic *Sal*I site of the gene was removed by a silent single base substitution maintaining the original amino acid sequence. The *phyA* gene was cloned with *Bam*HI and *Sal*I into pGEX-6P-1, yielding pWS25.

2.2.7 Real-Time Imaging of *L. pneumophila* Infection in *D. discoideum*

D. discoideum amoebae were harvested from approximately 70% confluent cultures. HL5 medium was removed and cultures were washed with 5 ml LoFlo medium and resuspended in fresh LoFlo medium. Cells were seeded (300 µl) at a density of $2 – 4 \times 10^5$/ml in 8-well µ-slides. Cells were allowed to adhere for 1 h, after which LoFlo medium was replaced. Microscope stage thermostat was set to regulate between 22°C and 25°C. Samples were viewed with a Leica TCS SP5 confocal microscope (HCX PL APO CS, objective 63x/1.4-0.60 oil; Leica Microsystems, Mannheim, Germany). For select applications, samples were observed with a Nikon eclipse TE300 microscope with Perkin Elmer UltraVIEW spinning disk system and Hamamatsu Orca ER CCD or Orca Flash 4.0 CMOS camera. A Nikon 100×/1.40 Plan Apo oil objective was used in combination with filters 488 – 10BP/525 – 50BP and 568 – 10BP/607 – 45BP. Data evaluation was carried out with Velocity 6.0.1.

To monitor rapid events, the amoebae were brought into focus on the microscope stage. Up to 5 µl of a *L. pneumophila* culture 10-fold diluted in LoFlo medium were introduced by submerging a pipette tip directly above the objective position. Video capture was initiated immediately as motile *L. pneumophila* arrived at the focal plane within seconds of addition. The focus was maintained manually and events were followed for up to a maximum of 15 min before moving to a fresh well to repeat the process.

To monitor slow (long-term) events, bacterial MOIs were calculated to represent an MOI between 5 and 20 in 300 µl LoFlo medium. LoFlo in the observation dishes was replaced by 300 µl LoFlo containing *L. pneumophila* (t = 0). Dishes were immediately centrifuged for 5 min at 1000 × *g*. Cells were brought into focus on the microscope stage. Three representative images for each strain were captured at defined time points. As images cannot be captured simultaneously, image acquisition was staggered so that capture was half completed when the specific time point was reached. To test for significance, a two-tailed t-test was applied assuming unequal variance.

2.2.8 Protein Purification

For the production of GST fusion proteins, *E. coli* BL21(DE3) containing pGEX-derivatives were induced at a cell density (OD600) of 0.6 with 0.5 mM isopropyl-1-thio-β-D-galacto-pyranoside (IPTG) for 4 h at 37°C in LB medium then lysed by French press. GST fusion proteins of LppA (pRM9, pSE7-10), PhyA (pWS25), LpnE (pSW13) and $P4C_{SidC}$ (pCR56) were purified using glutathione-sepharose beads in a batch procedure according to the manufacturer's recommendations. Products of pRM9 were also released from the bound GST-tag in cleavage buffer with PreScission Protease. The buffer was exchanged for TBS using PD-10 desalting columns. The solubility and purity of the protein preparations was analysed by SDS-PAGE and the concentration spectrophotometrically determined with the NanoDrop.

2.2.9 Protein-Lipid Overlays

In order to assess the products of LppA from various PI lipids, PIP-strips were treated with a 0.5 µg/ml LppA for 10 min. Membranes were washed three times for 10 min with PBS. PIP-strips were blocked for 1 h 4% fat-free milk powder in TBS-Tween (0.1% Tween-20 [v/v], pH 8.0) (Blocking buffer) then incubated overnight with 120 pmol/ml of the purified GST-fusion protein in fresh blocking buffer in a dark room at 4°C. The membrane was washed 3 times for 10 min with blocking buffer. The primary α-GST antibody was added (1:1000 dilution) in blocking buffer, and incubated for 2 h at room temperature. The membrane was washed 3 times for 10 min with blocking buffer before the secondary antibody (HRPO) was added (1:5000 dilution) in blocking buffer, and incubated for 1 h. The membrane was washed 3 times for 10 min with blocking buffer. The substrates of a chemiluminescence kit were mixed according to the manufacturer´s instructions and applied to the nitrocellulose membrane. Photo film was applied onto the membrane overtop of a transparent cellulose acetate sheet in a darkroom, and exposed the film. Films were developed immediately after exposure.

2.2.10 Phosphate Release Assay

Substrates to be tested were prepared in assay buffer (Tris-HCl 100 mM, NaCl 120 mM, pH 7.4) in a total volume of 25 µl/well. Enzymes to be tested were diluted in assay buffer to desired concentration in a total volume of 25 µl for each test well in a 384-well plate. 25 µl of enzyme mix containing 0.05 – 5 µg protein was rapidly added to each well to initiate the reaction. To do so, the pipette tip was touched to the bottom of the well, mixed 3 times rapidly without blowing out and extracted smoothly, releasing the remaining fluid. Reactions were carried out at 25°C. Malachite green acidic dye reagent

was mixed with the vanadate ion complex in a ratio of 100:1 at least 30 min before assay termination. Reactions were stopped by the addition of 25 µl of malachite green dye complex. After reaction termination, colour was allowed to develop for 20 min, after which absorbance was measured at 620 nm with a FLUOstar plate reader. Reaction start and stop times for different time points were staggered but always reflected the appropriate run-time and 20 minute colour development before measuring. Two to four wells were used for each time point. For the zero time point, a measure of assay background, the enzyme mix and malachite green mix were added simultaneously. All values for a series were standardized against the zero reading. A standard reference curve for phosphate release was generated using the Protein Tyrosine Phosphatase (PTP) Assay Kit and 1 mM phosphate standard according to manufacturer's instructions. To test for significance, a two-tailed t-test was applied assuming unequal variance.

2.2.11 Translocation Assays

To determine translocation of LppA, vector pSH108 encoding adenylate cyclase fusion proteins to the N-terminal of LppA was transformed to *L. pneumophila* wild-type and Δ*icmT* strains to quantify the production of cAMP in the host cell (Chen *et al.*, 2004). RAW 264.7 macrophages were seeded at 5×10^5/ml into 96-well plates in a final volume of 100 µl/well and incubated at 37°C overnight. The macrophages were infected (MOI 50) with *L. pneumophila* wild-type or Δ*icmT* harboring plasmid pSH108 grown for 21 h in AYE medium supplemented with 0.5 mM IPTG. After 30 min of infection, cells were washed with PBS and lysed with 200 µl sterile water for 10 min. Lysis was enhanced by shaking the plate on a microplate shaker. Intracellular cAMP was measured by using the cAMP Biotrak enzyme immuno assay system. To test for significance, a two-tailed t-test was applied assuming unequal variance.

2.2.12 Extracellular Growth Assays

L. pneumophila wild-type was inoculated with an OD_{600} of 0.1 to 200 µl AYE in 96-well plate format. Three wells were used per sample per test condition. After 12 h growth at 37°C and 600 rpm on a temperature controlled plate shaker, 10 mM phytate was added for 6 h to one growth set. After an additional 6 h, the bacteria were pelleted for 10 min at 1000 × *g* and carefully resuspended in fresh 37°C AYE medium. Growth on the plate shaker proceeded for another 12 h. OD_{600} measurements were taken with a FLUOstar plate reader and subtracted from input values.

Alternatively, *L. pneumophila* wild-type, Δ*lppA* mutant or wild-type harbouring pRM1 (M45-LppA) were inoculated with an OD_{600} of 0.1 to 200 µl AYE in 96-well plate format. Three wells were used

per sample per test condition (0 - 5 mM phytate). Unused wells were filled with 200 µl sterile water. Cultures were incubated on a temperature controlled plate shaker at 24°C and 600 rpm. Growth was measured after 5 days (OD_{600}).

Finally, wild-type *L. pneumophila* was also grown in 3 mL AYE cultures at 37°C. Micronutrient supplementation was carried out with $FeN_3O_9 \times 9H_2O$, $ZnCl_2$, $CaCl_2$ or $MgCl_2 \times 6H_2O$. Phytate (final concentration 10 mM) was added to cultures at a ratio of 1:1 with each micronutrient. Cultures were inoculated in triplicate at an OD_{600} of 0.1 and allowed to grow for 21 h. To test for significance, a two-tailed t-test was applied assuming unequal variance.

2.2.13 Competitive Growth Assay in *A. castellanii*

A. castellanii seeded 5 x 10^4 per well in a 96-well plate in Ac buffer were infected with a mixture of wild-type *L. pneumophila* and Δ*lppA* mutant bacteria at an MOI of 0.01. The assay was carried out for 18 d at 37°C. Every third day, the supernatant and lysed amoebae (0.8% saponin) were diluted 1:1000, and fresh amoebae were infected (50 µl homogenate per 200 µl amoebae culture volume), and aliquots were plated on plain CYE agar plates or plates containing kanamycin to determine relative colony forming units (CFU) between the two strains.

2.2.14 Intracellular Growth Assays and Imaging

Intracellular growth assays under phytate load were performed with *A. castellanii* or *D. discoideum* amoebae cultured with increasing concentrations of phytate. The compound was added at 2.5 mM and the concentration was increased every two days until cells were maintained in 5 or 10 mM phytate for *D. discoideum* and *A. castellanii* respectively. *L. pneumophila* wild-type, Δ*icmT*, Δ*lppA* harboring pNT28 (GFP), or Δ*lppA* harboring pWS31 (GFP, LppA) were inoculated in AYE with Cam (5 µg/ml) and IPTG (1 mM), and grown to early stationary phase. *A. castellanii* or *D. discoideum* were seeded 5 × 10^4/well in 200 µl LoFlo in a 96-well plate and allowed to adhere for 1 h. Each measured time point of the experiment required one 96-well plate with three allocated wells per strain. *L. pneumophila* cultures were diluted in LoFlo to 2.5 × 10^4/ml. Medium was removed from adhered cells and replaced with 200 µl of the *L. pneumophila* dilutions in LoFlo. Plates were centrifuged at 1000 × *g* for 5 min and incubated at 37°C for *A. castellanii* or 23°C *D. discoideum*. As an input control, 20 µl of a 1:100 dilution of each strain used for infection was plated onto CYE agar, and colonies were counted after 3 d incubation at 37°C.

After centrifugation, one plate for *A. castellanii* (t = 0) was imaged by confocal microscopy using a Nikon eclipse TE300 microscope with Perkin Elmer UltraVIEW spinning disk system and Hamamatsu Orca Flash 4.0 C-MOS camera. A Nikon 20× Plan Fluor objective was used in combination with filters 488 – 10BP/525 – 50BP and bright field. Image evaluation was carried out with Velocity 6.0.1 software. Confocal images of GFP channel and bright field were captured for each time point. Since GFP expression could vary between strains, quantitative plating assays were performed to complement microscope images. To this end, the infected cells were lysed after microscopic imaging at a given time point, diluted 1:1000, and plated to CYE agar. *D. discoideum* amoebae were lysed and plated without imaging. CFU counts for *L. pneumophila* growth in cells not cultured under phytate load followed the same procedure in absence of phytate supplementation. To test for significance, a two-tailed t-test was applied assuming unequal variance.

3 Results

3.1 The Early Phosphoinositide Pattern is Mediated by the Host Cell

The PI pattern observed during *L. pneumophila* infection could be separated into distinct programmed events. The first, discussed in this section, is the early macropinosome PI pattern upon internalization of *L. pneumophila* by the host cell. The following series of experiments demonstrates that the PI pattern in this event is independent of the Icm/Dot machinery. The progressive events, discussed in section **3.2**, see the transition from host-cell mediated to Icm/Dot mediated control of the PI pattern. All experiments directed at solving the PI pattern were carried out with real time imaging techniques developed specifically for observation of *Legionella*. In addition to enabling a defined, time-resolved analysis of the dynamics of host cell components, live cell imaging avoids common fixation problems, such as the destruction of epitopes and membrane architecture or the production of artefacts. PIs are important membrane constituents in a multitude of processes, especially in directing and coordinating vesicle traffic in the cell. *L. pneumophila* has adapted a strategy to manipulate phosphoinositide metabolism to promote its own survival and replication.

3.1.1 Acquisition and Clearance of PtdIns(3,4,5)P_3 from the *L. pneumophila* Macropinosome

The uptake of *L. pneumophila* was investigated on a single cell level in *D. discoideum* producing PH_{CRAC}-GFP as a probe for PtdIns(3,4,5)P_3 (and PtdIns(3,4)P_2). PtdIns(3,4,5)P_3 is the characteristic PI lipid produced on dynamic sections of the plasma membrane. In amoebae infected

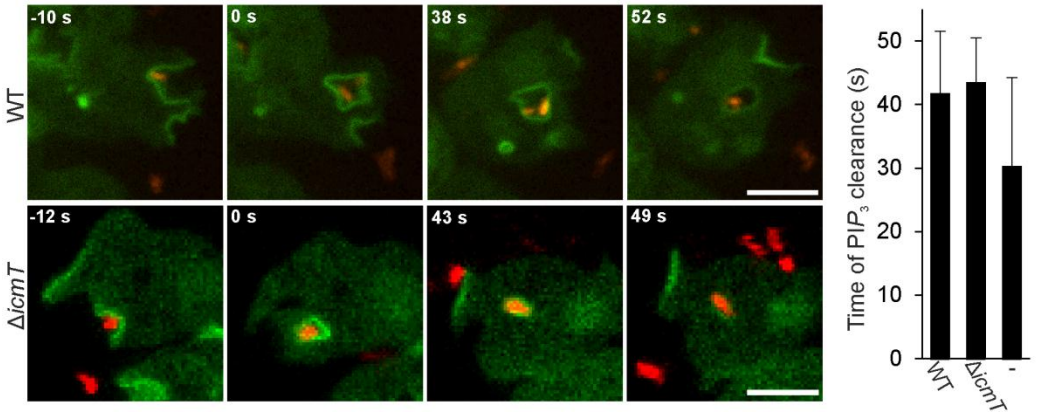

Figure 3.1 Transient accumulation of PtdIns(3,4,5)P_3 upon uptake of *L. pneumophila*. Time lapse image series for wild-type and Δ*icmT L. pneumophila* internalized by *D. discoideum* expressing PH_{CRAC}-GFP as a marker of PtdIns(3,4,5)P_3 (and PtdIns(3,4)P_2). The PI probe accumulates during formation of a macropinocytic cup and sealing of the macropinosome harbouring *L. pneumophila* (0 s), transiently persists on the internalized macropinosome, and finally dissociates from the vacuoles. Elapsed time from macropinosome formation to clearance of PtdIns(3,4,5)P_3 and PtdIns(3,4)P_2 from the uninfected macropinosome (-) or macropinosome containing *Legionella* as indicated was quantified. Data was collected for 6 replicates and 50 events were scored for each data set (mean ± SD). The zero time point was determined by the fusion of the membranes forming the macropinosome (infected and uninfected) and events were followed until probe dissociation. Scale bars 5 µm.

with *L. pneumophila*, PH_{CRAC}-GFP localized to macropinocytic cups and early macropinosomes. To analyze the role of the *L. pneumophila* Icm/Dot T4SS on PtdIns(3,4,5)P_3 dynamics during bacterial uptake, *D. discoideum* producing PH_{CRAC}-GFP were infected with either wild-type or Δ*icmT L. pneumophila* and observed on a time scale resolved to seconds (**Figure 3.1**). PtdIns(3,4,5)P_3 waves were constantly produced by *D. discoideum* in presence or absence of bacteria. The PI lipid accumulated with similar kinetics at every entry site observed to result in a macropinosome. Furthermore, PtdIns(3,4,5)P_3 was cleared with an average of about 42 seconds from macropinosomes containing *L. pneumophila*, regardless of whether vacuole contained wild-type or Δ*icmT*. PtdIns(3,4,5)P_3 clearance from macropinosomes in uninfected *D. discoideum* was also not significantly different. These results indicate that during uptake of wild-type and Icm/Dot-deficient *L. pneumophila* the PtdIns(3,4,5)P_3 dynamics are similar and comparable to uninfected amoebae.

All *L. pneumophila* observed entering the host cell did so exclusively in PtdIns(3,4,5)P_3-labelled macropinosomes. This observation was further supported by pharmacological inhibition of PI3K or actin polymerization, in which cells failed to internalize the bacteria (**Figure 3.2**). Concentrations of the PI3K inhibitor wortmannin (0.1 mM) adequate to silence PtdIns(3,4,5)P_3 production in mammalian cells do not suffice for *D. discoideum*. A concentration 40-fold higher was necessary to effectively abolish the PtdIns(3,4,5)P_3 wave. In absence of PtdIns(3,4,5)P_3, cells were still capable of directed polarization but incapable of internalizing *L. pneumophila*.

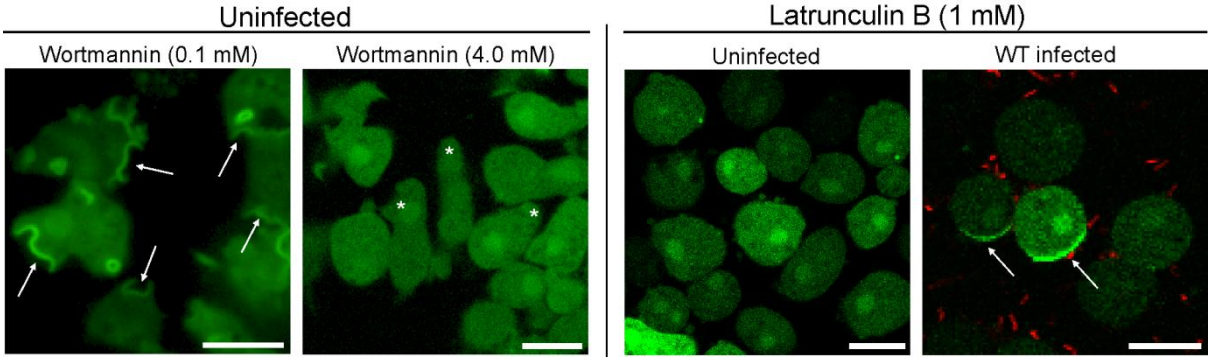

Figure 3.2 Pharmacological inhibition of PI3K or actin polymerization prevents uptake of *L. pneumophila*. Wortmannin treatment of 0.1 mM 1 h prior to observation in *D. discoideum* expressing PH_{CRAC}-GFP was not sufficient to disable the PtdIns(3,4,5)P_3 wave on dynamic membranes. A concentration of 4.0 mM was however able to abolish the PtdIns(3,4,5)P_3 wave. Latrunculin B treatment of 1 mM for 20 min caused *D. discoideum* to round and mostly detach from the observation dish. Upon infection of these cells with *L. pneumophila* wild-type, cells could produce a polarized PtdIns(3,4,5)P_3 wave at sites of stimulation, but were not permissive to the bacteria. Arrows indicate PtdIns(3,4,5)P_3 waves. Asterisks denote examples of dynamic cell membranes where a PtdIns(3,4,5)P_3 would be expected. Scale bars 10 µm.

Actin polymerization is also essential to the macropinocytic uptake process. As such, *D. discoideum* treated with the actin polymerization inhibitor latrunculin B are incapable of internalizing *L. pneumophila*. The cells round and struggle with lamellapodia formation. Nonetheless, they can still produce polarized waves of PtdIns(3,4,5)P_3.

3.1.2 Acquisition of PtdIns(3)*P* by the Internalized *L. pneumophila* Macropinosome

PtdIns(3)*P* is an endocytic marker synthesised by PI3K. Internalized vacuoles acquire this lipid shortly after uptake, directing them for endosome-lysosome fusion. To analyse the dynamics of PtdIns(3)*P* during *L. pneumophila* infection, *D. discoideum* was cultured producing the probe 2×FYVE-GFP. This probe specifically labels PtdIns(3)*P* with high sensitivity. A preliminary observation of *L. pneumophila* uptake into this cell system indicated that there was a short elapsed time between macropinosome closure and acquisition of PtdIns(3)*P*. In the microscope bright field, unlabeled projections were observed to surround a bacterium and then fuse. This fusion of the membranes to form a macropinosome was designated as the zero time point. From there, elapse time until the appearance of PtdIns(3)*P* could be measured (**Figure 3.3**). Wild-type and Δ*icmT* mutant *L. pneumophila* could spend several seconds in a macropinocytic cup before fusion of the projected amoebae lamellipodia. In the majority of cases, *L. pneumophila* was observed to escape the phagocyte prior to macropinosome closing, indicating that formation of and entrance into the macropinocytic cup was not tantamount to uptake of the bacteria.

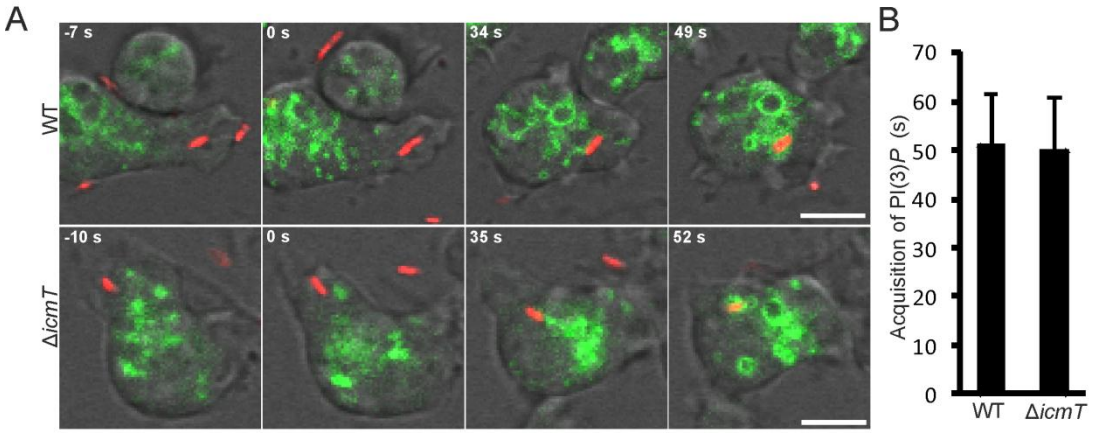

Figure 3.3 Rapid acquisition of PtdIns(3)*P* on *L. pneumophila* macropinosomes. (A) Time-lapse images of PtdIns(3)*P* acquisition by a newly internalized *Legionella*-containing macropinosome (wild-type or Δ*icmT*) in *D. discoideum* producing 2×FYVE-GFP. The image series shows the formation of a macropinocytic cup, fusion of the membranes to seal the macropinosome (t = 0 s), the internalized macropinosome prior to PtdIns(3)*P* acquisition, and finally acquisition of PtdIns(3)*P* by the macropinosome. (B) Quantification of PtdIns(3)*P* acquisition by recently internalized *L. pneumophila* macropinosomes from the time of macropinosome formation to the association of the 2×FYVE-GFP probe with the macropinosome. Data was collected for 5 replicates and a total of 40 events were scored for each strain (mean ± SD). Scale bars 5 µm.

The newly formed macropinosomes were dragged inward toward the cell by the retracting lamellipodia. After about 30 seconds, the macropinosomes were brought into proximity of the cellular PtdIns(3)*P* pool, and shortly thereafter acquired the PI lipid. PtdIns(3)*P* was acquired by both wild-type and Δ*icmT* macropinosomes on average of 50 seconds post uptake. Images better resolved for vesicle structure show uptake of wild-type *L. pneumophila* in an approximately 2.5 µm diameter

macropinosome followed by its apparent contact to PtdIns(3)*P*-rich membranes and acquisition of PtdIns(3)*P* (**Figure 3.4**).

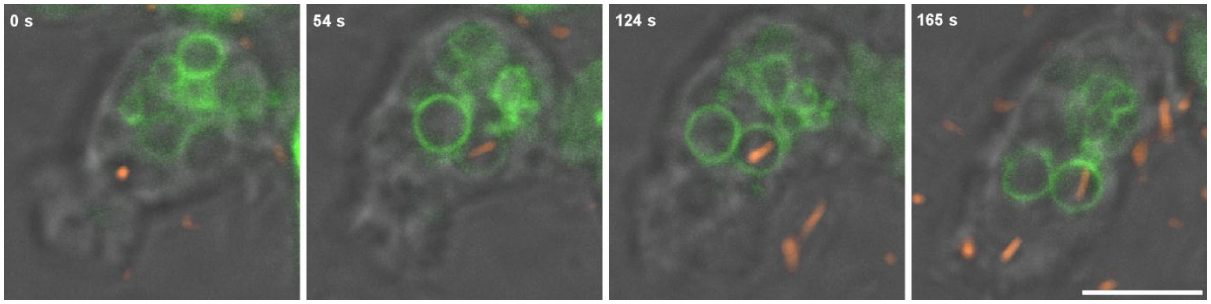

Figure 3.4 Rapid acquisition PtdIns(3)*P* resolved for vesicle structure. Acquisition of PtdIns(3)*P* by the internalized macropinosome in high resolution. Images show the newly internalized macropinosome (containing wild-type *L. pneumophila*) brought into proximity of the PtdIns(3)*P* pool and acquiring PtdIns(3)*P*, followed by intensification of the signal. Scale bar 5 µm.

As was determined for PtdIns(3,4,5)P_3, the acquisition of PtdIns(3)*P* is independent of the *L. pneumophila* Icm/Dot T4SS. The time course for the disappearance of PtdIns(3,4,5)P_3 / PtdIns(3,4)P_2 and the appearance of PtdIns(3)*P* also overlap. Up until this point in the infection, the host cell and not *L. pneumophila* controls these early interactions.

3.1.3 PtdIns(4)*P* is a Transient Lipid Component of the Macropinosome Membrane

Since internalized macropinosomes are derived from the PM, analysis was extended to PI lipids that are omnipresent on this organelle. In contrast to PtdIns(3,4,5)P_3 which is only transiently produced on the dynamic membrane, PtdIns(4)*P* and PtdIns(4,5)P_2 (section **3.1.4**) are resident constituents. *D. discoideum* amoebae stably producing the PtdIns(4)*P*-specific probe GFP-P4C$_{SidC}$ were used to characterize the dynamics of membrane PtdIns(4)*P* with high temporal resolution.

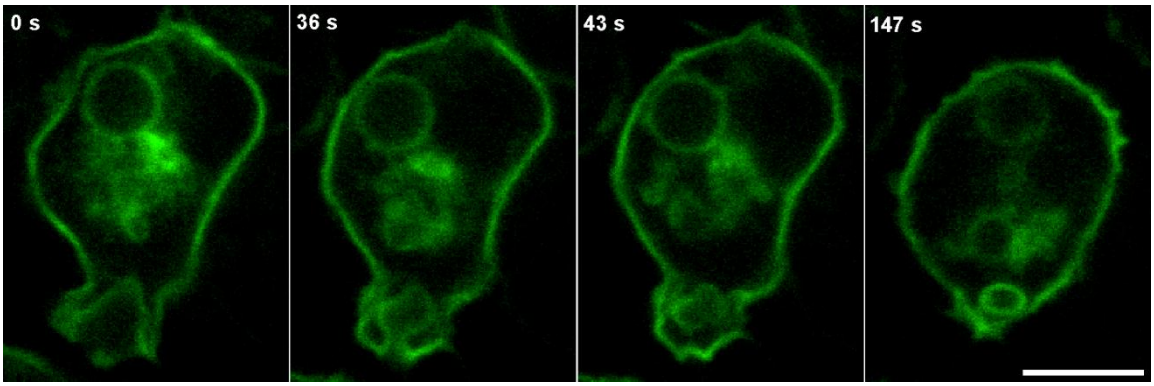

Figure 3.5 Transient localization of PtdIns(4)*P* on macropinosomes. In uninfected *D. discoideum* producing GFP-P4C$_{SidC}$, plasma membrane-derived PtdIns(4)*P* is present on the internalized macropinosome. Scale bar 5 µm.

In *D. discoideum*, the GFP-P4C$_{SidC}$ probe transiently localized to macropinocytic membranes for approximately 1 min after vacuole formation (**Figure 3.5**) until dissociation. Therefore, PtdIns(4)*P* could be considered an intrinsic component of a macropinosome internalizing *L. pneumophila*. Accordingly, PtdIns(4)*P* was identified immediately after uptake on macropinosomes containing both *L. pneumophila* wild-type and Δ*icmT* mutant bacteria (**Figure 3.6**). In both cases, the lipid was short-lived. The pool of PtdIns(4)*P* initially present on *Legionella* vacuoles was no longer detected beyond the first minutes after uptake of the bacteria. At 5 min p. i. GFP-P4C$_{SidC}$ localized to the plasma membrane and some internal vesicles of amoebae infected with either *L. pneumophila* wild-type or Δ*icmT* mutant bacteria, but no longer to bacteria-containing macropinosomes. The recovery of PtdIns(4)*P* from the *L. pneumophila* containing macropinosome is another process mediated by the host cell. This result also indicated that the PM-derived pool of PtdIns(4)*P* did not contribute to the PtdIns(4)*P* accumulation on the wild-type LCV (see **3.2.2**).

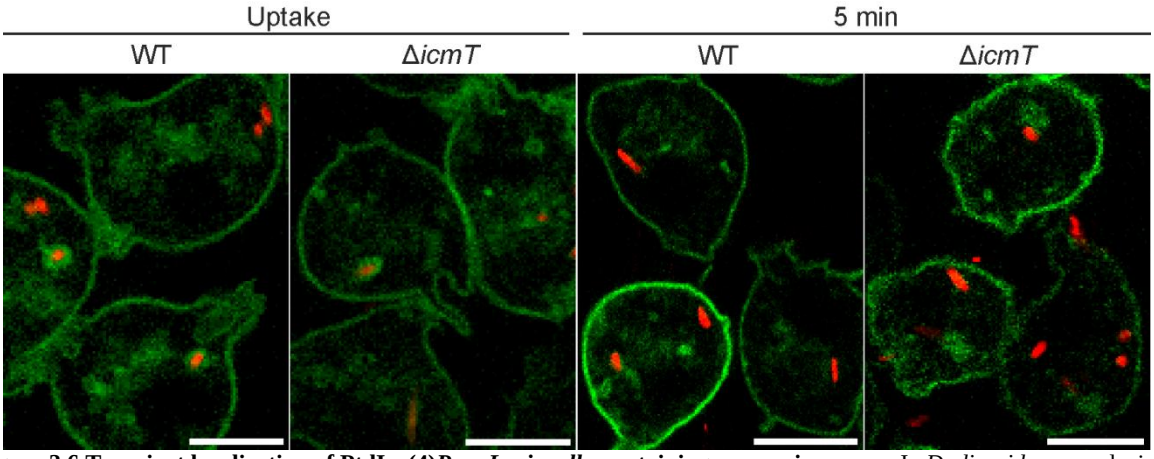

Figure 3.6 Transient localization of PtdIns(4)*P* on *Legionella*-containing macropinosomes. In *D. discoideum* producing GFP-P4C$_{SidC}$, PtdIns(4)*P* is transiently acquired as labeled by GFP-P4C$_{SidC}$ upon contact and uptake of *L. pneumophila* wild-type and Δ*icmT*. Scale bars 5 µm.

3.1.4 PtdIns(4,5)P_2 is Excluded from the Internalized Macropinosome

As with PtdIns(4)*P*, PtdIns(4,5)P_2 is constitutively present at the PM and the most abundant PI lipid in the cell. Analysis of this lipid was carried out with *D. discoideum* producing the PtdIns(4,5)P_2 probe PH$_{PLC\delta1}$-GFP. Contrary to PtdIns(4)*P*, PtdIns(4,5)P_2 was excluded from membranes forming a macropinosome. The lipid then reappeared on the plasma membrane after uptake of the macropinosome (**Figure 3.7A**). Accordingly, *L. pneumophila*-containing macropinosomes remained devoid of PtdIns(4,5)P_2. *L. pneumophila* did not accumulate this lipid on maturing LCVs (**Figure 3.7B**).

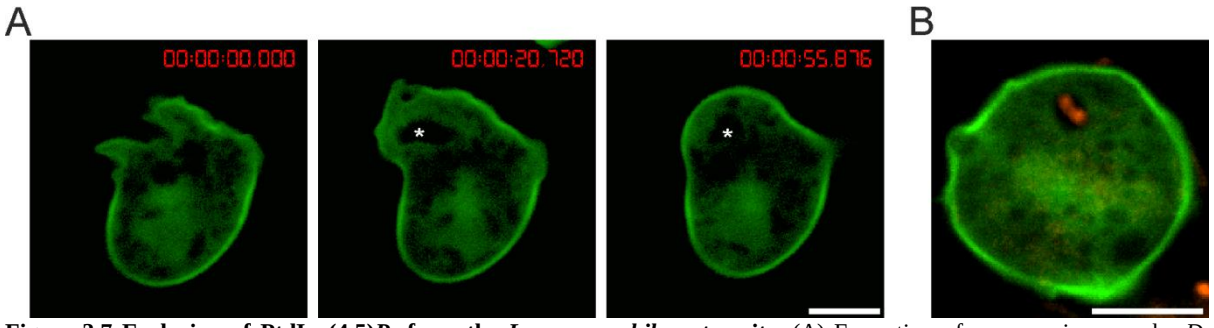

Figure 3.7 Exclusion of PtdIns(4,5)P_2 from the *L. pneumophila* entry site. (A) Formation of a macropinosome by *D. discoideum* producing the PtdIns(4,5)P_2 probe $PH_{PLC\delta1}$-GFP. The probe labels the resting plasma membrane but dissociates at dynamic membrane sites and does not label the internalized macropinosome (*). After macropinosome internalization, the probe re-localizes to the entry site on the plasma membrane. (B) Wild-type *L. pneumophila* does not accumulate PtdIns(4,5)P_2 (2 h p. i). Scale bars 5 µm.

3.2 The Icm/Dot-Dependent Phosphoinositide Pattern

3.2.1 Clearance of PtdIns(3)*P* from the LCV

In section **3.1.2**, it was demonstrated that PtdIns(3)*P* was acquired by the internalized *L. pneumophila* macropinosome independently of the Icm/Dot T4SS. In a follow up experiment in the same *D. discoideum* 2xFYVE-GFP strain, PtdIns(3)*P* was tracked for a prolonged time after initial infection (**Figure 3.8**). From the point at which the pathogen vacuoles acquire PtdIns(3)*P* up until 30 min of infection, there was no significant difference observed in the fraction of PtdIns(3)*P*-positive vacuoles containing wild-type or Δ*icmT L. pneumophila*. Based on single cell observation (section **3.1.2**), all internalized macropinosomes should acquire PtdIns(3)*P* as a programmed process. At 30 min p. i., around 90% of vacuoles were PtdIns(3)*P*-labelled, indicating that the vast majority have acquired the lipid. A major transition occurs for wild-type *L. pneumophila* between 30 and 60 min after infection, marked by a decrease from 90% to 35% of LCVs positive for the lipid. Meanwhile more than 80% of Δ*icmT* mutants remain positive for the lipid at 60 min p. i. This major PtdIns(3)*P* shedding by the wild-type LCV occurs at a very sensitive time which also sees drastic changes in host factor recruitment and PtdIns(4)*P* accumulation (**Figure 3.10**). By 2 h p. i., PtdIns(3)*P* was only detected on a small proportion of LCVs (15-20%). Over the same period of time, the percentage of PtdIns(3)*P*-positive vacuoles harboring Δ*icmT L. pneumophila* did not significantly decrease, and most macropinosomes containing the mutant bacteria retained the lipid. Thus, PtdIns(3)*P* is gradually cleared from LCVs, with the sharpest transition occurring between 30 min and 1 h after infection, whereas the majority of vacuoles containing Δ*icmT L. pneumophila* remain PtdIns(3)*P*-positive over the same time course.

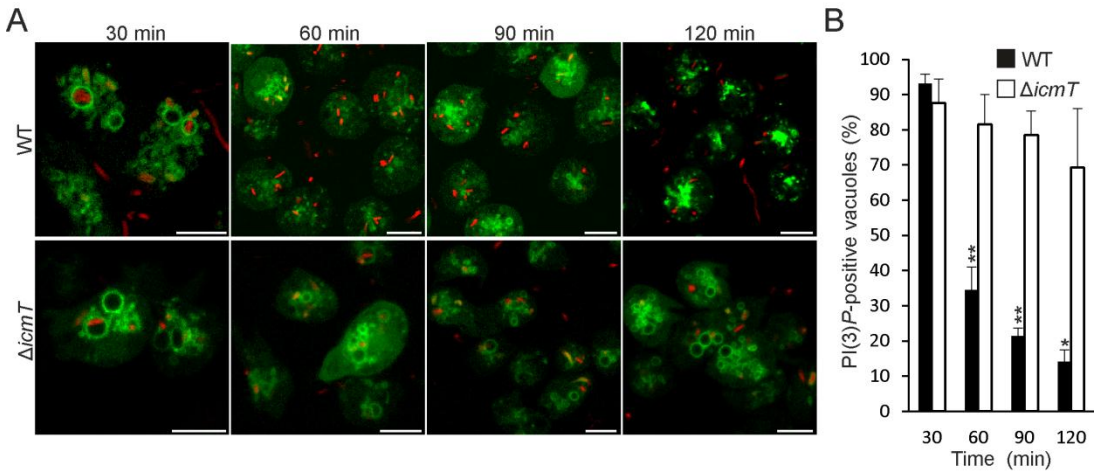

Figure 3.8 Loss of PtdIns(3)*P* from wild-type LCVs and persistence on Δ*icmT*-containing vacuoles. (A) Time-lapse images showing the clearance of PtdIns(3)*P* from wild-type LCVs over 120 min and persistence of PtdIns(3)*P* on vacuoles harboring Δ*icmT* in *D. discoideum* producing 2×FYVE-GFP. (B) Quantification of PtdIns(3)*P*-positive LCVs following infection (MOI 20) shows PtdIns(3)*P* clearance from wild-type LCVs but not from Δ*icmT*. Data was collected for 4 replicates and between 189 and 522 LCVs were scored for each strain per time point (mean ± SD). Asterisks denote statistical significance between wild-type and Δ*icmT* (**P*<0.005, ***P*<0.001). Scale bars 5 µm.

Changes in the PtdIns(3)*P* pattern are also significant beyond those observed up to 2 h after infection. Wild-type *L. pneumophila* eventually clears the lipid from all LCVs in time. No such LCVs containing replicating bacteria were observed to be positive for PtdIns(3)*P*. This observation was made upon examining infection at 8 h and beyond (**Figure 3.9**). An increasing number of Δ*icmT* mutants also lose PtdIns(3)*P*, which likely reflects degradation of the bacteria or conversion to the lipid to the late endosomal marker PtdIns(3,5)P_2. It should be noted that the general decrease or disappearance in 2xFYVE-GFP intensity is not a consequence of the cell's incapacity to produce functional markers at this time. GFP-P4C_{SidC} continues to be stably produced in advanced infection (see **3.2.2**).

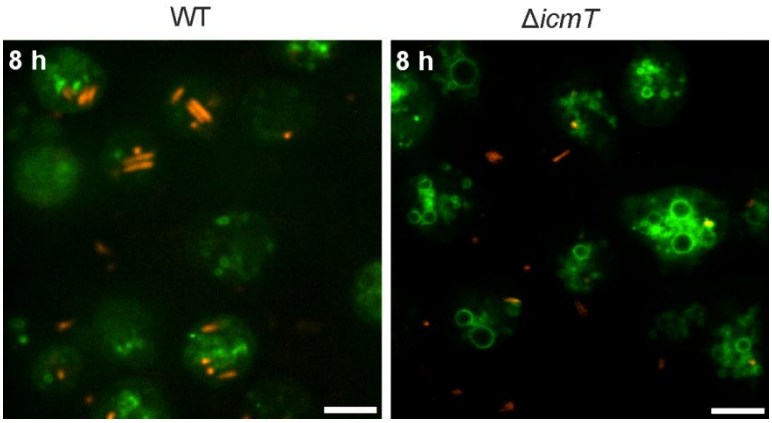

Figure 3.9 Replicating *L. pneumophila* 8 h p. i. (MOI 10) in *D. discoideum* producing 2×FYVE-GFP. The endocytic lipid marker PtdIns(3)*P* is not visible on any wild-type LCV containing replicating bacteria. There is also a general decrease in the PtdIns(3)*P* pool. Cells infected with Δ*icmT* show normal PtdIns(3)*P*-labelling of endocytic compartments. By this time, many of the Δ*icmT* bacteria, which do not replicate, have been degraded. Scale bars 5 µm.

3.2.2 Kinetics of PtdIns(4)*P* Acquisition by *L. pneumophila*

The PtdIns(4)*P* acquisition on *Legionella* vacuoles after the initial removal from macropinosomes was followed up to 2 h after infection. After the initial disappearance, PtdIns(4)*P* stably accumulated on wild-type LCVs (**Figure 3.10**). At 30 min p. i., more than 40% of LCVs were marked with PtdIns(4)*P* on vacuole membranes tightly surrounding the bacteria. The number of PtdIns(4)*P*-positive LCVs increased 1 or 2 h p. i. to more than 80% or 90%, respectively, and the vacuoles adopted the typical spherical shape. In parallel, the ratio of GFP-P4C$_{SidC}$ signal intensity on LCVs relative to the plasma membrane progressively and prominently increased. In stark contrast, PtdIns(4)*P* accumulation was not detectable on vacuoles containing Δ*icmT* mutant bacteria throughout the 2 h of infection. PtdIns(4)*P* therefore localizes to wild-type LCVs in a bi-phasic manner. After an initial transient presence on early macropinosomes controlled by the host cell, PtdIns(4)*P* steadily and stably accumulates on LCVs in a second phase, which is specific for wild-type *L. pneumophila* and controlled by the Icm/Dot T4SS.

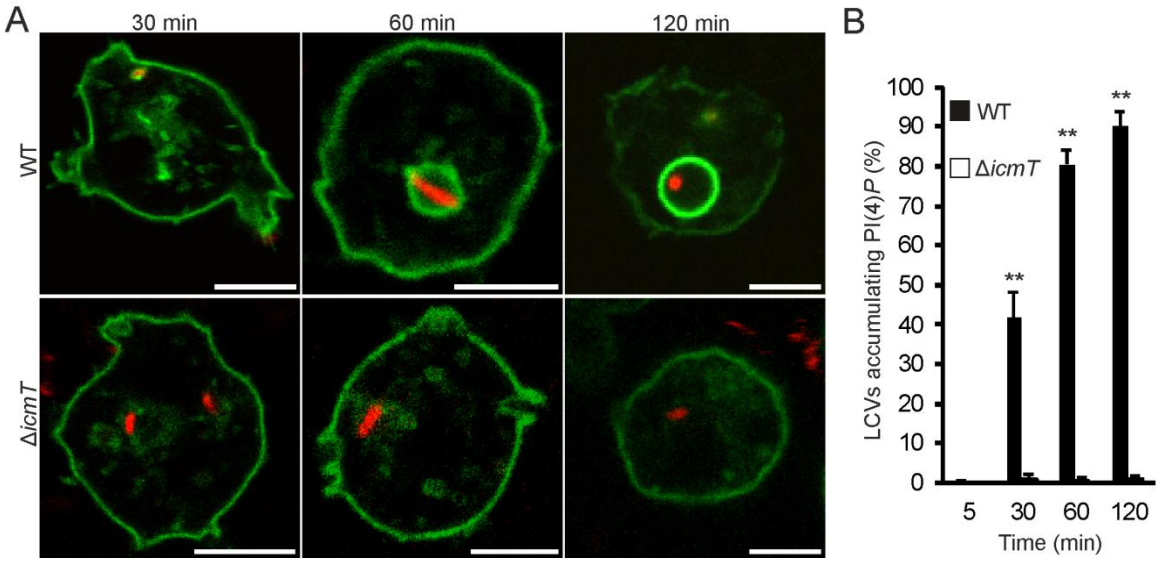

Figure 3.10 PtdIns(4)*P* accumulates on wild-type LCVs. (A) Time-resolved accumulation of PtdIns(4)*P* by *L. pneumophila* wild-type but not Δ*icmT* over the first 120 min of infection (MOI 10). (B) Quantification of PtdIns(4)*P* accumulation. Over 120 min of infection, wild-type LCVs accumulate PtdIns(4)*P* to a high level, while Δ*icmT* vacuoles do not. Data was collected for 3 replicates and a total of approximately 200 vacuoles were scored per strain for each time point (mean ± SD). Asterisks denote statistical significance between wild-type and Δ*icmT* (**P<0.001). Scale bars 5 µm.

Beyond the 2 h post infection, PtdIns(4)*P* persists on the LCV. The depicted large spherical LCVs observed in **Figure 3.10** eventually transition to form-fitted LCVs as the bacteria replicate and fill the space. **Figure 3.11** shows *L. pneumophila* wild-type bacteria after several rounds of replication, 18 h p. i. in *D. discoideum* expressing P4C$_{SidC}$-mRFPmars as the LCV marker. PtdIns(4)*P* is not cleared in time like other lipids, but persists as the staple feature of the LCV compartment until bacterial exodus, as far as could be observed.

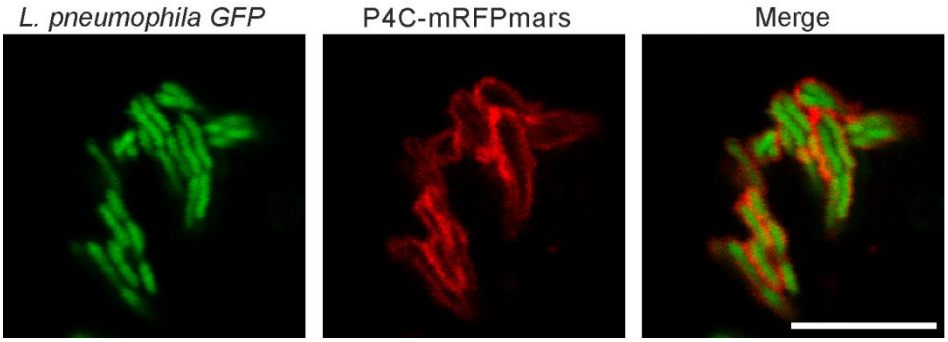

Figure 3.11 Long-term accumulation of PtdIns(4)*P* on LCVs. $P4C_{SidC}$-mRFPmars produced in *D. discoideum* infected with wild-type *L. pneumophila* tightly labels LCVs at 18 h p. i. Scale bar 5 µm.

3.3 Spatial Phosphoinositide Patterning during *L. pneumophila* Infection

3.3.1 Separation of Replicative and Endocytic Compartments

The cellular architecture of PtdIns(3)*P*-positive membranes was noticed to undergo changes along with the observed shedding of PtdIns(3)*P* from wild-type LCVs. To better characterize this observed effect, *D. discoideum* strains were constructed to produce tandem 2×FYVE-GFP and calnexin-mRFPmars to simultaneously label PtdIns(3)*P* and the recruited ER LCV marker calnexin.

In *D. discoideum*, the probe 2×FYVE-GFP labels endocytic vesicles throughout the cell. Amoebae infected with *L. pneumophila* Δ*icmT* could not be distinguished from uninfected cells in terms of their vesicle structure (**Figure 3.12**, see also **Figure 3.13**). The avirulent bacteria did not cause any observable rearrangements of the host cell membrane organization or vesicle structure. Conversely, *D. discoideum* infected with wild-type *L. pneumophila* showed a notably different membrane architecture. PtdIns(3)*P*-positive membranes were condensed, and the large characteristic PtdIns(3)*P*-labelled vesicles were no longer visible. As indicated in section **3.2.1**, over the course of 2 h of infection, PtdIns(3)*P* was removed from the replication-permissive wild-type LCV. Here it can be observed that the ER marker compartment surrounding the LCV is free of PtdIns(3)*P*. The re-arrangement of PtdIns(3)*P*-positive compartments coincided with and followed clearance of the endocytic PtdIns(3)*P* from LCVs.

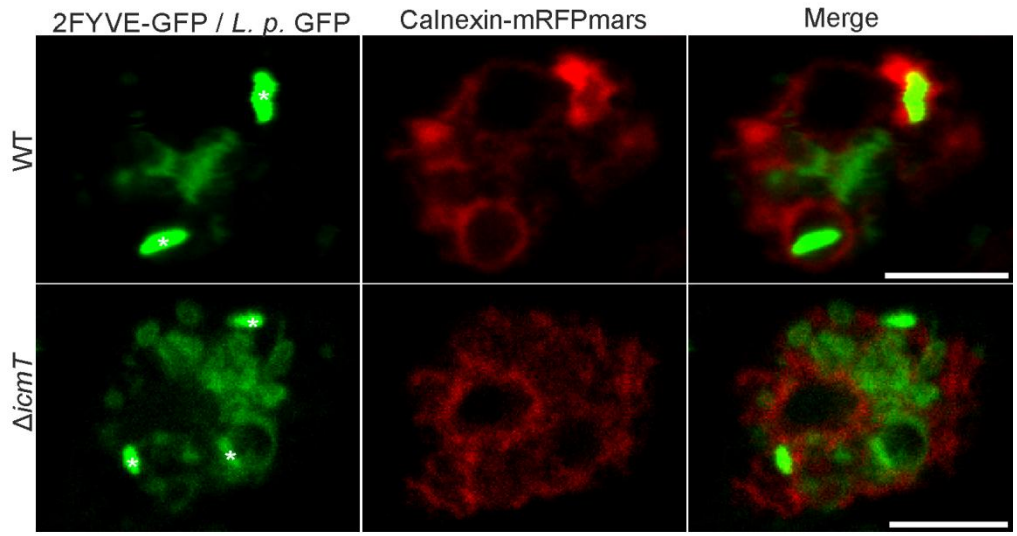

Figure 3.12 Redistribution of PtdIns(3)*P*-positive membranes upon *L. pneumophila* infection. Separation of the replication-permissive ER compartment (labeled by calnexin-mRFPmars) and the endocytic marker PtdIns(3)*P* (labeled by 2×FYVE-GFP) was observed in wild-type *L. pneumophila*-infected *D. discoideum* producing both probes. LCVs were clear of endocytic membranes. PtdIns(3)*P* remained distributed and vesicular in cells infected with Δ*icmT* mutants. Images were taken 2 h p. i. Asterisks denote bacteria. Scale bar 5 µm.

3.3.2 Condensation of Endocytic Membranes

The distribution of PI lipids in *D. discoideum* using 2×FYVE-GFP and P4C$_{SidC}$-mRFPmars as probes for PtdIns(3)*P* and the LCV marker PtdIns(4)*P* respectively was also analyzed. As was the case for the previously described *D. discoideum* system (**Figure 3.12**), it was observed 2 h p. i. that wild-type *L. pneumophila* LCVs which were PtdIns(4)*P*-positive were entirely separated from condensed PtdIns(3)*P*-positive membranes (**Figure 3.13**).

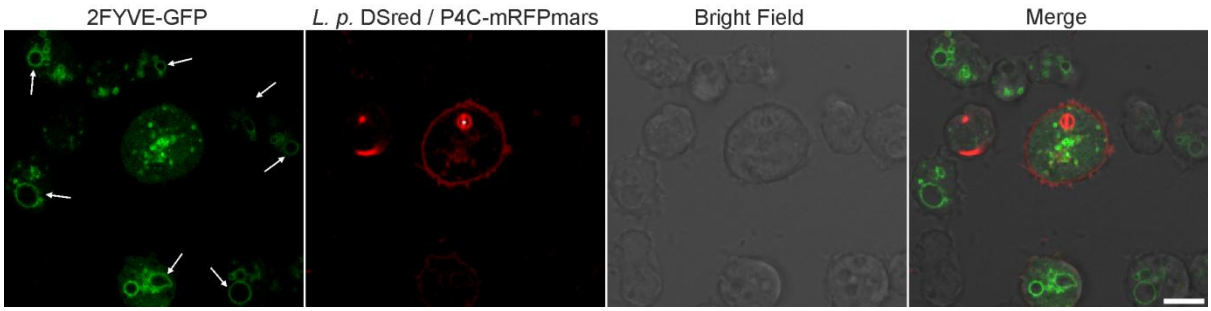

Figure 3.13 Condensation of endocytic membranes. Images of *D. discoideum* producing tandem 2×FYVE-GFP and P4C$_{SidC}$-mRFPmars 2 h p. i. with wild-type *L. pneumophila*. The LCV is separate from the condensed mass of PtdIns(3)*P* in the cell, but moreover, the characteristic large vesicles present in uninfected surrounding cells (arrows) are not visible in the infected cells (MOI 5). Asterisk represents *L. pneumophila* in cell of interest. Scale bar 5 µm.

In surrounding uninfected cells, the characteristic PtdIns(3)*P*-positive vesicles were clearly visible. Quantification for the presence of these vesicles revealed that more than 90% of uninfected or Δ*icmT*-infected amoebae contained these structures, whereas only 10% or less of the amoebae infected with wild-type *L. pneumophila* retained them at 2 h p. i. (**Figure 3.14**).

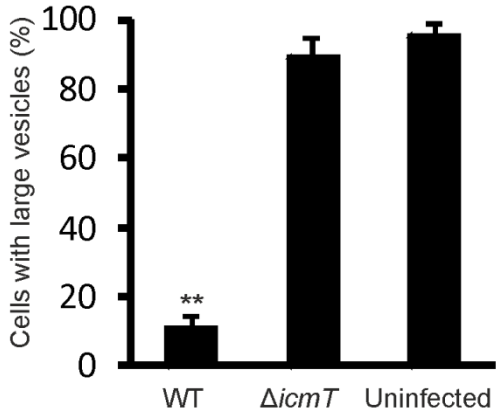

Figure 3.14 Compacting of PtdIns(3)*P*-labeled vesicles. The integrity of the large vesicles was assessed and quantified from the distribution of the 2xFYVE-GFP probe and bright field images for *D. discoideum* infected for 2 h with wild-type or Δ*icmT L. pneumophila* or uninfected amoebae producing 2×FYVE-GFP. Asterisks denote statistical significance of decrease compared to uninfected cells (***P*<0.001).

The infection of *D. discoideum* with wild-type *L. pneumophila* thus appears to trigger major remodeling of PtdIns(3)*P*-positive membranes and apparent disintegration of the tubular endosomal network, as well as a complete separation of the endocytic PtdIns(3)*P*-positive compartments from the replication permissive PtdIns(4)*P*-positive LCVs.

3.3.3 Morphology of the LCV during *L. pneumophila* Replication

Three-dimensional imaging of the LCV structure indicated that cells infected with multiple *L. pneumophila* wild-type bacteria formed an LCV network. *D. discoideum* expressing P4C$_{SidC}$-GFP showed that LCVs are not randomly distributed within the cell, but rather are held in close proximity to each other, giving the appearance of a networked stack. The identifying LCV marker PtdIns(4)*P* is enriched in the membrane that tightly surrounds the replicating bacteria (**Figure 3.15**).

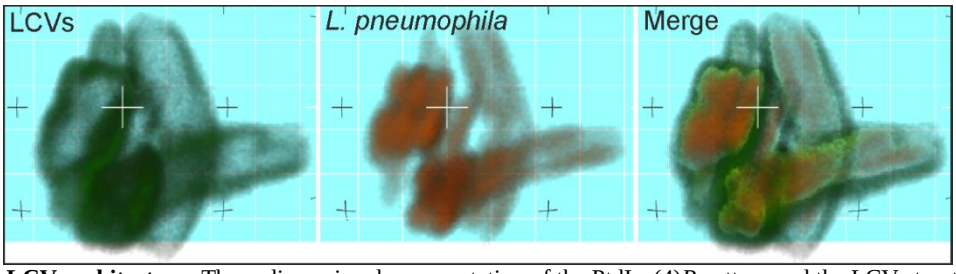

Figure 3.15 LCV architecture. Three-dimensional representation of the PtdIns(4)*P* pattern and the LCV structure 18 h p. i. for wild-type *L. pneumophila*-infected *D. discoideum* producing GFP-P4C$_{SidC}$. In this single cell, LCVs adopt a shape that is tight to the replicating bacteria in a layered assembly.

3.4 PtdIns(4)*P* Accumulation Precedes and is Independent of ER Recruitment

LCVs are reported to attach to and fuse with the ER during the course of their maturation (Swanson *et al.*, 1995; Tilney *et al.*, 2001; Robinson and Roy, 2006). As demonstrated in **Figure 3.10**, the kinetics of PtdIns(4)*P* acquisition and calnexin recruitment to LCVs (Ragaz *et al.*, 2008) are very similar, yielding around 80% and 90% PtdIns(4)*P* or calnexin-positive LCVs at 1 and 2 h p. i. This temporally similar accumulation presented itself as an opportunity to showcase the power of live imaging with tandem fluorescent probe expression. A *D. discoideum* strain was constructed producing tandem $P4C_{SidC}$-mRFPmars and calnexin-GFP with intent of observing the interplay of PtdIns(4)*P* and the ER and discriminating between the markers on a time resolved scale.

LCVs were imaged at 1, 2 and 8 h p. i. The PtdIns(4)*P* probe $P4C_{SidC}$-mRFPmars labelled spherical LCVs that were formed by 1 h and maintained spherical shape 8 h p. i. (**Figure 3.16A**). At 1 h p. i. wild-type LCVs defined by a discrete ring of PtdIns(4)*P* were loosely surrounded by ER membrane. This observation indicated that the acquisition of PtdIns(4)*P* preceded and was independent of ER attachment. Under live cell microscopy conditions, the calnexin-GFP probe surrounded the discrete PtdIns(4)*P*-positive LCV membrane but showed no indication of fusion at the 8 hour observation point. Up until that point, visual observation and histogram plot data indicated that the immediate LCV membrane and ER layers were resolvable separate entities. These results support the notion that PtdIns(4)*P*-positive membrane is formed early during LCV maturation and serves as an anchoring platform for PtdIns(4)*P*-binding *L. pneumophila* effector proteins which promote later steps of LCV formation.

To empirically show that the formation of a PtdIns(4)*P*-positive membrane precedes the recruitment of ER, the infection series was repeated with the *L. pneumophila* Δ*sidC-sdcA* mutant strain (Ragaz *et al.*, 2008) which is defective for ER recruitment but does not affect other PI dynamics (Weber *et al.*, 2014). Upon infection of *D. discoideum* producing $P4C_{SidC}$-mRFPmars and calnexin-GFP with Δ*sidC-sdcA* mutant *L. pneumophila*, PtdIns(4)*P*-positive LCVs were formed as for wild-type bacteria. However, the recruitment of calnexin-GFP to PtdIns(4)*P*-positive LCVs was severely impaired, yielding obvious PtdIns(4)*P*-positive LCVs without indication of ER interaction. LCVs with Δ*sidC-sdcA* mutant *L. pneumophila* acquired calnexin-GFP-positive membranes later and to a lesser extent (**Figure 3.16B**). At 2 h p. i. LCVs containing Δ*sidC-sdcA* bacteria had recruited sections of the ER, but the interaction was still incomplete and loose. Moreover, on LCVs surrounded by ER membrane, large gaps were present between the two membranes. Finally at 8 h p. i., LCVs harbouring Δ*sidC-sdcA* mutant or wild-type *L. pneumophila* were similar, with the PtdIns(4)*P*-rich LCV in tight association with, but still separated from the surrounding ER. These findings indicate that the formation of a PtdIns(4)*P*-positive LCV, binding of bacterial effectors and further interactions with

cell organelles are sequential steps during LCV maturation, where the LCV remains a distinct compartment with a discrete PtdIns(4)*P* identity.

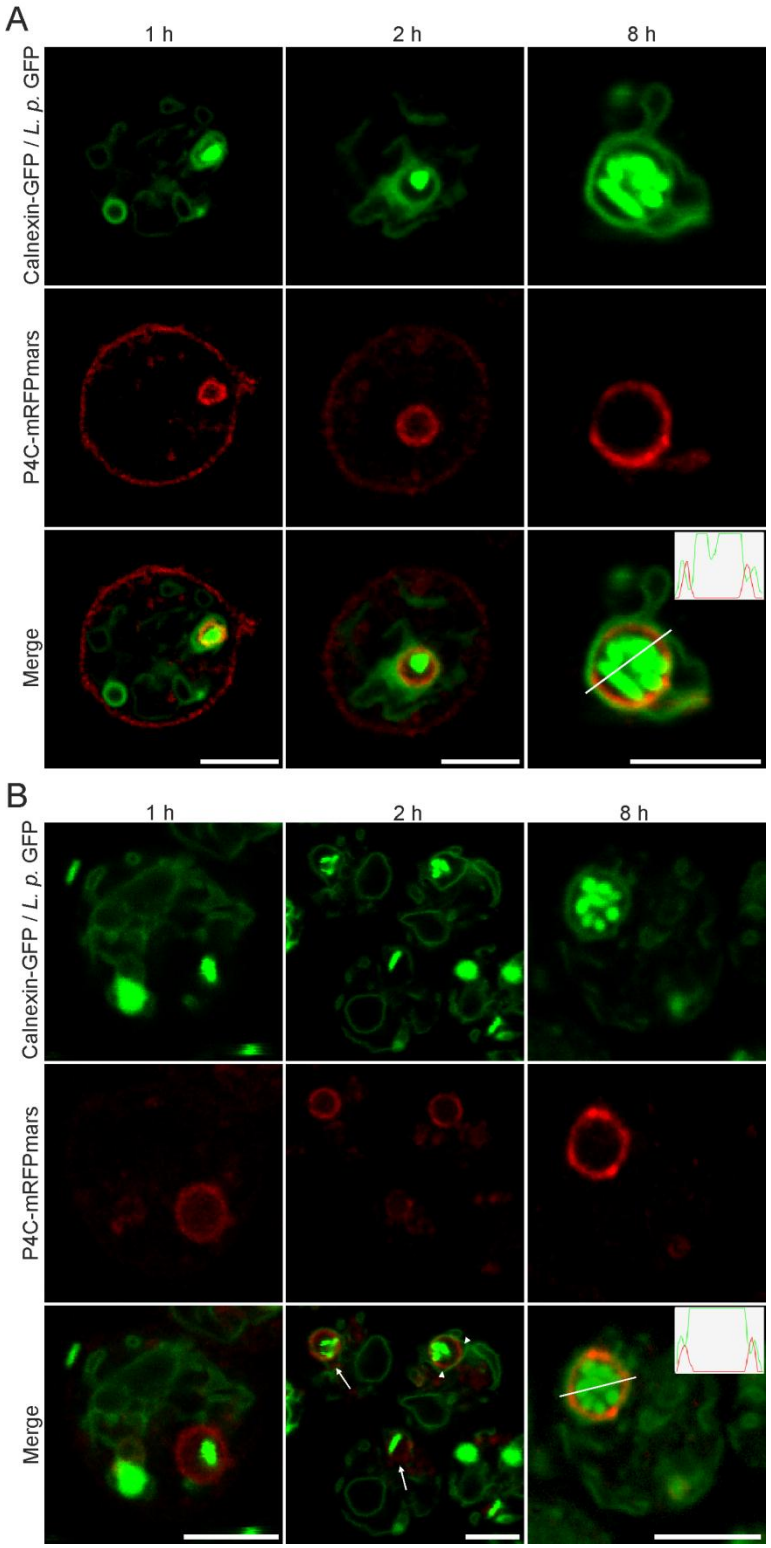

Figure 3.16 Progressive coating of PtdIns(4)*P*-positive LCVs with ER membranes. (A) *D. discoideum* producing tandem calnexin-GFP and $P4C_{SidC}$-mRFPmars were infected with *L. pneumophila* wild-type (MOI 5). The image series shows a loose layer of ER wrapping around a PtdIns(4)*P*-labeled LCV (1 h), an ER network in tight association to the LCV (2 h), and replicating *L. pneumophila* in a discrete PtdIns(4)*P* vacuole surrounded by membranous ER (8 h). (B) *D. discoideum* producing tandem calnexin-GFP and $P4C_{SidC}$-mRFPmars were infected with *L. pneumophila* Δ*sidC-sdcA*, a strain defective for ER acquisition by LCVs. The image series shows an LCV positive for PtdIns(4)*P* in absence of ER association (1 h), partial or loose association of the ER network with LCVs (2 h), and replicating *L. pneumophila* in a discrete PtdIns(4)*P*-positive vacuole, with which the membranous ER is ultimately in tight association (8 h). Arrows indicate LCVs incompletely surrounded by calnexin-GFP-labeled ER or gaps between the LCV and surrounding ER network. The inset histograms in the merged images (8 h) show that the maximum fluorescence intensities of the GFP and mRFPmars signals around the LCV do not directly overlap. Scale bars 5 µm.

To further substantiate the case that the LCV membrane and the ER are tightly associated by separate entities, the host cell factor Arf1 was expressed in *D. discoideum* calnexin-GFP as an mRFPmars fusion **(Figure 3.17)**. This *D. discoideum* strain infected was infected as prior with wild-type *L. pneumophila*. The acquired fluorescence images indicate that the GFP and mRFPmars probes overlap. This feat is evidenced by the fluorescence intensity plot, indicating that subtle differences in localization can be discriminated with the applied techniques in microscopy, and are not an artefact of chromatic aberration.

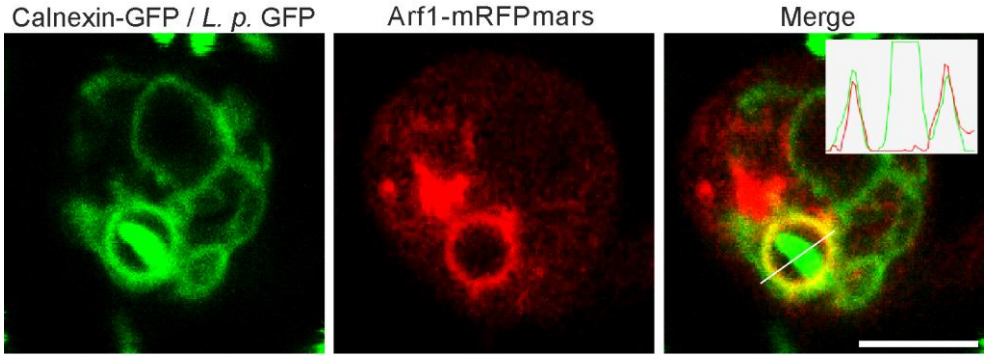

Figure 3.17 Co-localization of Arf1-mRFPmars with calnexin-GFP on LCVs. Arf1-mRFPmars and calnexin-GFP co-produced in *D. discoideum* co-localize on *L. pneumophila* wild-type LCVs at 2 h p. i. The histogram indicates that the fluorescence intensity maxima overlap. This overlap is visualized as a yellow ring around the LCV. Scale bar 5 µm.

3.5 Discovery of LppA as an *in Vitro* Phosphoinositide Phosphatase

A PSI-BLAST search using the phosphatase consensus sequence HCxxGxxRT identified the *L. pneumophila* 36.3 kDa protein Lpg2819 as a putative protein tyrosine phosphatase II of the dual specificity phosphatase (DSP) superfamily. Lpg2819 is conserved among the sequenced *L. pneumophila* strains (including Philadelphia-1, Paris, Lens, Corby, Alcoy, 130b/AA100, Lorraine), as well as in *L. longbeachae* (64% identity), *L. shakespearei* (64% identity), and *L. dumoffii* (62% identity). This catalytic sequence is also the identifying feature of PI phosphatases. The predicted catalytically active site of LppA (HCRGGKGRT) is almost identical to the mammalian PI 3-phosphatase PTEN (HCR/KAGKGRT) and similar to the mycobacterial PI phosphatase MptpB (HCFAGKDRT) (**Figure 3.18**).

LppA **HCRGGKGRT**
PTEN **HCKAGKGRT**
MptpB **HCFAGKDRT**
SidP **SCVSGKDRK**
SidF **GCKSNNDRG**

Figure 3.18 P-loop alignment of LppA and select PI phosphatases. The predicted P-loop of LppA from *L. pneumophila* was aligned to human PTEN, *M. tuberculosis* MptpB, and *L. pneumophila* SidP and SidF.

3.5.1 Phosphoinositide Phosphatase Activity of LppA

PI phosphatase activity LppA towards di-octyl PI lipids was tested *in vitro* (**Figure 3.19**). LppA dephosphorylated the di-phosphorylated PIs PtdIns(3,4)P_2 and PtdIns(4,5)P_2 very efficiently, followed by PtdIns(3,4,5)P_3 as a rapidly metabolized substrate. PtdIns(3,5)P_2 was turned over with approximately 20-fold lower efficiency than the best substrates. The monophosphorylated PIs proved to be very poor substrates, but nonetheless capable of being converted. A 100-fold higher amount of enzyme was required to observe poor activity towards PtdIns(3)*P*, PtdIns(4)*P* or PtdIns(5)*P*.

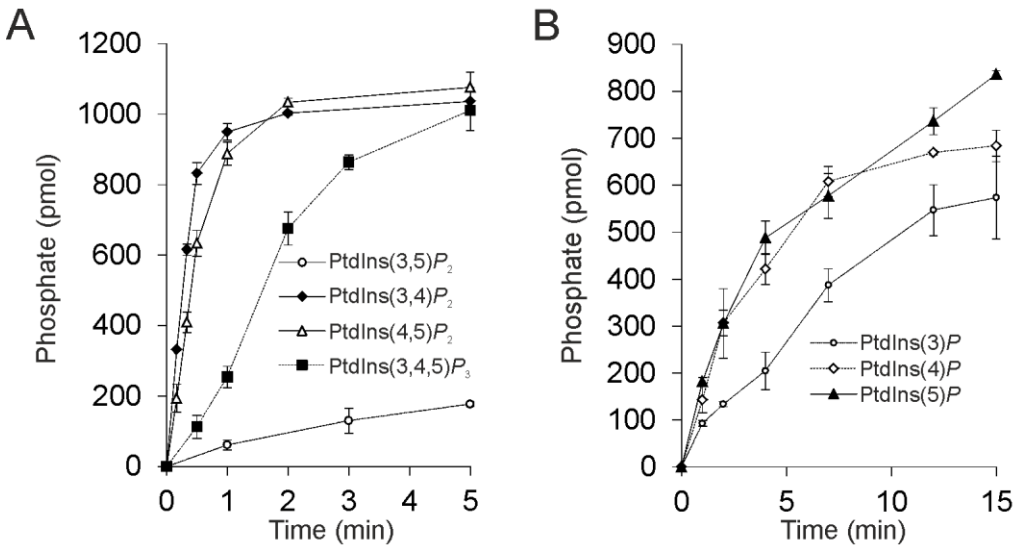

Figure 3.19 The cysteine phosphatase LppA hydrolyses PIs *in vitro*. Hydrolysis of PI lipids by $LppA_{\Delta 1\text{-}16}$ was measured for the time indicated above with 1 nmol di-octyl PI lipids and (A) 0.05 µg or (B) 5 µg protein, respectively. PI phosphatase activity was measured by phosphate release as a malachite green vanadate dye complex. Reactions proceeded at 25°C. Absorbance at 620 nm was measured 20 min after termination of each reaction.

3.5.2 Phosphoinositide Products of LppA

To analyze the *in vitro* PI product(s) generated by LppA, nitrocellulose membranes spotted with all 7 PIs and other lipids (PIP strips) were treated with LppA and subsequent protein-lipid overlay (**Figure 3.20**). The GST-$P4C_{SidC}$ probe bound on untreated control membranes exclusively to the PtdIns(4)*P* spot. In contrast, on membranes pre-treated with LppA, GST-$P4C_{SidC}$ also bound to the spots initially occupied by PtdIns(3,4)P_2, PtdIns(4,5)P_2 or PtdIns(3,4,5)P_3, indicating that PtdIns(4)*P* is the product of the phosphatase. LppA-treated membranes which were overlaid with GST-LpnE to detect PtdIns(3)*P* bound only to the initial PtdIns(3)*P* spot, indicating that no PtdIns(3)*P* was produced by the phosphatase. To control for complete metabolism of the lipids, the same membrane was then again overlaid with GST-$P4C_{SidC}$, and returned the same result as previous, meaning that PtdIns(4)*P* was produced.

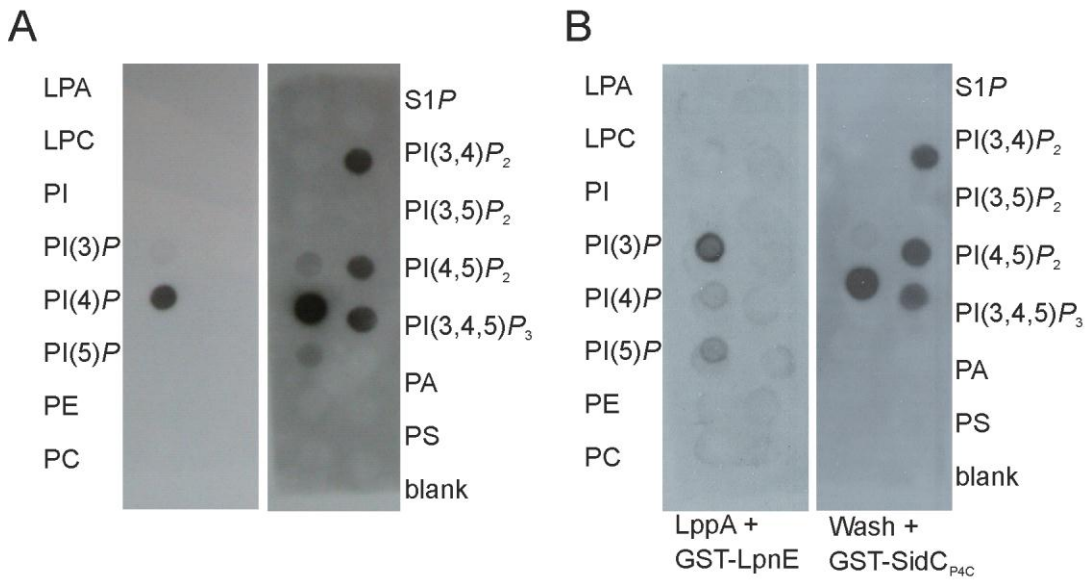

Figure 3.20 LppA produces PtdIns(4)*P* *in vitro*. (A) Nitrocellulose membranes with PI and other lipids (100 pmol/spot) were treated (right panel) or not (left panel) with purified $LppA_{\Delta 1\text{-}16}$ (submerged in 0.5 µg/µl, 10 min), and binding of the PtdIns(4)*P* probe GST-$P4C_{SidC}$ was analyzed using an anti-GST antibody. (B) A membrane as described in (A) was treated with LppA and then overlaid with the PtdIns(3)*P* probe GST-LpnE (left membrane). After development, the same membrane was washed and overlaid again with GST-$P4C_{SidC}$ showing that PtdIns(4)*P* was the unique product (right membrane). Left lane (both panels): lysophosphatidic (LPA), lysophosphocholine (LPC), phosphatidylinositol (PtdIns), phosphoinositide (PtdIns(x)*P*), phosphatidylethanolamine (PE), phosphatidylcholine (PC). Right lane (both panels): sphingosine-1-phosphate (S1*P*), phosphoinositide (PtdIns(x)*P*), phosphatidic acid (PA), phosphatidylserine (PS).

3.5.3 LppA is Produced and Translocated but does not Influence the LCV PtdIns(4)*P* Pattern

LppA was produced in *L. pneumophila* wild-type strains at early stationary phase. Western blots using an anti-LppA antibody detected the protein in lysates of wild-type *L. pneumophila*, and to a higher degree in strains producing LppA from vectors pWS31 and pRM1 (**Figure 3.21A**). LppA was not a known substrate of the Icm/Dot T4SS. To determine whether LppA is translocated into the host cell, an N-terminal fusion with the calmodulin-dependent adenylate cyclase CyaA that enables assessment of cAMP production upon translocation of the fusion protein to host cell cytoplasm was used. RAW 246.7 macrophages were infected with wild-type *L. pneumophila* or the translocation-defective Δ*icmT* mutant strain producing the CyaA-LppA fusion protein (**Figure 3.21B**). Calmodulin-dependent production of cAMP was only observed upon infection with wild-type *L. pneumophila*. LppA therefore represents a new substrate of the Icm/Dot T4SS. This finding implies that LppA has access to the host cell cytoplasm and performs an intracellular function.

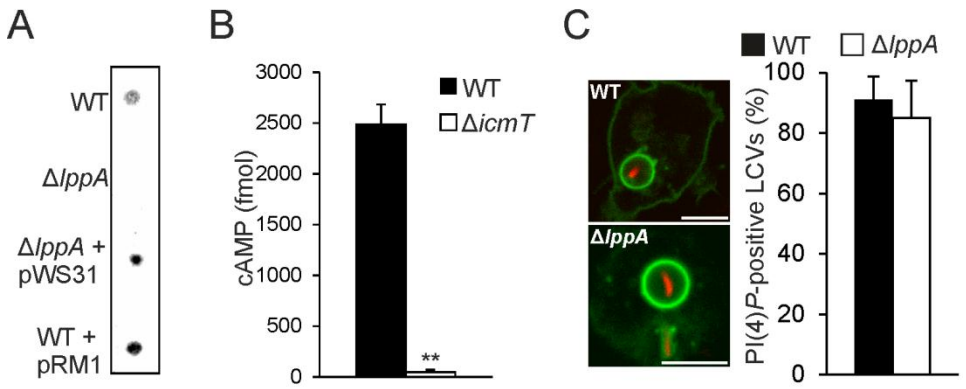

Figure 3.21 LppA is type-IV translocated but does not influence LCV PtdIns(4)*P*. (A) Anti-LppA dot blot of *L. pneumophila* lysates from cultures grown to early stationary phase. (B) LppA is a substrate of the Icm/Dot T4SS. RAW 264.7 macrophages were infected with wild-type or Δ*icmT L. pneumophila* harboring pSH108 (CyaA-LppA). Levels of cAMP (mean ± SD, four duplicate experiments) were measured 30 min post infection (MOI 50). (C) Live imaging of *D. discoideum* GFP-P4C$_{SidC}$ infected with wild-type or Δ*lppA L. pneumophila* (pSW1, DsRed) at an MOI 10. Images were taken 2 h p. i. at 23°C. PtdIns(4)*P*-positive LCVs were quantified. At least 100 LCVs were counted for each sample 2 h p. i. Scale bars, 5 µm.

The translocation of LppA and efficient hydrolysis of PI lipids to yield PtdIns(4)*P in vitro* presented a good case for the involvement of LppA in modulating the LCV PtdIns(4)*P* pattern. Therefore, live cell imaging was carried out using P4C$_{SidC}$-GFP to compare the dynamics of PtdIns(4)*P* accumulation on LCVs harbouring wild-type or Δ*lppA* mutant bacteria (**Figure 3.21C**). Upon infection of *D. discoideum* amoebae expressing GFP-SidC$_{P4C}$ with *L. pneumophila*, LCVs harbouring wild-type or Δ*lppA L. pneumophila* accumulated PtdIns(4)*P* to the same level within 2 h post infection. LCVs were similar in size and GFP-SidC$_{P4C}$ signal intensity. LCVs were scored for the presence of PtdIns(4)*P* 2 h post infection with either strain. In both wild-type and Δ*lppA* mutant bacteria, around 90% of all LCVs were labelled by the P4C$_{SidC}$-GFP probe. Thus, in spite of its *in vitro* PI metabolism, the translocated *L. pneumophila* PI phosphatase does not appear to modulate the LCV PI pattern in infected cells.

3.5.4 Substrate Range and Intracellular Localization of LppA

LppA phosphatase activity was tested against a broader range of substrates. Phosphoinositide lipids bear significant resemblance to the inositol phosphates, which make up the head group of the PI lipids. Therefore, if the *in vitro* PI phosphatase activity observed for LppA in **Figure 3.19** was not facilitated by specific recognition of fatty acid tails, the activity should also apply to the equivalent inositol phosphate compounds.

As such, LppA was capable of metabolising inositol phosphates, and at rates comparable to the PI lipid on which the equivalent head group appears. **Table 3.1** shows the relative turnover rates of both PI lipids and InsP_x compounds by LppA. The phosphatase was not, however, able to convert

Ins*P* to Ins, nor was it able to catalyze the release of phosphate from the phosphotyrosine moiety of the phosphoryulated insulin receptor or epidermal growth factor receptor.

Table 3.1 Broad substrate range of LppA and relative turnover rates.

Substrate	LppA activity
PtdIns(3,4,5)P_3	Fast
PtdIns(3,4)P_2	Very Fast
PtdIns(4,5)P_2	Very Fast
PtdIns(3,5)P_2	Moderate
PtdIns(3)*P*	Slow
PtdIns(4)*P*	Slow
PtdIns(5)*P*	Slow
Ins*P*	Negligible
InsP_2	Slow (analogous to PtdIns(x)*P*)
Ins(1,3,4,5)P_4	Fast (analogous to PtdIns(3,4,5)P_3)
Ins(1,3,4,6)P_4	Fast
Phosphotyrosine residue	Negligible

An additional two assays provided mounting evidence that LppA did not specifically interact with PI lipids in the cell. The intracellular localization of LppA in *D. discoideum* ectopically producing LppA-GFP revealed that the localization of the protein is cytoplasmic, and not specific for any given PI-enriched membrane (**Figure 3.22A**). Furthermore, protein-lipid overlays using LppA and catalytically inactive LppA demonstrated that the phosphatase does not bind to any PI lipids, or any other lipids on the multi-lipid membranes (**Figure 3.22B**). This experiment was conducted with the expectation that the catalytically inactive LppA would remain bound to its potential PI substrate without hydrolyzing.

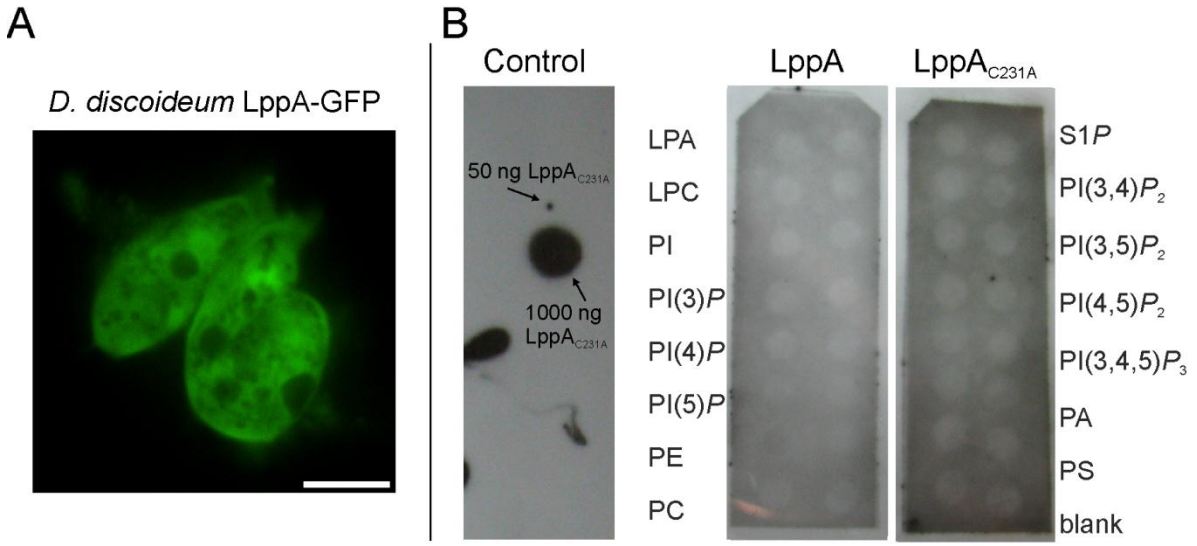

Figure 3.22 Cellular localization and lack of PI binding of LppA. (A) *D. discoideum* was transfected with vector pWS27 for regulated extra-chromosomal expression of LppA-GFP. The fusion protein shows cytoplasmic distribution within the cell. (B) Protein-lipid overlay of PI-spotted nitrocellulose membranes. The affinity purified anti-LppA antibody efficiently recognizes LppA$_{C231A}$ spotted on a control membrane. LppA and catalytically inactive LppA$_{C231A}$ were applied to PI-spotted membranes (0.5 µg/µl) for 2 h. Membranes were washed and stained with an anti-LppA antibody, followed by HRPO-coupled mouse anti-rabbit secondary antibody. Prolonged exposure of the membranes revealed that neither LppA nor LppA$_{C231A}$ bind to PIs. Left lane (both panels): lysophosphatidic (LPA), lysophosphocholine (LPC), phosphatidylinositol (PtdIns), phosphoinositide (PtdIns(x)*P*), phosphatidylethanolamine (PE), phosphatidylcholine (PC). Right lane (both panels): sphingosine-1-phosphate (S1*P*), phosphoinositide (PtdIns(x)*P*), phosphatidic acid (PA), phosphatidylserine (PS).

3.6 Characterization of LppA as Translocated Cysteine Phytase

3.6.1 Alignment of LppA to Established or Predicted Cysteine Phytases

In light of the broad substrate range of LppA (**Table 3.1**), investigation shifted to examine the phosphate-saturated inositol compound, phytate (InsP_6). A closer bioinformatic inspection of LppA revealed an overall similarity to predicted cysteine phytases of *Clostridium* (39% identity), *Stigmatella* (36% identity), and the well characterized cysteine phytase PhyA of *S. ruminantium* (30% identity) (**Figure 3.23**). The P-loop consensus sequence of *Legionella* spp. is strictly conserved in the predicted phytases of *Clostridium acetobutylicum* and *Stigmatella aurantiaca*. This finding alluded to LppA potentially being more closely related to phytases than to PI phosphatases. LppA was characterized as a cysteine phytase in the subsequent sections.

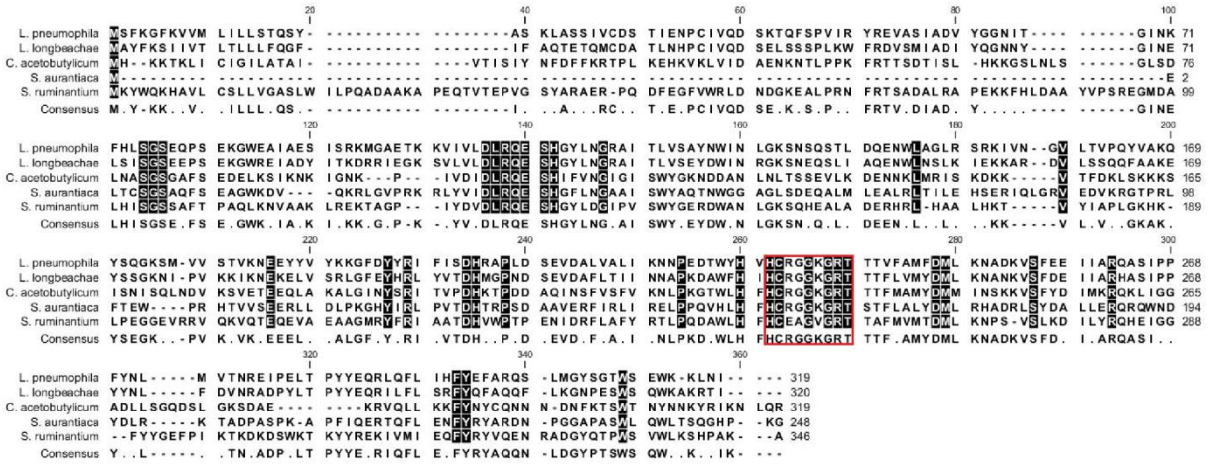

Figure 3.23 Alignment of cysteine phytases and P-loops. Alignment of (predicted) cysteine phytases of *Legionella pneumophila* (LppA), *Legionella longbeachae*, *Stigmatella aurantica*, *Clostridium acetobutylicum*, and *Selenomonas ruminantium* (PhyA) in order of decreasing homology to LppA. The red box highlights the predicted or established P-loop catalytic active sites of LppA and PhyA respectively, as well as for putative phytases from *L. longbeachae*, *S. aurantiaca*, and *C. acetobutylicum*.

3.6.2 Phytase Activity of LppA and Mutagenesis of Catalytic Residues

Phosphate release assays were performed to test potential phytase activity of LppA, compared to activity of *S. ruminantium* PhyA. Under the conditions tested, GST-LppA hydrolyzed phytate at an initial rate of 5 pmol/s per µg, confirming its activity as a phytase (**Figure 3.24A**). The turnover rate by GST-LppA was approximately twice as fast as for GST-PhyA tested under the same conditions. Point mutations were made to the putative catalytic motif to determine which amino acids were essential for enzymatic activity (**Figure 3.24B**). Mutations of the catalytic residues Cys231 or Arg237 to Ala resulted in loss of phytase activity. Replacing Gly236 with a bulky and charged amino acid, Asp, also abolished phytate hydrolysis, while changing Lys235 to Ala did not alter phytase activity. Therefore, *L. pneumophila* produces a cysteine phytase, which under the given conditions *in vitro*, shows a two-fold higher activity than PhyA. The assays were carried out at 25°C and at neutral pH to loosely simulate the conditions in an infected amoeba. It is therefore important to note that PhyA has an optimal activity at acidic pH and higher temperature inside the rumen. LppA, like PhyA, contains the conserved amino acids Cys_{215} and Arg_{221} implicated in catalysis.

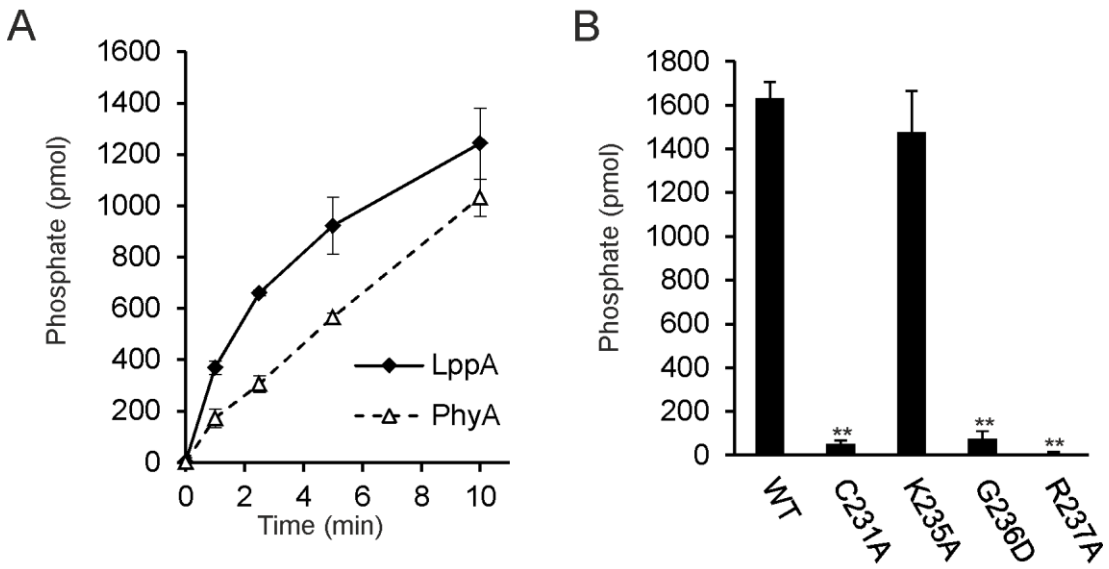

Figure 3.24 LppA is a cysteine phytase *in vitro*. (*A*) Hydrolysis of phytate by GST-LppA$_{\Delta 1\text{-}16}$ and GST-PhyA. (B) Activity of GST-LppA$_{\Delta 1\text{-}16}$ point mutations of putative catalytically essential residues. For all reactions (A and B), enzyme activity was measured by phosphate release as a malachite green vanadate dye complex. Reactions proceeded at 25°C with 2 nmol phytate and 0.5 µg protein for up to (A) 10 min or (B) 15 min. Absorbance at 620 nm was measured 20 min after termination of each reaction. Data shown are means and standard deviation (SD) of triplicates and are representative of three independent experiments (** $P < 0.005$).

3.7 Identification of Phytate as Growth Inhibitory to *L. pneumophila*

3.7.1 Phytate is a Bacteriostatic Agent

In a preliminary screening, *D. discoideum* was infected with wild-type *L. pneumophila* under conditions of 10 mM phytate, 10 mM inositol, or no treatment. Compared to the untreated group of cells, phytate treatment tended to slow bacterial replication, while its precursor inositol appeared to enhance it (**Figure 3.25A**). This result provided the first insights into phytate as a potential agent of intracellular bacterial growth inhibition.

To investigate the effect of phytate on the growth of *L. pneumophila* in AYE broth, the compound was added to a bacterial culture in early exponential growth phase (**Figure 3.25B**). Under these conditions, 10 mM phytate caused growth stasis of *L. pneumophila*. After 6 h, the bacteria were pelleted, resuspended in fresh AYE medium and let grow again. After removal of phytate, *L. pneumophila* resumed growth at the initial rate. Therefore, phytate is not toxic to *L. pneumophila*, but reversibly inhibits growth in what is a bacteriostatic rather than a bactericidal effect.

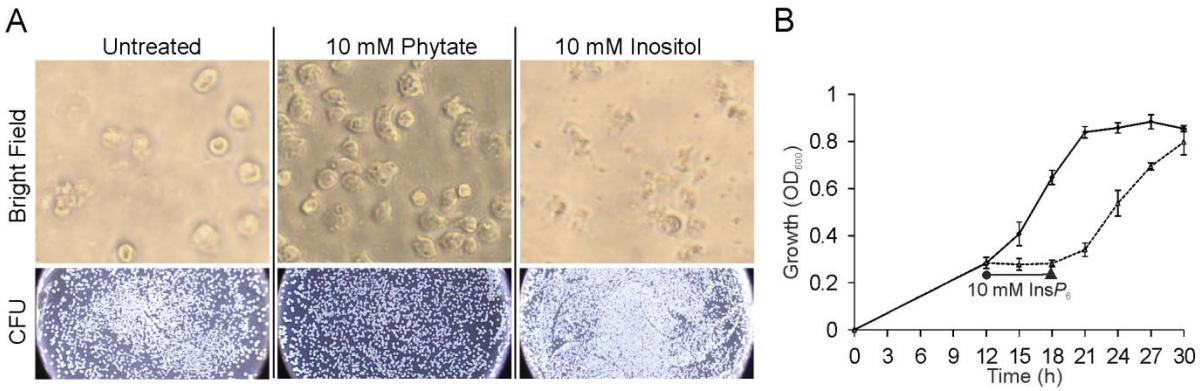

Figure 3.25 Phytate treatment protects *D. discoideum* from *L. pneumophila* infection and reversibly inhibits bacterial growth in broth. (A) *D. discoideum* in MB medium was treated with 10 mM phytate or its precursor inositol 1 h prior to infection (MOI 2) with wild-type *L. pneumophila*. Cells were imaged 24 h after infection, and samples of each were plated on CYE agar to compare relative colony forming units (CFU). (B) Phytate is bacteriostatic for *L. pneumophila*. Wild-type *L. pneumophila* was inoculated at an OD_{600} of 0.1 in AYE medium, and growth was measured by OD_{600} every 3 h from 12-30 h. At 12 h, 10 mM phytate (InsP_6) was added for 6h (dashed line), the bacteria were pelleted, resuspended in fresh AYE medium and allowed to grow again. The control without phytate was treated the same way.

3.7.2 LppA Overexpression and Micro-nutrient Substitution Revert the Effect of Phytate

Following the determination of phytate as a growth-inhibitory agent, it was assessed if LppA produced by *L. pneumophila* could provide relief from the compound. To this end, *L. pneumophila* wild-type, Δ*lppA*, or wild-type overproducing LppA were grown in AYE supplemented with 0-5 mM phytate (**Figure 3.26A**). Growth was monitored by measuring the optical density of the culture. In absence of phytate, the *L. pneumophila* strains grew comparably. The addition of phytate inhibited bacterial growth in a dose-dependent manner, and 5 mM of the compound completely abolished bacterial replication. Whereas *L. pneumophila* lacking *lppA* was only slightly more susceptible towards phytate, the wild-type strain overproducing LppA grew significantly better at phytate concentrations ranging from 1-4 mM. There appears to be a threshold concentration of phytate that does not adversely affect growth. Generally, a 2 to 3 mM concentration of phytate is tolerated, probably owing to the availability of nutrients in the complex AYE medium. LppA overexpression does under these conditions confer a distinct growth advantage.

In order to demonstrate that the bacteriostatic effect of phytate on *L. pneumophila* was attributable to metal ion micro-nutrient complexation, iron, zinc, magnesium, or calcium were added in equimolar concentrations to phytate in bacterial AYE cultures and growth was assessed. Where 10 mM phytate (or EDTA) completely blocked the growth of *L. pneumophila*, the concomitant addition of 10 mM of a given micro-nutrient reverted the inhibition (**Figure 3.26B**). It could thereby be shown that phytate was causing growth stasis through micro-nutrient deprivation.

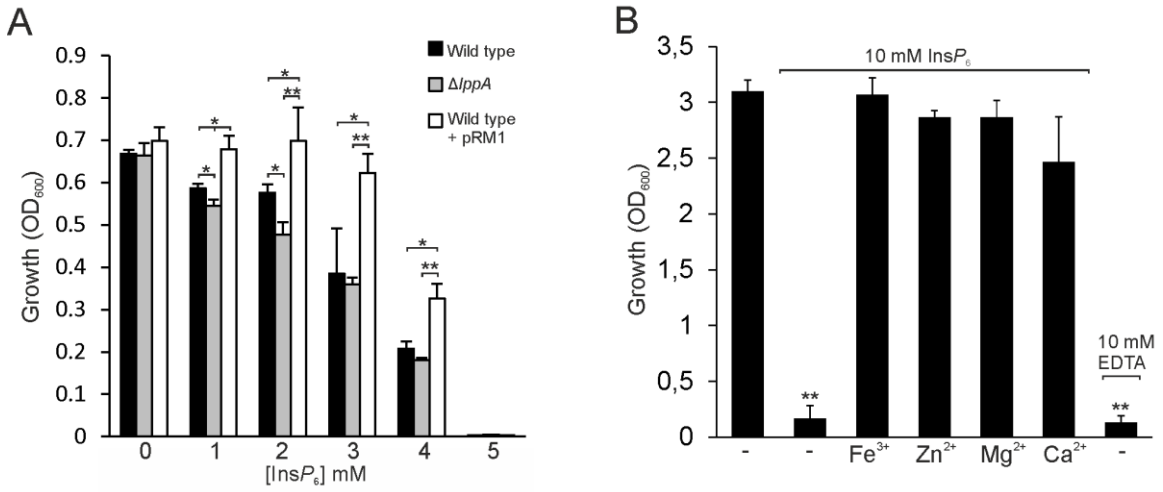

Figure 3.26 Growth inhibition of *L. pneumophila* is counteracted by LppA or micro-nutrient supplementation. (A) *L. pneumophila* wild-type or Δ*lppA* harboring pCR33 (vector), or wild-type harboring pRM1 (LppA overexpression) were grown in AYE supplemented with 0-5 mM InsP_6 for 5 d at 24°C. (B) *L. pneumophila* wild-type was grown for 21 h in AYE containing 10 mM InsP_6 or 10 mM of the indicated micro-nutrients (iron, zinc, magnesium, or calcium). 10 mM EDTA alone was used as a control for chelation. Data (A and B) represent means ± SD of triplicates (*P < 0.05, **P < 0.005).

3.8 LppA Does Not Affect Intracellular Replication in Untreated Phagocytes

The progression to the extracellular growth assays (**section 3.7**) was to test if LppA had a significant role in intracellular replication in untreated amoebae. In absence of phytate, intracellular replication for wild-type, Δ*lppA* or complemented Δ*lppA* strains was not significantly different (**Figure 3.27A,B**). Wild-type and the Δ*lppA* mutant were also evenly matched in competitive growth over 18 d (**Figure 3.27C**). LppA therefore does not play a major role in pathogenesis under the tested conditions.

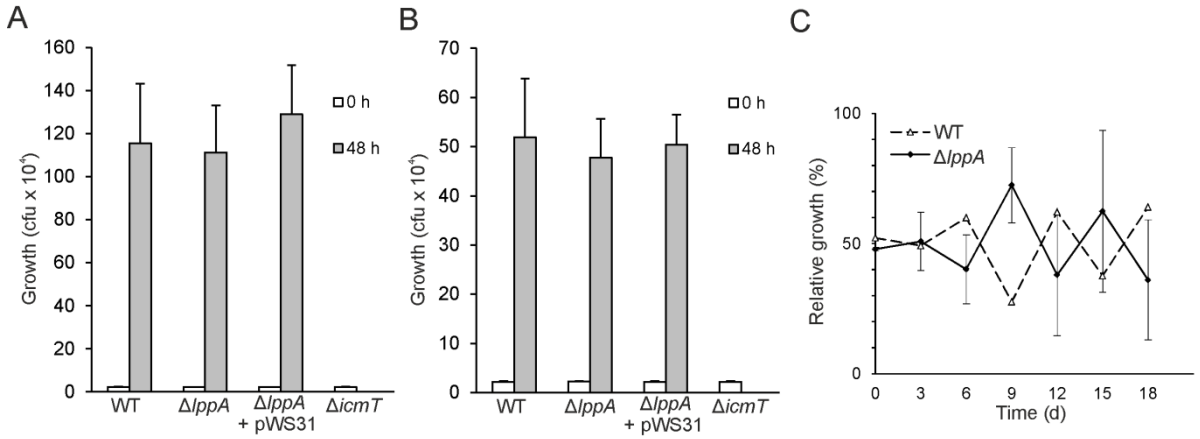

Figure 3.27 Intracellular growth and competition of *L. pneumophila* in amoebae. (A) *A. castellanii* cultured in absence of phytate were infected (MOI 1, 37°C) with *L. pneumophila* wild-type, Δ*lppA* or Δ*icmT* harboring pNT28 (GFP), or Δ*lppA* harboring pWS31 (GFP, LppA), and intracellular growth was determined by CFU at 0 (input) and 48 h post infection. (B) Infections of *D. discoideum* carried out as in (A) with an incubation temperature of 23°C. (C) *A. castellanii* was co-infected (1:1 ratio, MOI 0.01) in 96-well plates with *L. pneumophila* wild-type and Δ*lppA* mutant bacteria, and grown at 37°C for 18 d. Every third day, supernatant and lysed amoebae were diluted 1:1000, fresh amoebae were infected (50 µl homogenate per 200 µl culture), and aliquots were plated on CYE agar plates (plain or kanamycin) to determine CFU. Data represent means ± SD of triplicates and are representative of three independent experiments.

3.9 LppA Promotes Intracellular Replication Under Phytate Load

In previous sections, phytate was identified as a reversible bacteriostatic agent (section **3.7**) and LppA was not necessary for *L. pneumophila* replication in amoebae under standard laboratory conditions (section **3.8**). To determine whether LppA might play a role in intracellular replication under phytate conditions, *L. pneumophila*, *A. castellanii* or *D. discoideum* were pre-loaded with the compound. To this end, the amoebae were initially treated with 2.5 mM phytate, and the concentration was increased every two days up to 10 mM for *A. castellanii* or 5 mM for *D. discoideum*. Shortly before an experiment, the amoebae were washed and suspended in LoFlo medium. The phytate-loaded amoebae were then infected with GFP-producing *L. pneumophila* wild-type, Δ*icmT*, Δ*lppA* or complemented Δ*lppA* strains. Bright field and GFP-fluorescence microscopy images were taken for infected *A. castellanii*. Images immediately following infection show an even distribution of amoebae and *L. pneumophila* (**Figure 3.28A**). After 48 h, amoebae infected with wild-type *L. pneumophila* or the complemented Δ*lppA* mutant strain had predominantly rounded up, characteristic to advanced *L. pneumophila* infection. The bright field channel shows that the majority of the cells are filled with bacteria, many of which are producing GFP. Note that the GFP-production was not under antibiotic selection at this point, and therefore, was notably low and heterogeneous for the complementation strain producing a short-lived GFP. In contrast, amoebae infected with *L. pneumophila* lacking *lppA* remained largely attached, the morphology of most amoebae was similar to cells infected with Δ*icmT*, and only a few amoebae were observably filled with bacteria. By 72 h post infection, *A. castellanii* infected with wild-type *L. pneumophila* were full of actively moving bacteria ready for exit (video observation), and most amoebae infected with the complemented Δ*lppA* mutant strain had burst, releasing many bacteria. Replication of the Δ*lppA* mutant strain increased over the 48 h time point, but was still considerably lower than replication of wild-type or complementation strains, and many cells resembled the Δ*icmT*-infected amoebae.

Intracellular growth of the *L. pneumophila* strains in phytate-loaded *A. castellanii* or *D. discoideum* was also quantified by determining colony forming units (CFU) (**Figure 3.28B,C**). Colony counts at the onset of infection were even across all strains, and Δ*icmT* mutant bacteria used as a negative control disappeared over time. Using CFU as readout for intracellular replication, significantly fewer bacteria lacking *lppA* were counted after 48 or 72 h infection, and the growth defect was fully complemented by providing the gene on a plasmid. Thus, the *L. pneumophila* translocated phytase LppA provides an intracellular growth advantage in phytate-loaded *A. castellanii* or *D. discoideum* amoebae.

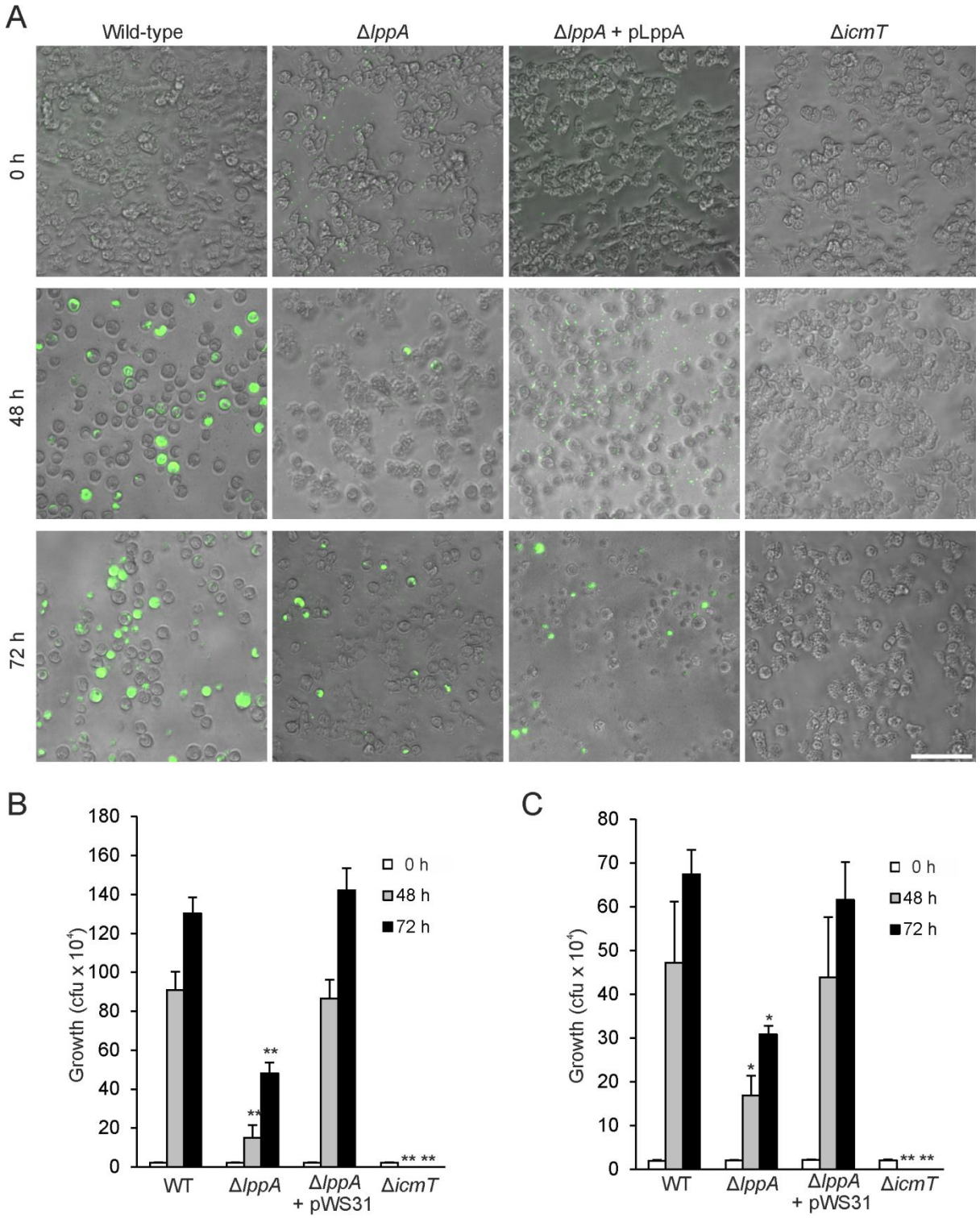

Figure 3.28 LppA promotes intracellular replication of *L. pneumophila* under phytate load. (A) *A. castellanii* amoebae cultured in presence of 10 mM phytate were infected (MOI 1, 37°C) with *L. pneumophila* wild-type, Δ*lppA* or Δ*icmT* harboring pNT28 (GFP), or Δ*lppA* harboring pWS31 (GFP, LppA). Bright field and GFP-fluorescence images for infected *A. castellanii* were taken at 0, 48 or 72 h post infection. Scale bar, 50 µm. (B) CFU counts for intracellular replication of *L. pneumophila* strains corresponding to images in (A). (C) CFU counts for intracellular replication of above-listed *L. pneumophila* strains at 23°C in *D. discoideum* pre-loaded with 5 mM phytate. Data show means ± SD of triplicates and are representative of three independent experiments (*$p < 0.05$, ** $p < 0.005$).

4 Discussion

Phosphoinositides play a central role in the assembly of the LCV and coordination of bacterial effectors. In spite of the importance of these lipids, a characterization of the PI lipid pattern of the LCV was all but nonexistent. Nonetheless, conceptual models were generated based on assumptions and speculations about the LCV PI pattern. This thesis presents a thorough spatiotemporal characterization of the very dynamic LCV PI pattern, thereby providing a global frame of reference and context for the interaction of specific *L. pneumophila* effectors with a given PI lipid in time. As such, the comprehensive PI pattern established in this work is used to re-evaluate existing schemes. The use of live cell imaging with tandem probes for observing interacting processes also provided a new way to consider the interaction of the LCV with the ER, and revealed new insights into how the pathogen avoids degradation.

In the course of the LCV PI lipid characterization, *L. pneumophila* PI phosphatases were sought which could potentially modulate these lipids. LppA satisfied all conditions of a PI phosphatase *in vitro* but had no influence on the LCV PI pattern. The primary structure of LppA was however even more closely related to that of cysteine-phytases. Biochemistry experiments revealed LppA as an efficient phytase. Subsequent cellular experiments showed that LppA was indeed a novel Icm/Dot secreted phytase. The abundant environmental compound phytate was, in the process, identified as a bacteriostatic agent through its ability to chelate metal ion micro-nutrients. LppA in turn could assist the bacteria during intracellular replication under phytate load.

4.1 Solving the LCV Phosphoinositide Pattern

A comprehensive spatiotemporal LCV PI pattern was established during the course of this thesis. Prior to this characterization, it was only known that PtdIns(4)*P* accumulated on the LCV dependent on the Icm/Dot T4SS (Weber *et al.*, 2006), but the timeline and extent of accumulation remained to be resolved. PtdIns(3)*P* was even less well characterized but circumstantially proposed to be a component of the LCV, in spite of its identity as a marker of the endocytic pathway (Weber *et al.*, 2009; Harding *et al.*, 2013; Finsel *et al.*, 2013). The lipids PtdIns(5)*P* and PtdIns(3,5)P_2 were not expected to interact with the LCV, given their localization to the nuclear membrane and late endosomes, respectively. The newly characterized LCV PI pattern for *L. pneumophila* infection is presented in section **4.1.5** (**Figure 4.1**).

4.1.1 Uptake of *L. pneumophila* Requires PtdIns(3,4,5)P_3 and PtdIns(3,4)P_2

The discrepancy in uptake efficiency ranging from 3 to 10-fold between wild-type and Icm/Dot mutants prompted speculation about the uptake mechanism employed by *L. pneumophila* (Hilbi *et al.*, 2001). Efforts were made to understand the origin of the difference, with emphasis on the T4SS. Resulting studies presented arguments for or against the requirement of PI3Ks for efficient uptake of *L. pneumophila* (Peracino *et al.*, 2010; Weber *et al.*, 2006). Although there is an obvious difference in the efficiency with which wild-type and Δ*icmT* mutants enter a cell, this difference reflects a population statistic. Live cell imaging enabled a high magnification examination of *L. pneumophila* uptake on a single cell level. This time-resolved experimentation showed that all *L. pneumophila* were taken up exclusively in PtdIns(3,4,5)P_3-rich macropinosomes and that the lipid persisted to the same extent regardless of whether the macropinosome contained wild-type, Icm/Dot mutants, or no *L. pneumophila* at all. In all cases, a PtdIns(3,4,5)P_3-rich cup was formed, followed by a fusion of the projected lamellipodia to form a PtdIns(3,4,5)P_3-rich macropinosome. From fusion of the membranes, the PH_{CRAC}-GFP label persisted for an average of 42 s. Re-evaluation of the original wortmannin treatment of 0.1 mM (Weber *et al.*, 2006) revealed that the concentration was not sufficient to inhibit the propagation of PtdIns(3,4,5)P_3 waves. Concentrations of wortmannin upwards of 40-fold higher were necessary to abolish the PI3K activity in *D. discoideum*. A functional cytoskeleton also proved necessary for *L. pneumophila* uptake. When the actin polymerization was paralyzed by latrunculin B, the bacteria were no longer internalized, in spite of the cell's continued ability to generate polarized PtdIns(3,4,5)P_3 waves. It could therefore be concluded that wild-type *L. pneumophila* and Icm/Dot deficient mutants are taken up by *D. discoideum* in the same way that the host cell internalizes macropinosomes. Thus, although there may be a tendency for promotion of bacterial uptake by the T4SS, it is not a prerequisite and the uptake mechanism itself is dependent on the host cell machinery.

The probe PH_{CRAC}-GFP labels both PtdIns(3,4,5)P_3 and PtdIns(3,4)P_2. Since a difference in the combined clearance times of these lipids from macropinosomes was not observed between strains, it was not likely that the presence of the individual species differed between strains. In previous studies using probes that discriminate between PtdIns(3,4,5)P_3 and PtdIns(3,4)P_2, it was observed that PtdIns(3,4,5)P_3 was present until macropinosome closure, while PtdIns(3,4)P_2 accounted for the larger fraction of the signal persistence otherwise observed with PH_{CRAC}-GFP (Dormann *et al.*, 2004). This step represents a direct conversion of PtdIns(3,4,5)P_3 to PtdIns(3,4)P_2 by SHIP (Cox *et al.*, 2001).

4.1.2 Participation of the Plasma Membrane Lipid PtdIns(4,5)P_2

The PM localized lipid PtdIns(4,5)P_2, accounting for the largest PI fraction in the cell, is a bystander in the development of the LCV. The internalization of *L. pneumophila* by macropinocytosis relies on the formation of PtdIns(3,4,5)P_3 at the entry site. PtdIns(4,5)P_2 on the PM is converted to PtdIns(3,4,5)P_3, which directs assembly of actin into dendritic structures (Gerisch *et al.*, 2009; Gerisch, 2010). Uptake of *L. pneumophila* by *D. discoideum* required formation of a macropinocytic cup and could not be discriminated from macropinosome formation (section **4.1.1**). Dynamic sections of PM forming such a cup were rich in PtdIns(3,4,5)P_3, but excluded PtdIns(4,5)P_2. After internalization of a newly formed macropinosome, the PtdIns(4,5)P_2 was regenerated at the PM site of uptake. In essence, PM PtdIns(4,5)P_2 does not make contact with the macropinosome, nor does it detectably occur on the LCV throughout infection. In keeping with the mechanism of macropinocytic uptake, *L. pneumophila* does not act on PM PtdIns(4,5)P_2 like the pathogens *S. enterica* and *S. flexneri* which infect non-phagocytic cells and require their own PI phosphatases to metabolize PtdIns(4,5)P_2 to PtdIns(5)*P*. This conversion destabilizes the plasma membrane to permit entry of the bacteria (Niebuhr *et al.*, 2002; Terebiznik *et al.*, 2002).

4.1.3 Acquisition and Clearance of PtdIns(3)*P*

The presence or occurrence of PtdIns(3)*P* on the LCV remained to be characterized. As *L. pneumophila* escapes the endocytic pathway, it was hypothesized that PtdIns(3)*P* either did not accumulate on the LCV or was rapidly cleared (Peracino *et al.*, 2010; Toulabi *et al.*, 2013). The proposed absence of PtdIns(3)*P* from the LCV, however, conflicted with reports of secreted effectors (e.g. LtpD, RidL) that specifically bound that lipid and could be detected in immonufluorescence beyond the first hour of infection (Harding *et al.*, 2013; Finsel *et al.*, 2013). Using *D. discoideum* expressing 2xFYVE-GFP, the dynamics of PtdIns(3)*P* were thoroughly characterized on the internalized macropinosome and followed from the seconds preceding uptake to several hours after infection.

The initial appearance of PtdIns(3)*P* on the internalized macropinosome was evident approximately 50 s after uptake. At that point PtdIns(3)*P* rapidly coated the macropinosome in a sharp transition. The appearance of PtdIns(3)*P* on the macropinosome directly followed clearance of PtdIns(3,4,5)P_3/PtdIns(3,4)P_2 (42 s). Statistically, the clearance/appearance times were not significantly different, but the PtdIns(3)*P* was most likely synthesized from PtdIns by the class III PI3K (Vieira *et al.*, 2001). Contrary to pre-conceived notions of PtdIns(3)*P* (Toulabi *et al.*, 2013), wild-type *L. pneumophila* macropinosomes did not avoid acquisition of the classical endocytic marker PtdIns(3)*P*, but acquired the lipid along the same time course and to the same extent as internalized

pathogen vacuoles containing Icm/Dot-deficient bacteria. The acquisition of PtdIns(3)*P* on the internalized macropinosome was therefore not avoided by Icm/Dot effectors. This PtdIns(3)*P* acquisition means that the host remains in control of the PI pattern for at least the first minute of infection.

Further challenging the notion that wild-type *L. pneumophila* avoids accumulating endocytic PtdIns(3)*P*, the lipid was not directly cleared from the LCV by the pathogen after its acquisition. Instead, virtually all LCVs remained PtdIns(3)*P*-positive 30 min after infection. At this point, the wild-type PtdIns(3)*P* pattern still could not be discriminated from that of a Icm/Dot mutant. However Between 30 and 60 min p.i., PtdIns(3)*P* was shed, leaving only about 35% of vacuoles PtdIns(3)*P*-positive. The remaining PtdIns(3)*P* was gradually lost down to a measured 20% of vacuoles by 120 min. All wild-type LCVs eventually completely lost PtdIns(3)*P*, in that no LCV with replicating bacteria was observed to be PtdIns(3)*P*-positive. In contrast, PtdIns(3)*P* persisted on vacuoles harboring Icm/Dot-deficient bacteria to a level that did not significantly decrease between 30 and 120 min after infection. The tendency however pointed to a reduction in this lipid in time. After several hours, but still before degradation of the bacteria by the host endocytic machinery, these vacuoles generally lost PtdIns(3)*P*. The lipid was most likely converted to PtdIns(3,5)P_2 by a type III PI 5-kinase, in keeping with the fate PtdIns(3)*P* on late endosomes (Nicot and Laporte, 2008).

L. pneumophila has evolved a strategy to exploit even the defining PI lipid of the host's endocytic pathway, meanwhile avoiding acidification. One can propose that the multiple effector proteins which anchor to PtdIns(3)*P* on the LCV exert their function effectively within the first 60 min of infection, as the lipid undergoes gradual clearance during 30 and 60 min. After 60 min, the LCV is well established and already rich in PtdIns(4)*P* (see **4.1.4**), representing a replication-permissive compartment. The loss of PtdIns(3)*P* very likely correlates to the task completion by PtdIns(3)*P*-binding effectors, which work to lay the foundation for successful LCV establishment. The loss of PtdIns(3)*P* in itself is an intriguing process in which the entire cellular PtdIns(3)*P* pool undergoes changes. It is not clear whether PtdIns(3)*P* on the LCV is metabolized or repositioned in the cell. PtdIns(3)*P*-rich endocytic membranes were notably condensed and compacted, with near total loss of vesicle structure. Interestingly, this architectural rearrangement represented a complete separation of the endocytic compartment from the replication-permissive compartment. As such, *L. pneumophila* appears to further avoid acidification and assure security of its environment by disabling the host cell's digestive machinery.

4.1.4 Bi-phasic Acquisition of PtdIns(4)*P*

PtdIns(4)*P* was to this point the best characterized PI lipid in the *L. pneumophila* infection. There are diverse pools of PtdIns(4)*P* in the cell, most associated with the Golgi or PM (De Matteis *et al.*, 2005; Balla *et al.*, 2005). The probe GFP-P4C$_{SidC}$ has the unique feature that it primarily labels the PM, with less intense cytoplasmic vesicle labeling (Ragaz *et al.*, 2008). This feature was used to follow PtdIns(4)*P* on the PM during the uptake of *L. pneumophila*. As with PtdIns(3,4,5)P_3 (**4.1.1**), PtdIns(4)*P* was a component of the macropinocytic cup and internalized macropinosome. The notable difference however was that the intensity of PtdIns(4)*P* was unchanged (within limits of resolution) between resting and active membrane. Observation of uninfected *D. discoideum* revealed that PtdIns(4)*P* was an intrinsic component of the macropinosome derived from the PM, but was lost within minutes of vacuole endocytosis, and therefore only transiently present. This scheme was true for macropinosomes of both wild-type and Icm/Dot-deficient *L. pneumophila*, both of which acquired PtdIns(4)*P* upon uptake, and promptly lost the lipid. Therefore, the initial PtdIns(4)*P* was not part of the PtdIns(4)*P* fraction which later accumulated on the wild-type LCV.

Live cell imaging of *L. pneumophila* infection revealed both the kinetics and the extent of PtdIns(4)*P* accumulation on the LCV. After the initial transient appearance of PtdIns(4)*P*, it did not reappear on vacuoles harbouring Icm/Dot-deficient bacteria, but steadily accumulated and intensified on the wild-type LCV. First signs of accumulation generally appeared around 30 min p.i., at which point 40% of LCVs had a detectable level of PtdIns(4)*P*, as observed with the sensitive probe. A novel aspect is the degree of accumulation observed. By 2 h p.i., the PtdIns(4)*P* labeling on the LCV was so intense that it drowned out all other PtdIns(4)*P* labeling in the cell. At that time, LCVs appeared perfectly spherical, about 4 µm in diameter. From this point, the signal intensity did not appear to intensify further, but the morphology of the LCV underwent changes in the following hours.

PtdIns(4)*P* was the only PI lipid found to persist on the LCV during infection. It also discretely labelled the immediate LCV membrane throughout the infection. It is not surprising that a multitude of *L. pneumophila* effectors exploit this lipid to anchor to the LCV. The defining role of PtdIns(4)*P* in the LCV interaction with the ER is discussed in section **4.2**, while the potential sources of PtdIns(4)*P* accumulation are discussed in section **4.3.3**.

4.1.5 Integrated Model of the Dynamic LCV PI Pattern during *L. pneumophila* Infection

The integrated LCV PI model compiled from all PI observation data is presented in **Figure 4.1**. The model presents the critical events in the PI pattern from the seconds preceding uptake of *L. pneumophila* by the host cell up to 2 h of infection. The early events are mediated by the host cell, following which the Icm/Dot T4SS takes over the PI modulation to establish the replicative niche.

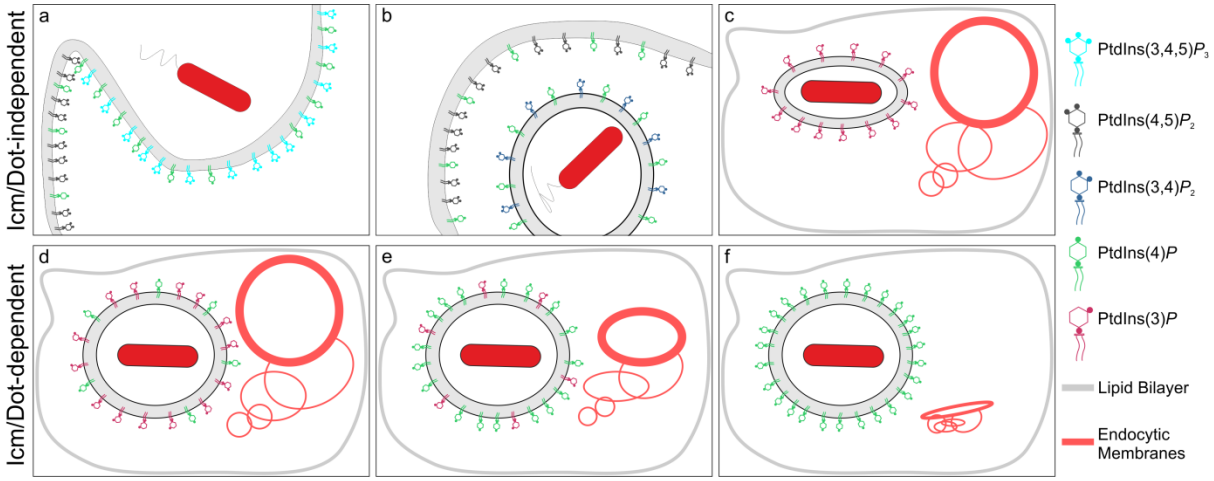

Figure 4.1 Integrated model of the dynamic LCV phosphoinositide pattern during *L. pneumophila* infection. (a) A macropinocytic cup forms rich in PtdIns(3,4,5)P_3 from phosphorylation of plasma membrane (PM) PtdIns(4,5)P_2 by class I PI3K. PtdIns(4)*P* continues to line the cup at the same detectable extent as on the surrounding PM. PtdIns(4,5)P_2 is confined to the PM external to the cup. *L. pneumophila* navigates into the cup. (b) The lamellipodia forming the cup fuse to form an internalized macropinosome. At this point, the PtdIns(3,4,5)P_3 is metabolized to PtdIns(3,4)P_2, likely by SHIP. Both PI(3,4)P_2 and PtdIns(4)*P* persist on the newly formed macropinosome for under a minute. PM PtdIns(4,5)P_2 is regenerated at the entry site immediately after uptake of the macropinosome. (c) Both PtdIns(3,4)P_2 and PtdIns(4)*P* are lost from the LCV and PtdIns(3)*P* rapidly appears immediately after, on average 50 s after uptake, likely through the action of class III PI3K. The PtdIns(3)*P*-rich macropinosome is in close proximity to a network of PtdIns(3)*P*-labeled endocytic vesicles. (d) Approximately 30 min post infection, the first signs of PtdIns(4)*P* appear on the LCV. PtdIns(3)*P* remains the dominating LCV PI lipid, unchanged over the first 30 min. (e) 60 min post infection, PtdIns(4)*P* dominates the LCV PI-lipid identity. PtdIns(3)*P* has undergone significant loss, now present on only 35% of LCVs. Remodelling of cellular endocytic membranes becomes evident. (f) By 120 min of infection and beyond, PtdIns(4)*P* accumulates to a high degree and remains the only detectable PI lipid on the LCV. Significant changes have occurred to the total cellular PtdIns(3)*P*. Endocytic vesicles have been condensed and compacted, segregated from the replication-permissive LCV. Steps (a) – (c) are common to both wild-type and Δ*icmT L. pneumophila*. Steps (d) – (f) are mediated by the Icm/Dot T4SS.

4.2 LCV Architecture and Interaction with the Endoplasmic Reticulum

Since the discovery that the ER interacts with the LCV (Swanson and Isberg, 2005; Kagan and Roy, 2002), this process has been a major centre of focus in the research on LCV development. The standard model for ER acquisition by the LCV was outlined in **Figure 1.1**. The results presented in section **3.4** shed new light on the importance of PtdIns(4)*P* for rough ER recruitment and present a conceptual advance in that the ER does not fuse with the LCV for a prolonged time.

SidC has long been regarded as a tethering protein in which the C-terminal section contains the PtdIns(4)*P*-binding $P4C_{SidC}$ domain and the N-terminal mediates ER vesicle interaction (Ragaz *et al.*, 2008). A recent N-terminal crystal structure indicated that SidC was consistent with dimensions observed for host cell tethers, but that was the extent of the structural similarity (Horenkamp *et al.*, 2014; Gazdag *et al.*, 2014). These studies proposed the SidC N-terminal structure as novel claim to support the tether hypothesis. However, a subsequent structural and biochemical exploration of an independently crystallized structure reclassified SidC as a ubiquitin ligase (Hsu *et al.*, 2014).

The importance of the ER to the infection has been under debate, since the absence of the effector SidC was reported to delay or abolish ER recruitment to the LCV without showing an intracellular replication phenotype (Ragaz *et al.*, 2008). In addition to this report, live cell imaging revealed that the ER does associate with the Δ*sidC-sdcA* mutant LCV in time, and eventually resembles wild-type association (**Figure 3.16**). This figure shows that ER was not detectable on the PtdIns(4)*P*-rich Δ*sidC-sdcA* mutant LCV 1 h after infection, and that loose and incomplete ER contacts are made in the ensuing hour. By 8 h p.i., both wild-type and Δ*sidC-sdcA* mutant strains display a similar degree of LCV ER association. The classical consideration of SidC as a tethering protein created a roadblock in a model trying to explain why firm ER-LCV contacts could be established in time. Since the role of SidC was re-classified to facilitating ER protein recruitment to the LCV, one could propose that when the LCV eventually does associate with the ER, it may have the intact tethering mechanism to make the normal association.

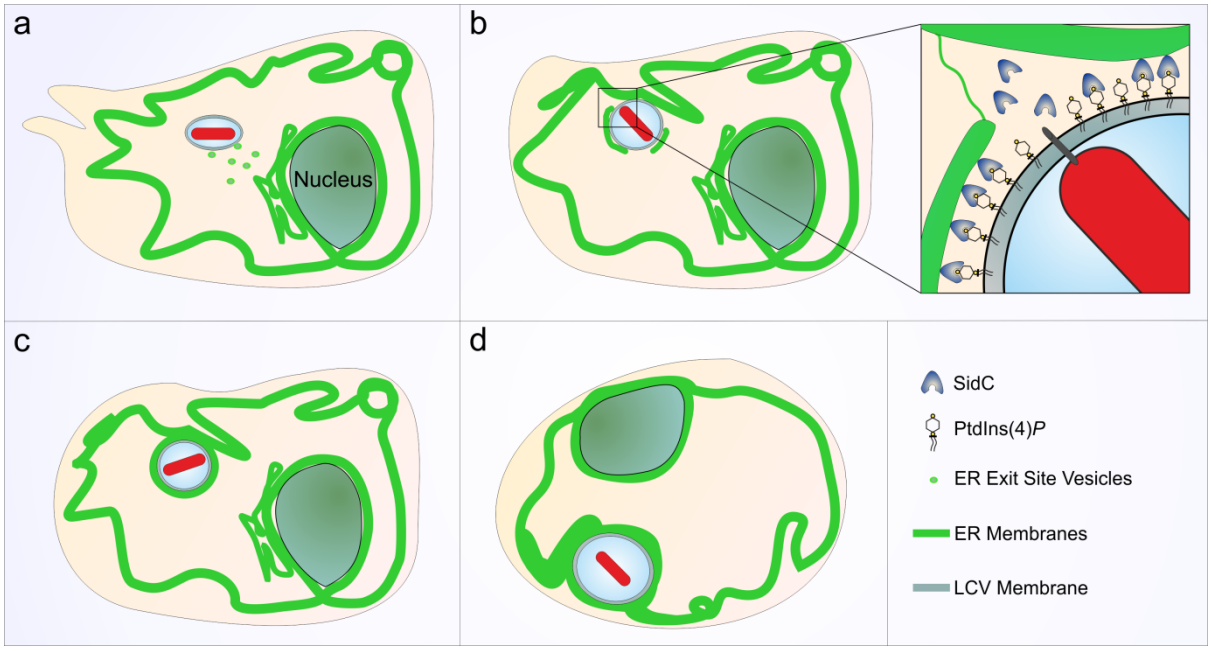

Figure 4.2 Revised model for endoplasmic reticulum association with the LCV. (a) 15 – 30 min post uptake, the *L. pneumophila* vacuole associates with vesicles derived from the ER exit sites. The vesicles serve as a source of membrane and PtdIns. The developing LCV begins to transition from tight to spacious as it acquires membrane. (b) Beyond 30 min, the LCV starts to associate with the physical organelle of the rough ER. The inset shows that PtdIns(4)*P* is formed on the LCV prior to ER deposition around the LCV. SidC, which is necessary for efficient ER recruitment, binds to the PtdIns(4)*P* where it facilitates LCV-ER interaction. This period represents partial and incomplete attachment of the LCV to the ER. (c) By 60 min of infection, the ER completely surrounds the LCV. (d) By 120 min post infection, the LCV lumen has increased and ER association around the LCV has thickened, but the LCV membrane is still discernible from the ER.

LCVs containing a Δ*sidC-sdcA* mutant do not suffer in size. LCVs containing a Δ*sidJ-sdjA* mutant were significantly smaller and less viable compared to the normal state (Liu and Luo, 2007). Interestingly, SidC localizes to the LCV, whereas SidJ does not, while both of these effectors were

shown to facilitate ER recruitment to the LCV. Although SidC is generally considered to recruit ER vesicles to the LCV, this work provides clear evidence that SidC promotes association of the physical ER organelle with the LCV. The different function of SidJ might be that it initially recruits ER exit site vesicles to supply membrane and PtdIns to the LCV, allowing it to transition from a tight to a spacious vacuole. Based on these reflections, a new generic model for ER interaction with the LCV is proposed in **Figure 4.2**.

4.3 Phosphoinositide Phosphatases in the *L. pneumophila* Infection

LppA provided a candidate for a secreted PI phosphatase in *L. pneumophila*. The *in vitro* biochemistry of LppA pointed to a PI phosphatase readily metabolizing poly-phosphorylated PIs to yield PtdIns(4)*P*. However, any experiments designed to observe a PI-phosphatase function of LppA in the cell right up to sophisticated real-time imaging with PI-specific probes yielded no PI-related differences attributable to the *lppA* gene (**4.3.1**). The newly characterized LCV PI pattern (**4.1.5**) provided much needed context for the consideration of potential pathogen-secreted PI phosphatases (**4.3.2**). While the source(s) of PtdIns(4)*P* accumulation on the LCV remain(s) elusive, possible roles of pathogen-secreted PI phosphatases and host cell components are discussed (**4.3.3**).

4.3.1 Uptake and Replication were not Affected by an *lppA* Deletion.

Invasive pathogens possess a series of strategies to enter a host cell. An entrance strategy employed by *S. enterica* and *S. flexneri* is to disrupt PM PI lipid homeostasis with a secreted PI phosphatase (Niebuhr *et al.*, 2002; Terebiznik *et al.*, 2002). Accordingly, based on *in vitro* biochemistry (**3.5.1**), LppA was initially theorized to contribute to the clearance of poly-phosphorylated PIs to encourage faster sealing of the macropinosome. In addition to the fact that *lppA* did not influence the uptake efficiency of *L. pneumophila* into the host cell, the PI lipids at play were later found to be modulated independently of the Icm/Dot T4SS. Under normal conditions, *lppA*-deficient mutants followed the same LCV PI progression as wild-type *L. pneumophila* and showed normal intracellular replication. A disturbance in growth was first observed for the mutant strain in the presence of phytate (see **4.4**).

4.3.2 Secreted PI Phosphatases in the *L. pneumophila* Infection

The *L. pneumophila* effector SidF was presented as a unique PI phosphatase responsible for LCV PtdIns(4)*P* production. *In vitro*, it metabolized PtdIns(3,4,5)P_3 to PtdIns(4,5)P_2 and PtdIns(3,4)P_2 to PtdIns(4)*P*. Based on these findings, combined with the information that SidF localized to the LCV 2 h p.i. (Banga *et al.*, 2007; Hsu *et al.*, 2012), it was proposed that SidF could be responsible for PtdIns(4)*P* production on the LCV. SidP followed as the second PI phosphatase to be published for *L. pneumophila*. In contrast to SidF, SidP metabolized PtdIns(3,5)P_2 to PtdIns(3)*P* and PtdIns(3)*P* to PtdIns *in vitro* (Toulabi *et al.*, 2013). Based on the biochemistry, SidP was hypothesized to metabolize PtdIns(3)*P* on the early phagosome, preventing accumulation and helping the pathogen evade the endocytic pathway. The proposed mechanism of action for each is summarized in **Figure 4.3**.

Though plausible, the proposed mechanisms of SidF and SidP appear to be flawed due to the absence of starting substrates and/or incomplete understanding in the lipid composition of the LCV, which is newly presented in **Figure 4.1**. The first problem with the SidF model is that PtdIns(3,4,5)P_3 and PtdIns(3,4)P_2 are only briefly present on the newly internalized macropinosome (< 60 s) and are cleared independently of the Icm/Dot T4SS. The subsequent and intrinsically related issue is that PtdIns(4)*P* accumulation only begins over 20 min after PtdIns(3,4,5)P_3 and PtdIns(3,4)P_2 are cleared. Nonetheless, a *sidF* deletion mutant was reported to show a reduced amount of PtdIns(4)*P* on the LCV, as determined by reduced detection of SidC (Hsu *et al.*, 2012). The quality of the immunofluorescence images provided in the aforementioned study could be improved, but nonetheless present a further conflict. SidC binds PtdIns(4)*P* specifically and recruits elements of the ER to the LCV. As such, ER recruitment to the LCV is absent or delayed in a *sidC-sdcA* deletion mutant (Ragaz *et al.*, 2008). Yet, the same group reported that *sidF* deletion did not affect ER protein recruitment (i.e. calnexin) to the LCV (Banga *et al.*, 2007) while simultaneously reporting that SidC was significantly reduced on the LCV (Hsu *et al.*, 2012). SidF was originally characterized as an anti-apoptotic protein. The connection between an anti-apoptotic function and LCV PtdIns(4)*P* accumulation function for a single effector is not intuitive and would benefit from further study.

SidF makes its case as a PI phosphatase based on its *in vitro* biochemistry and models of other intracellular pathogens that employ PI phosphatases as virulence factors. Experiments only examined SidF localization to the LCV 2 h after infection (Banga *et al.*, 2007). It has therefore not been demonstrated that SidF localizes to the LCV in the first minute of infection when the proposed substrates, PtdIns(3,4,5)P_3 and PtdIns(3,4)P_2, are present on the internalized macropinosome. One could alternatively propose, based on SidF's subcellular localization to the ER network through its N-terminal sequence (Hsu *et al.*, 2012), that its localization to the LCV occurs as a passenger via the ER recruitment to the LCV and is therefore mediated by SidC.

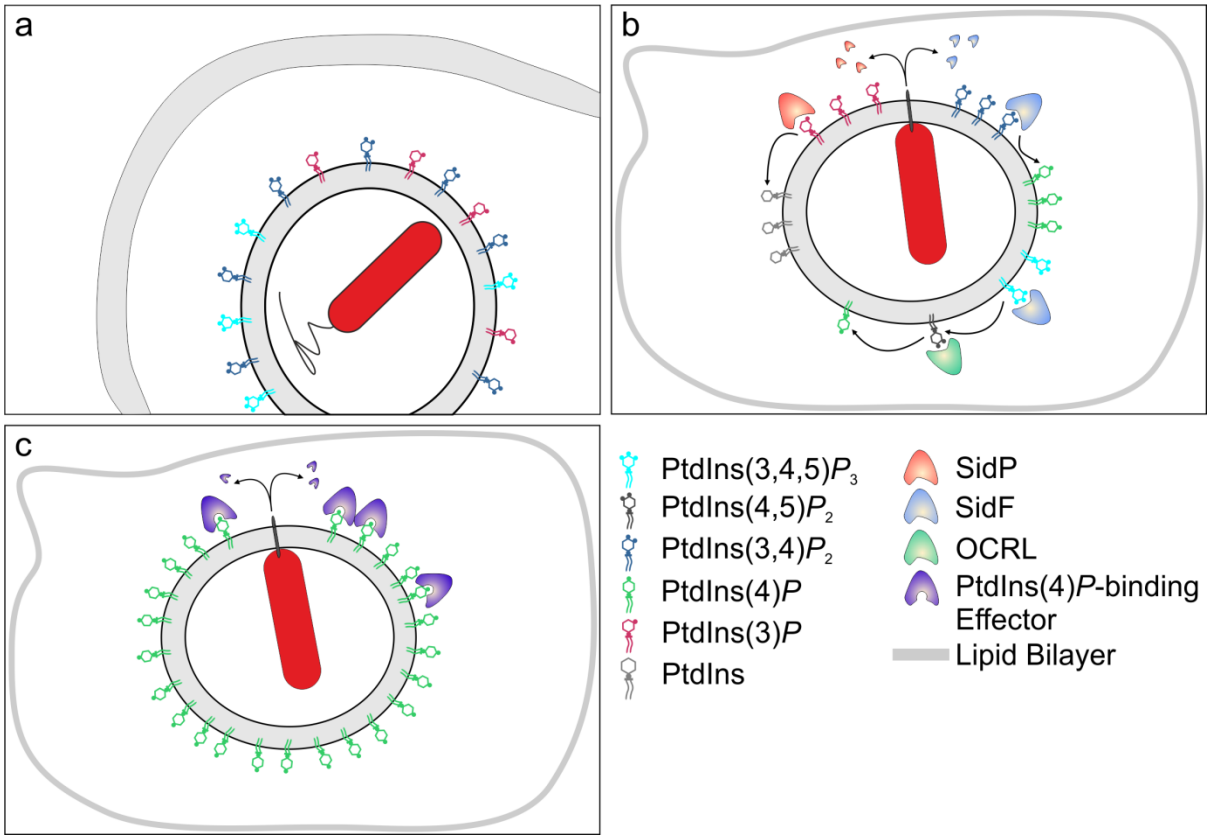

Figure 4.3 Literature model for the mechanism of action of proposed *L. pneumophila* PI phosphatases SidF and SidP. (a) *L. pneumophila* is internalized in a vacuole with PI lipid species PtdIns(3,4,5)P_3, PtdIns(3,4)P_2, and PtdIns(3)*P*. (b) SidP clears PtdIns(3)*P* to PtdIns, allowing the LCV to escape the endocytic pathway. SidF clears PtdIns(3,4)P_2 to PtdIns(4)*P*, both contributing to PtdIns(4)*P* accumulation on the LCV and preventing PI 4-phosphatases from making PtdIns(3)*P*. SidF also converts PtdIns(3,4,5)P_3 to PtdIns(4,5)P_2, which is further metabolized to PtdIns(4)*P* by 5-phosphatases like OCRL. (c) PtdIns(4)*P*-binding effectors anchor to the LCV. The timeline of events (a) – (c) is not specified.

SidP on the other hand was shown to ectopically complement a yeast phosphatase deletion *in vitro* without evidence of an intracellular growth or PI phenotype in *L. pneumophila*-infected cells (Toulabi *et al.*, 2013). The authors build on the assumption that PtdIns(3)*P* is rapidly removed from the wild-type phagosome and moreover, prevented from accumulating. The combined action of SidF and SidP was also the subject of speculation, emphasizing that the presence of two pathogen-secreted PI 3-phosphatases likely means that PtdIns(3)*P* removal from the phagosome is critical for bacterial survival (Toulabi *et al.*, 2013). Although the wild-type LCV incontestably escapes the endocytic pathway and subsequent degradation, the flaw in the hypothesized SidP mode of action is that PtdIns(3)*P* accumulates on both wild-type and Icm/Dot deficient *L. pneumophila* macropinosomes within 60 s of uptake and persists to the same extent for at least 30 min after infection. It cannot as of yet be ruled out that SidP might contribute to the gradual removal of PtdIns(3)*P* from the wild-type LCV beyond the first 30 min of infection, but it most probably does not enable early removal of this lipid or prevent it from accumulating. The notion of rapid PtdIns(3)*P* elimination does not account for the presence of *L. pneumophila* effectors (e.g. LtpD, SetA and RidL) which were reported on the LCV 1 h after infection. The intracellular function relating to the *in vitro* PI metabolism of SidF and SidP

therefore remains to be shown. The comprehensive dynamic PI pattern characterized and presented in **Figure 4.1** re-enforces the importance of the frame of reference to hypothesis generation about PI-interacting effectors.

4.3.3 PtdIns(4)*P* Accumulation and Pathogen-Secreted PI Phosphatases

LppA was discovered as a putative PI phosphatase. It was characterized with broad PI substrate range, producing PtdIns(4)*P* as its unique product *in vitro*, indicating that *L. pneumophila* might employ a PI phosphatase, prior to the publication of SidF and SidP. The logical progression was to investigate its role in PtdIns(4)*P* production on the LCV. A diverse array of assays, the most sensitive of which examined real-time accumulation of PtdIns(4)*P* on the LCV, did not reveal a PI-related phenotype of the *lppA*-deletion strain. These findings demonstrated that the *in vitro* biochemistry was not intrinsically related to the intracellular function of the protein. LppA was subsequently attributed to phytate metabolism and to providing relief for the pathogen under phytate stress (see **4.4**).

The idea that *L. pneumophila* would require a PI phosphatase to gain entry into a host cell (**4.3.1**) or to shape the LCV PI pattern (**4.3.2**) stems from other intracellular pathogens which employ these very strategies. There are two fundamental strategic differences between *L. pneumophila* and, for example *S. enterica* or *M. tuberculosis*. *L. pneumophila* is an environmental bacterium with an amoeboid species as natural host, but it can infect multiple unrelated hosts and has a large repertoire of over 300 effector proteins. Other pathogens have evolved to infect one specific cell type and have refined their effector repertoire accordingly. *S. enterica* and *M. tuberculosis* secrete about 30 and 50 effectors respectively, including an indispensable PI phosphatase. In absence of *Salmonella* SopB, the SCV does not form and infection cannot proceed. If *Mycobacterium* is missing MptpB, PtdIns(3)*P* accumulates on the MCV and leads to acidification of the vacuole. As such, it would seem an evolutionary lapse for *L. pneumophila* to rely on a single PI phosphatase to carry out critical functions like PtdIns(4)*P* generation on the LCV. This grab-bag effector strategy for multiple host colonization casts further doubt on the individual contribution of SidF to the LCV PI pattern. A second strategic difference concerns the uptake of the pathogen into the host cell. *L. pneumophila*, like *M. tuberculosis*, infects professional phagocytes and does not need to force its entry. In contrast, *S. enterica* and *S. flexneri* infect non-phagocytic cells and require a PI phosphatase to disrupt the host cell plasma membrane, enabling entry.

Another aspect to consider is the robustness and importance of PtdIns(4)*P* accumulation on the LCV. From real-time observation of PI dynamics with PI-specific fluorescent probes, PtdIns(4)*P* was the only PI lipid whose accumulation was subject to a functional Icm/Dot T4SS, and was

therefore the defining PI lipid of the LCV. It persisted for the entire duration of infection, as far as could be observed. To appreciate the robustness of PtdIns(4)*P* accumulation on the LCV, one must consider the available sources of PtdIns(4)*P* in the host cell. The Golgi is a PtdIns(4)*P*-rich organelle to which the small GTPase Arf1 localizes (De Matteis *et al.*, 2005). Arf1 itself recruits the class IIIβ PI4K to promote traffic along the secretory pathway (Godi *et al.*, 1999). The secreted effector RalF recruits Arf1 to the LCV, but does not affect intracellular replication of *L. pneumophila* nor does it impair acquisition of SidC by the LCV (Urwyler *et al.*, 2009b). Although Arf1 localizes to the LCV, the PI4K IIIβ was never observed to make the same association, thereby likely explaining why a Δ*ralF* mutant shows no PtdIns(4)*P* defect (Urwyler *et al.*, 2009b). It was therefore proposed that direct fusion of PtdIns(4)*P*-rich vesicles with the LCV was a more likely source.

Such a mechanism of PtdIns(4)*P*-labeled vesicle fusion with the LCV seems rather plausible. Following uptake of *L. pneumophila* in a macropinosome, the vacuole remains void of PtdIns(4)*P* for the ensuing 20 to 25 min (**3.2.2**). During this time, the LCV intercepts vesicles from ER exit sites (Kagan and Roy, 2002). PtdIns(4)*P* is formed at ER exit sites where it mediates exit of secretory vesicles (Blumental-Perry *et al.*, 2006). The LCV in turn intercepts these secretory vesicles. Phosphorylation of PtdIns in the ER is kept in check through a high presence of the PI-monophosphatase Sac1, but vesicles can be released with a PtdIns(4)*P* identity (Hughes *et al.*, 2000; Balla, 2013). One could propose that the early interception of the these exit site vesicles, possibly mediated by SidJ, contributes to the gradual increase in LCV volume and PtdIns(4)*P* intensification over the first 30 – 40 min of infection. In the presence of sufficient PtdIns(4)*P*, SidC could bind and mediate the ensuing physical interaction of the LCV with the ER structure.

Another potential source of PtdIns(4)*P*, the PI 5-phosphatase Dd5P4, has already been implicated in modulating LCV PtdIns(4)*P* levels (Weber *et al.*, 2009). Dd5P4 (homologue to OCRL1) is recruited to the LCV by LpnE, which itself binds to PtdIns(3)*P*. Paradoxically, the absence of Dd5P4 promotes more rapid interaction of the ER with the LCV despite reduced binding of SidC, and impairs the transition of the LCV from tight to spacious vacuole. In this case, intracellular replication of *L. pneumophila* was unexpectedly enhanced.

With over 400 proteins in the *L. pneumophila* genome containing the Cx_5R signature deemed necessary for PI phosphatase activity (Hsu *et al.*, 2012), it is quite possible that other examples of *in vitro* PI phosphatases exist beyond LppA, SidF, and SidP and that PtdIns(4)*P* accumulation is a multifaceted process involving multiple sources.

4.4 Implications of LppA and Phytate for Metabolism and Virulence

Phytate is among the most abundant phosphate compounds in nature and a potent metal ion chelator owing to its high negative charge. In this report, the chelating properties of phytate were identified as contributing to extracellular and intracellular bacteriostasis. *L. pneumophila* has an elevated requirement for iron (Reeves *et al.*, 1981), and the standard growth medium AYE accordingly contains an approximate 30-fold excess of 0.6 mM iron. This iron dependency provides a rationale for the susceptibility of *L. pneumophila* towards phytate, but traces of calcium, magnesium, zinc, manganese and molybdenum also stipulate the minimum requirement for growth (Reeves *et al.*, 1981). As such, the bacteria possess a number of iron uptake systems which include the siderophore legiobactin and the ferrous iron transmembrane transporter FeoB (Cianciotto, 2007). Siderophore-like activity in *L. pneumophila* has been reported for conditions of iron starvation with similar bacteriostatic chelators (Goldoni *et al.*, 1991). The sensitivity of *L. pneumophila* to phytate suggests that under the conditions tested, the bacteria do not prioritize phytate as a source of phosphorus or as a siderophore for iron, in contrast to the described role of phytate for *X. oryzae* (Chatterjee *et al.*, 2003) and *P. aeruginosa* (Smith *et al.*, 1994; Hirst *et al.*, 1999), respectively.

Amoebae, namely the social soil amoeba *D. discoideum*, produce phytate in the millimolar range (Martin *et al.*, 1987; Stephens and Irvine, 1990). Under the laboratory conditions tested, the homeostatic concentration of phytate was not sufficient to impair growth of an *lppA*-deficient *L. pneumophila* strain. However, *D. discoideum* and *A. castellanii* proved to have a higher capacity for phytate tolerance and storage. The amoebae pre-loaded with phytate restricted intracellular growth of *L. pneumophila* in an *lppA*-dependent manner. The physiological concentration of phytate in free-living amoebae cannot be ascertained, nor can it be said how sensitive wild *L. pneumophila* strains are to micro-nutrient concentration differences when more factors are at play in the environment. As proof of principle, *L. pneumophila* strains lacking *lppA* were significantly more susceptible to phytate in amoebae in which the phytate concentration was artificially enhanced.

LppA presents the first instance of a type IV-secreted phytase. Furthermore, the obligate intra-amoebal bacterium *Candidatus Protochlamydia amoebophila* produces a putative cysteine phytase with 32% identity to LppA (Lim *et al.*, 2007). This finding suggests that the phytate-containing compartment communicates with the bacterial symbiont and that degradation of intracellular phytate might also be beneficial for survival and replication of this bacterium. Protozoa take up solutes and small particles via macropinocytosis. These macropinosomes likely also communicate with LCVs. The results presented in this report emphasize the critical role of micro-nutrients for intracellular pathogens. Environmentally acquired or host-synthesized phytate might function together with transporters that remove metal ions from the pathogen vacuole forming an anti-bacterial strategy against vacuolar pathogens through micro-nutrient depletion. Accordingly, the

transmembrane proteins Nramp-1 and Nramp-2 were shown to pump iron from vacuoles (LCV) into the cytoplasm of *D. discoideum* (Bozzaro *et al.*, 2013; Peracino *et al.*, 2013). While the eukaryotic cell limits the availability of micro-nutrients through ion efflux and chelation, the intracellular pathogen *L. pneumophila* has developed countermeasures to the bacteriostatic strategy (**Figure 4.4**).

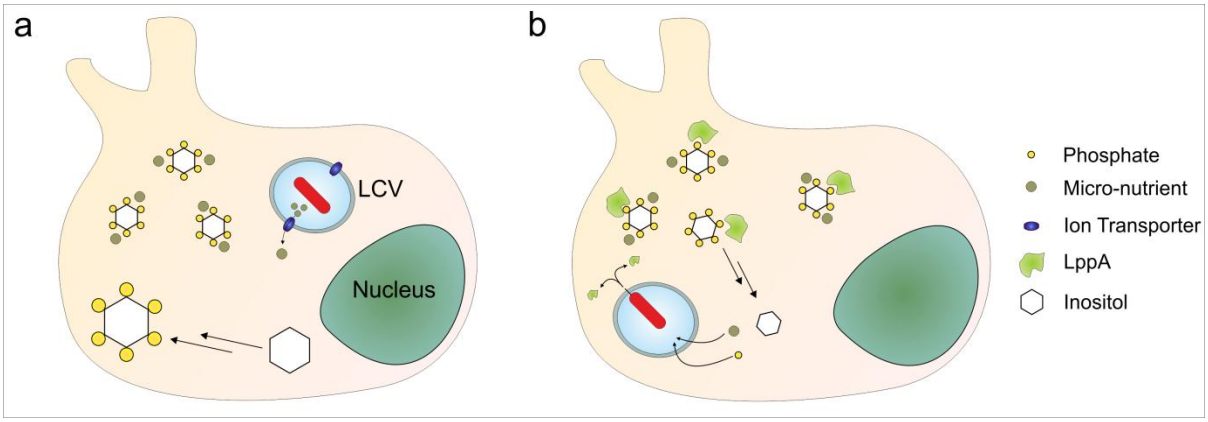

Figure 4.4 LppA assists in micro-nutrient acquisition in amoebae. (a) Phytate (InsP_6) is synthesized to millimolar quantities in amoebae. Phytate is a potent chelator and complexes metal ion micro-nutrients. The amoeba also produces metal ion transporters which cause efflux of micro-nutrients from the LCV. (b) *L. pneumophila* translocates LppA into the host cell cytoplasm. LppA metabolizes phytate, increasing bioavailability of phosphate, inositol, and micro-nutrients, which can then be transported into the LCV by their respective transport routes.

Although LppA also hydrolyzes poly-phosphorylated PI lipids *in vitro*, only the phytase activity appeared to be relevant in infected cells. Cysteine phytases are characterized by the catalytic motif HCX_2GX_2R, of which the Cys and Arg residues are catalytically essential and His and Gly are important for P-loop conformation (Chu *et al.*, 2004). While the catalytic motif of LppA (HCRGGKGRT) is 66% identical to PhyA (HCEAGVGRT), it is more closely related to the mammalian PI 3-phosphatase PTEN (HCR/KAGKGRT) with 89% identity. Since both PTEN and LppA effectively metabolize PtdIns(3,4,5)P_3 and the main PI product of LppA *in vitro* is PtdIns(4)*P*, it was initially hypothesized that LppA could function as a PI phosphatase in infected cells. Such a function could not be validated in *L. pneumophila*-infected cells. Other *L. pneumophila* Icm/Dot substrates SidF and SidP are reported *in vitro* PI phosphatases. As was the case with LppA, the function of these enzymes may not directly relate to the bench-top biochemistry (see **4.3**).

4.5 Live Cell Imaging for Observation of *L. pneumophila* Infection

The use of live cell imaging for time lapse observation has clear advantages compared to fixed preparations: it is the best way to view intact membrane and vesicle structure, meanwhile allowing the operator to follow the same group of cells through time (**Figure 4.5**). Although the use of antibody staining is generally not possible with live cells (save for the use of microinjection), labeling of organelle structures or cell compartments can be accomplished in addition to PI labeling by cells expressing multiple fluorescent fusion constructs.

A short-term observation protocol was developed to follow rapid and immediate changes in the LCV PI pattern on a single cell level. This method allowed capture of events that proceed too rapidly to be captured in fixed sections. It also provided a wealth of sequential information that would otherwise be missed between time points. This protocol was ideal for observing PI changes upon bacterial uptake and the ensuing minutes. Another protocol was developed for time lapse observation on the basis of capturing hundreds of cells at a given time to yield a large statistical sample. The quality of the statistics was dependent on the uniform distribution of infecting *L. pneumophila* and a simultaneous infection of the cells. This protocol is suited for observing slower processes of PI accumulation or loss and changes in cellular architecture, which may occur over a timespan of hours.

During the first experiments after the transition from fixed samples to live imaging, it was observed that cells infected with *L. pneumophila* rounded and detached from the substratum. A closer look at this phenomenon revealed that this rounding followed a very reliable timeline, usually starting around 45 min post infection when the LCV had formed contacts to the ER, and completing detachment about 15 min later. The onset of rounding could be slightly accelerated or delayed with respective increase or decrease in the infectious load. This Icm/Dot-dependent cell detachment not surprisingly represents a technical problem for washing and fixation, and thus a major loss of experimental information. The most heavily infected cells were more likely to be lost during slide preparation, as they underwent the most advanced rounding. This loss of cells with more advanced infection has the potential to confound statistics which evaluate the presence of an element on the LCV over time. The implication is that the quantification would shift to favour a larger proportion of cells with less advanced infection, and therefore underestimate a count. Live cell imaging has no cell loss from the imaging dishes. What used to be a technical problem in slide preparation proved to be an asset in live imaging. Detached cells drifted to the center of the observation dish where they conveniently aligned edge to edge to allowing the operator to capture significantly more events per image. This feature was especially helpful for quantifications which allowed only a narrow window to capture images for a given time point.

Perhaps the biggest asset of live imaging is that it enables observation of the same group of cells from start to finish in an experiment. This continuity provides an advantage over static microscopy which requires that a given test group be sacrificed for imaging, meaning that imaging of subsequent time points is always of different samples. Through the time resolution of seconds in real time imaging, uptake of *L. pneumophila* into a host cell could be characterized, settling incongruities surrounding involvement of PtdIns(3,4,5)P_2 and PI3K (**3.1.1**), while capturing a yet unknown event in which PtdIns(4)*P* transiently occurs on the macropinosome (**3.1.3**).

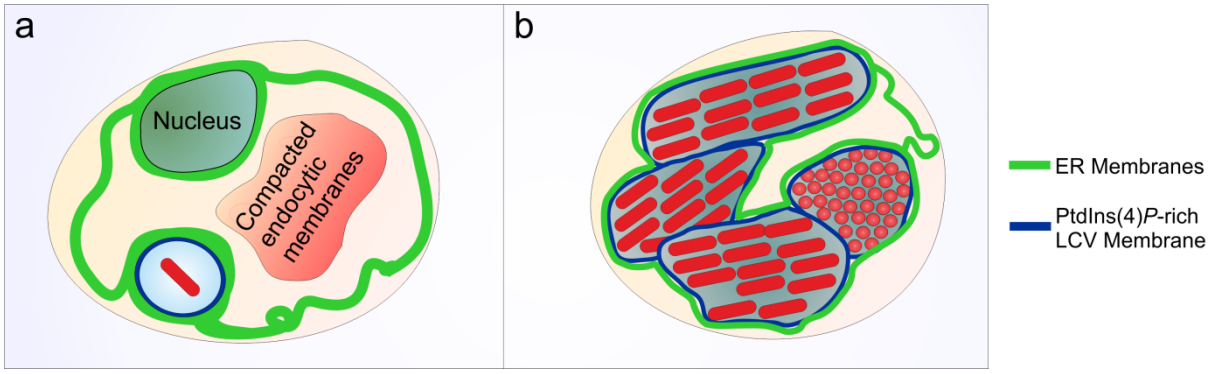

Figure 4.5 Live cell imaging preserves fine membrane structure. (a) Tandem probe analysis in live imaging allowed continuous observation of the change in PtdIns(3)*P* vesicle structure without disturbing the system. The compacting or destruction of endocytic vesicles and membranes could not be attributed to fixation artefact. (b) Intact ER and LCV membranes were observed in immediate proximity of each other without indication of fusion.

Depending on the application, fixation of cells may be necessary. Following live cell imaging, cells can be fixed directly in the observation dishes, antibody stained, and mounted *in situ* in a viscous mounting medium. Fixation has the obvious benefit that the sample being observed is almost entirely still, allowing for prolonged captures without blurring. The drawback is that fixation causes physical changes to membrane structures, including shrinking and collapsing. Live cell imaging leaves fine structures intact, but at the cost of effective capture time. One solution is to optimize imaging techniques suited to balance exposure time, resolution, and signal to noise ratio. Such was accomplished to make the discovery that PtdIns(4)*P* was acquired by the LCV prior to and independently of the ER and remained a separate entity for at least the first 8 h of infection (**3.4**). This finding was also made possible by the ectopic expression of two different fluorophore-labeled probes in the host cell, allowing visualization of parallel processes.

4.6 Concluding Remarks

This thesis established an LCV PI pattern as a frame of reference and demonstrated its importance to effector binding and interaction with the LCV. Knowing which steps of the LCV PI pattern development are Icm/Dot-dependent and which lipids are present at which time will guide future studies interested in these lipids. The PI reference should also guide hypotheses which intrinsically rely on the presence of specific on the LCV at a given time. Microscopic techniques were developed for imaging the *L. pneumophila* infection in order to solve the dynamic LCV PI pattern. In the process, it was discovered that PtdIns(4)*P*, rather than the long regarded ER membrane, forms the defining feature of the replication-permissive LCV. PtdIns(4)*P* accumulation on the LCV was shown to precede and occur independently of physical interaction with the ER network. Further challenging the standard model of ER fusion with the LCV, it was demonstrated that the PtdIns(4)*P*-rich LCV membrane remains a distinct compartment, discernible from the ER for at least the observed 8 h. Future studies can explore the type of connection and communication the two compartments form, and types of inter-communication between LCVs and the ER network. One can additionally investigate how PtdIns(4)*P* is generated on the LCV, how PtdIns(3)*P* is removed, and how the general changes occur to disable the host cell's endocytic machinery. The importance and robustness of PtdIns(4)*P* accumulation on the LCV may indeed mean that *L. pneumophila* does not rely on a pathogen-secreted PI phosphatase to generate the lipid, but rather a collection of omnipresent host phosphatases. The effector LppA which like others satisfied the *in vitro* conditions for a PI phosphatase, proved instead to be a phytase assisting the pathogen with nutrient acquisition. As such, it was proposed that micro-nutrient deprivation by the host cell is an effective anti-microbial strategy, and that bacterial phytases represent a virulence factor against starvation.

5 References

Agranoff, B. W., Bradley, R. M., and Brady, R. O. (1958) The enzymatic synthesis of inositol phosphatide. *Journal of Biological Chemistry* **233**, 1077-1083

Altman, E., and Segal, G. (2008) The response regulator CpxR directly regulates expression of several *Legionella pneumophila icm/dot* components as well as new translocated substrates. *Journal of bacteriology* **190**, 1985-1996

Andrews, H. L., Vogel, J. P., and Isberg, R. R. (1998) Identification of linked *Legionella pneumophila* genes essential for intracellular growth and evasion of the endocytic pathway. *Infection and immunity* **66**, 950-958

Arasaki, K., and Roy, C. R. (2010) *Legionella pneumophila* promotes functional interactions between plasma membrane syntaxins and Sec22b. *Traffic* **11**, 587-600

Attree, O., Olivos, I. M., Okabe, I., Bailey, L. C., Nelson, D. L., Lewis, R. A., Mclnnes, R. R., and Nussbaum, R. L. (1992) The Lowe's oculocerebrorenal syndrome gene encodes a protein highly homologous to inositol polyphosphate-5-phosphatase.

Bakowski, M. A., Braun, V., Lam, G. Y., Yeung, T., Do Heo, W., Meyer, T., Finlay, B. B., Grinstein, S., and Brumell, J. H. (2010) The phosphoinositide phosphatase SopB manipulates membrane surface charge and trafficking of the *Salmonella*-containing vacuole. *Cell host & microbe* **7**, 453-462

Balla, A., Tuymetova, G., Tsiomenko, A., Várnai, P., and Balla, T. (2005) A plasma membrane pool of phosphatidylinositol 4-phosphate is generated by phosphatidylinositol 4-kinase type-III alpha: studies with the PH domains of the oxysterol binding protein and FAPP1. *Molecular biology of the cell* **16**, 1282-1295

Balla, T. (2013) Phosphoinositides: tiny lipids with giant impact on cell regulation. *Physiological reviews* **93**, 1019-1137

Bandyopadhyay, P., Xiao, H., Coleman, H. A., Price-Whelan, A., and Steinman, H. M. (2004) Icm/dot-independent entry of *Legionella pneumophila* into amoeba and macrophage hosts. *Infection and immunity* **72**, 4541-4551

Banga, S., Gao, P., Shen, X., Fiscus, V., Zong, W.-X., Chen, L., and Luo, Z.-Q. (2007) *Legionella pneumophila* inhibits macrophage apoptosis by targeting pro-death members of the Bcl2 protein family. *Proceedings of the National Academy of Sciences* **104**, 5121-5126

Barnett, G. (1994) Manure P fractionation. *Bioresource technology* **49**, 149-155

Batty, I., Van der Kaay, J., Gray, A., Telfer, J., Dixon, M., and Downes, C. (2007) The control of phosphatidylinositol 3,4-bisphosphate concentrations by activation of the Src homology 2 domain containing inositol polyphosphate 5-phosphatase 2, SHIP2. *Biochem. J* **407**, 255-266

Behnia, R., and Munro, S. (2005) Organelle identity and the signposts for membrane traffic. *Nature* **438**, 597-604

Bennett, T. L., Kraft, S. M., Reaves, B. J., Mima, J., O'Brien, K. M., and Starai, V. J. (2013) LegC3, an effector protein from *Legionella pneumophila*, inhibits homotypic yeast vacuole fusion *in vivo* and *in vitro*. *PloS one* **8**, e56798

Benson, R. F., and Fields, B. S. (1998) Classification of the genus *Legionella*. in *Seminars in respiratory infections*

Beresford, N., Patel, S., Armstrong, J., Szoor, B., Fordham-Skelton, A., and Tabernero, L. (2007) MptpB, a virulence factor from *Mycobacterium tuberculosis*, exhibits triple-specificity phosphatase activity. *Biochem. J* **406**, 13-18

Berridge, M. J. (1984) Inositol trisphosphate and diacylglycerol as second messengers. *Biochemical Journal* **220**, 345

Berridge, M. J. (1993) Inositol trisphosphate and calcium signalling. *Nature* **361**, 315-325

Blumental-Perry, A., Haney, C. J., Weixel, K. M., Watkins, S. C., Weisz, O. A., and Aridor, M. (2006) Phosphatidylinositol 4-phosphate formation at ER exit sites regulates ER export. *Developmental cell* **11**, 671-682

Bollin, G., Plouffe, J., Para, M., and Hackman, B. (1985) Aerosols containing *Legionella pneumophila* generated by shower heads and hot-water faucets. *Applied and environmental microbiology* **50**, 1128-1131

Bominaar, A. A., Van Dijken, P., Draijer, R., and Van Haastert, P. J. (1991) Developmental regulation of the Inositol 1,4,5-trisphosphate phosphatases in *Dictyostelium discoideum*. *Differentiation* **46**, 1-5

Bozzaro, S., Buracco, S., and Peracino, B. (2013) Iron metabolism and resistance to infection by invasive bacteria in the social amoeba *Dictyostelium discoideum*. *Frontiers in cellular and infection microbiology* **3**

Brassinga, A. K. C., Hiltz, M. F., Sisson, G. R., Morash, M. G., Hill, N., Garduno, E., Edelstein, P. H., Garduno, R. A., and Hoffman, P. S. (2003) A 65-kilobase pathogenicity island is unique to Philadelphia-1 strains of *Legionella pneumophila*. *Journal of bacteriology* **185**, 4630-4637

Brenner, D. J., Steigerwalt, A. G., and McDade, J. E. (1979) Classification of the Legionnaires' disease bacterium: *Legionella pneumophila*, genus novum, species nova, of the family Legionellaceae, familia nova. *Annals of internal medicine* **90**, 656-658

Brombacher, E., Urwyler, S., Ragaz, C., Weber, S. S., Kami, K., Overduin, M., and Hilbi, H. (2009) Rab1 guanine nucleotide exchange factor SidM is a major phosphatidylinositol 4-phosphate-binding effector protein of *Legionella pneumophila*. *Journal of Biological Chemistry* **284**, 4846-4856

Brüggemann, H., Hagman, A., Jules, M., Sismeiro, O., Dillies, M. A., Gouyette, C., Kunst, F., Steinert, M., Heuner, K., Coppee, J. Y., and Buchrieser, C. (2006) Virulence strategies for infecting phagocytes deduced from the *in vivo* transcriptional program of *Legionella pneumophila*. *Cellular microbiology* **8**, 1228-1240

Burns, D. L. (2003) Type IV transporters of pathogenic bacteria. *Current opinion in microbiology* **6**, 29-34

Burstein, D., Zusman, T., Degtyar, E., Viner, R., Segal, G., and Pupko, T. (2009) Genome-scale identification of *Legionella pneumophila* effectors using a machine learning approach. *PLoS pathogens* **5**, e1000508

Cambronne, E. D., and Roy, C. R. (2007) The *Legionella pneumophila* IcmSW complex interacts with multiple Dot/Icm effectors to facilitate type IV translocation. *PLoS pathogens* **3**, e188

Cazalet, C., Rusniok, C., Brüggemann, H., Zidane, N., Magnier, A., Ma, L., Tichit, M., Jarraud, S., Bouchier, C., and Vandenesch, F. (2004) Evidence in the *Legionella pneumophila* genome for exploitation of host cell functions and high genome plasticity. *Nature genetics* **36**, 1165-1173

Chatterjee, S., Sankaranarayanan, R., and Sonti, R. V. (2003) PhyA, a secreted protein of *Xanthomonas oryzae pv. oryzae*, is required for optimum virulence and growth on phytic acid as a sole phosphate source. *Molecular plant-microbe interactions* **16**, 973-982

Chen, J., De Felipe, K. S., Clarke, M., Lu, H., Anderson, O. R., Segal, G., and Shuman, H. A. (2004) *Legionella* effectors that promote nonlytic release from protozoa. *Science* **303**, 1358-1361

Cho, W., and Stahelin, R. V. (2005) Membrane-protein interactions in cell signaling and membrane trafficking. *Annu. Rev. Biophys. Biomol. Struct.* **34**, 119-151

Choudhury, R., Diao, A., Zhang, F., Eisenberg, E., Saint-Pol, A., Williams, C., Konstantakopoulos, A., Lucocq, J., Johannes, L., and Rabouille, C. (2005) Lowe syndrome protein OCRL1 interacts with clathrin and regulates protein trafficking between endosomes and the trans-Golgi network. *Molecular biology of the cell* **16**, 3467-3479

Christie, P. J. (2001) Type IV secretion: intercellular transfer of macromolecules by systems ancestrally related to conjugation machines. *Molecular microbiology* **40**, 294-305

Christie, P. J., and Vogel, J. P. (2000) Bacterial type IV secretion: conjugation systems adapted to deliver effector molecules to host cells. *Trends in microbiology* **8**, 354-360

Chu, H. M., Guo, R. T., Lin, T. W., Chou, C. C., Shr, H. L., Lai, H. L., Tang, T. Y., Cheng, K. J., Selinger, B. L., and Wang, A. H. (2004) Structures of *Selenomonas ruminantium* phytase in complex with persulfated phytate: DSP phytase fold and mechanism for sequential substrate hydrolysis. *Structure* **12**, 2015-2024

Cianciotto, N. P. (2007) Iron acquisition by *Legionella pneumophila*. *Biometals* **20**, 323-331

Cirillo, J. D., Cirillo, S. L., Yan, L., Bermudez, L. E., Falkow, S., and Tompkins, L. S. (1999) Intracellular growth in *Acanthamoeba castellanii* affects monocyte entry mechanisms and enhances virulence of *Legionella pneumophila*. *Infection and immunity* **67**, 4427-4434

Clarke, M. (2010) Recent insights into host-pathogen interactions from *Dictyostelium*. *Cellular microbiology* **12**, 283-291

Clarke, M., Engel, U., Giorgione, J., Muller-Taubenberger, A., Prassler, J., Veltman, D., and Gerisch, G. (2010) Curvature recognition and force generation in phagocytosis. *BMC Biol* **8**, 154

Clarke, M., Köhler, J., Arana, Q., Liu, T., Heuser, J., and Gerisch, G. (2002) Dynamics of the vacuolar H^+-ATPase in the contractile vacuole complex and the endosomal pathway of *Dictyostelium* cells. *Journal of cell science* **115**, 2893-2905

Clemens, D. L., Lee, B.-Y., and Horwitz, M. A. (2000) Deviant Expression of Rab5 on Phagosomes Containing the Intracellular Pathogens *Mycobacterium tuberculosis* and *Legionella pneumophila* Is Associated with Altered Phagosomal Fate. *Infection and immunity* **68**, 2671-2684

Cockcroft, S., and Garner, K. (2011) Function of the phosphatidylinositol transfer protein gene family: is phosphatidylinositol transfer the mechanism of action? *Critical reviews in biochemistry and molecular biology* **46**, 89-117

Cornelis, G. R., and Van Gijsegem, F. (2000) Assembly and function of type III secretory systems. *Annual Reviews in Microbiology* **54**, 735-774

Cox, D., Dale, B. M., Kashiwada, M., Helgason, C. D., and Greenberg, S. (2001) A Regulatory Role for Src Homology 2 Domain–Containing Inositol 5′-Phosphatase (Ship) in Phagocytosis Mediated by Fcγ Receptors and Complement Receptor 3 (αMβ2; Cd11b/Cd18). *The Journal of experimental medicine* **193**, 61-72

De Felipe, K. S., Glover, R. T., Charpentier, X., Anderson, O. R., Reyes, M., Pericone, C. D., and Shuman, H. A. (2008) *Legionella* eukaryotic-like type IV substrates interfere with organelle trafficking. *PLoS pathogens* **4**, e1000117

De Felipe, K. S., Pampou, S., Jovanovic, O. S., Pericone, C. D., Senna, F. Y., Kalachikov, S., and Shuman, H. A. (2005) Evidence for acquisition of *Legionella* type IV secretion substrates via interdomain horizontal gene transfer. *Journal of bacteriology* **187**, 7716-7726

De Groot, C., and Golterman, H. (1993) On the presence of organic phosphate in some Camargue sediments: evidence for the importance of phytate. *Hydrobiologia* **252**, 117-126

De Matteis, M. A., and Godi, A. (2004) PI-loting membrane traffic. *Nature cell biology* **6**, 487-492

De Matteis, M., Di Campli, A., and Godi, A. (2005) The role of the phosphoinositides at the Golgi complex. *Biochimica et Biophysica Acta (BBA)-Molecular Cell Research* **1744**, 396-405

Declerck, P. (2010) Biofilms: the environmental playground of *Legionella pneumophila*. *Environmental microbiology* **12**, 557-566

Derré, I., and Isberg, R. R. (2004) *Legionella pneumophila* replication vacuole formation involves rapid recruitment of proteins of the early secretory system. *Infection and immunity* **72**, 3048-3053

Desjardins, M. (2003) ER-mediated phagocytosis: a new membrane for new functions. *Nature Reviews Immunology* **3**, 280-291

Di Paolo, G., and De Camilli, P. (2006) Phosphoinositides in cell regulation and membrane dynamics. *Nature* **443**, 651-657

Dondero Jr, T. J., Rendtorff, R. C., Mallison, G. F., Weeks, R. M., Levy, J. S., Wong, E. W., and Schaffner, W. (1980) An outbreak of Legionnaires' disease associated with a contaminated air-conditioning cooling tower. *New England Journal of Medicine* **302**, 365-370

Dormann, D., Weijer, G., Dowler, S., and Weijer, C. J. (2004) *In vivo* analysis of 3-phosphoinositide dynamics during *Dictyostelium* phagocytosis and chemotaxis. *Journal of cell science* **117**, 6497-6509

Dove, S. K., Cooke, F. T., Douglas, M. R., Sayers, L. G., Parker, P. J., and Michell, R. H. (1997) Osmotic stress activates phosphatidylinositol-3, 5-bisphosphate synthesis. *Nature* **390**, 187-192

Dove, S. K., McEwen, R. K., Mayes, A., Hughes, D. C., Beggs, J. D., and Michell, R. H. (2002) Vac14 Controls PtdIns(3,5)P_2 Synthesis and Fab1-Dependent Protein Trafficking to the Multivesicular Body. *Current biology* **12**, 885-893

Downes, C., Gray, A., Fairservice, A., Safrany, S., Batty, I., and Fleming, I. (2005) The regulation of membrane to cytosol partitioning of signalling proteins by phosphoinositides and their soluble headgroups. *Biochemical Society Transactions* **33**, 1303-1307

Drayer, A. L., Van der Kaay, J., Mayr, G. W., and Van Haastert, P. (1994) Role of phospholipase C in *Dictyostelium*: formation of inositol 1, 4, 5-trisphosphate and normal development in cells lacking phospholipase C activity. *The EMBO journal* **13**, 1601

Dressman, M. A., Olivos-Glander, I. M., Nussbaum, R. L., and Suchy, S. F. (2000) Ocrl1, a PtdIns(4,5)P_2 5-phosphatase, is localized to the trans-Golgi network of fibroblasts and epithelial cells. *Journal of Histochemistry & Cytochemistry* **48**, 179-189

Dreyfus, L. A. (1987) Virulence associated ingestion of *Legionella pneumophila* by HeLa cells. *Microbial pathogenesis* **3**, 45-52

Erdmann, K. S., Mao, Y., McCrea, H. J., Zoncu, R., Lee, S., Paradise, S., Modregger, J., Biemesderfer, D., Toomre, D., and De Camilli, P. (2007) A role of the Lowe syndrome protein OCRL in early steps of the endocytic pathway. *Developmental cell* **13**, 377-390

Faix, J., Gerisch, G., and Noegel, A. A. (1992) Overexpression of the csA cell adhesion molecule under its own cAMP-regulated promoter impairs morphogenesis in *Dictyostelium*. *Journal of Cell Science* **102**, 203-214

Fajardo, M., Schleicher, M., Noegel, A., Bozzaro, S., Killinger, S., Heuner, K., Hacker, J., and Steinert, M. (2004) Calnexin, calreticulin and cytoskeleton-associated proteins modulate uptake and growth of *Legionella pneumophila* in *Dictyostelium discoideum*. *Microbiology* **150**, 2825-2835

Feeley, J. C., Gibson, R. J., Gorman, G. W., Langford, N. C., Rasheed, J. K., Mackel, D. C., and Baine, W. B. (1979) Charcoal-yeast extract agar: primary isolation medium for *Legionella pneumophila*. *Journal of clinical microbiology* **10**, 437-441

Fernandez-Moreira, E., Helbig, J. H., and Swanson, M. S. (2006) Membrane vesicles shed by *Legionella pneumophila* inhibit fusion of phagosomes with lysosomes. *Infection and immunity* **74**, 3285-3295

Fields, B., Shotts, E., Feeley, J., Gorman, G., and Martin, W. (1984) Proliferation of *Legionella pneumophila* as an intracellular parasite of the ciliated protozoan *Tetrahymena pyriformis*. *Applied and environmental microbiology* **47**, 467-471

Fields, B. S. (1996) The molecular ecology of legionellae. *Trends in microbiology* **4**, 286-290

Fields, B. S., Fields, S. R. U., Loy, J. N. C., White, E. H., Steffens, W., and Shotts, E. B. (1993) Attachment and entry of *Legionella pneumophila* in *Hartmannella vermiformis*. *Journal of Infectious Diseases* **167**, 1146-1150

Finsel, I., Ragaz, C., Hoffmann, C., Harrison, C. F., Weber, S., Van Rahden, V. A., Johannes, L., and Hilbi, H. (2013) The *Legionella* effector RidL inhibits retrograde trafficking to promote intracellular replication. *Cell host & microbe* **14**, 38-50

Fischer, M., Haase, I., Simmeth, E., Gerisch, G., and Müller-Taubenberger, A. (2004) A brilliant monomeric red fluorescent protein to visualize cytoskeleton dynamics in *Dictyostelium*. *FEBS letters* **577**, 227-232

Franke, J., and Kessin, R. (1977) A defined minimal medium for axenic strains of *Dictyostelium discoideum*. *Proceedings of the National Academy of Sciences of the United States of America* **74**, 2157

Fraser, D. W., Tsai, T. R., Orenstein, W., Parkin, W. E., Beecham, H. J., Sharrar, R. G., Harris, J., Mallison, G. F., Martin, S. M., McDade, J. E., Shepard, C. C., and Brachman, P. S. (1977) Legionnaires' disease: description of an epidemic of pneumonia. *The New England journal of medicine* **297**, 1189-1197

Gagnon, E., Duclos, S., Rondeau, C., Chevet, E., Cameron, P. H., Steele-Mortimer, O., Paiement, J., Bergeron, J. J., and Desjardins, M. (2002) Endoplasmic reticulum-mediated phagocytosis is a mechanism of entry into macrophages. *Cell* **110**, 119-131

Gary, J. D., Wurmser, A. E., Bonangelino, C. J., Weisman, L. S., and Emr, S. D. (1998) Fab1p is essential for PtdIns(3)*P* 5-kinase activity and the maintenance of vacuolar size and membrane homeostasis. *The Journal of cell biology* **143**, 65-79

Gazdag, E. M., Schöbel, S., Shkumatov, A. V., Goody, R. S., and Itzen, A. (2014) The structure of the N-terminal domain of the *Legionella* protein SidC. *Journal of structural biology* **186**, 188-194

Gazdag, E. M., Streller, A., Haneburger, I., Hilbi, H., Vetter, I. R., Goody, R. S., and Itzen, A. (2013) Mechanism of Rab1b deactivation by the *Legionella pneumophila* GAP LepB. *EMBO reports* **14**, 199-205

Gerisch, G. (2010) Self-organizing actin waves that simulate phagocytic cup structures. *BMC Biophysics* **3**, 7

Gerisch, G., Ecke, M., Schroth-Diez, B., Gerwig, S., Engel, U., Maddera, L., and Clarke, M. (2009) Self-organizing actin waves as planar phagocytic cup structures. *Cell Adh Migr* **3**, 373-382

Glick, T. H., Gregg, M. B., Berman, B., Mallison, G., Rhodes, W. W., and Kassanoff, I. (1978) Pontiac fever an epidemic of unknown etiology in a health department: I. Clinical and epidemiologic aspects. *American journal of epidemiology* **107**, 149-160

Godi, A., Pertile, P., Meyers, R., Marra, P., Di Tullio, G., Iurisci, C., Luini, A., Corda, D., and De Matteis, M. A. (1999) ARF mediates recruitment of PtdIns-4-OH kinase-β and stimulates synthesis of PtdIns(4,5)P_2 on the Golgi complex. *Nature cell biology* **1**, 280-287

Goldoni, P., Visca, P., Pastoris, M. C., Valenti, P., and Orsi, N. (1991) Growth of *Legionella* spp. under conditions of iron restriction. *Journal of medical microbiology* **34**, 113-118

Greub, G., and Raoult, D. (2004) Microorganisms resistant to free-living amoebae. *Clinical microbiology reviews* **17**, 413-433

Hacker, U., Albrecht, R., and Maniak, M. (1997) Fluid-phase uptake by macropinocytosis in *Dictyostelium*. *Journal of Cell Science* **110**, 105-112

Hagele, S., Kohler, R., Merkert, H., Schleicher, M., Hacker, J., and Steinert, M. (2000) *Dictyostelium discoideum*: a new host model system for intracellular pathogens of the genus *Legionella*. *Cellular microbiology* **2**, 165-171

Harding, C. R., Mattheis, C., Mousnier, A., Oates, C. V., Hartland, E. L., Frankel, G., and Schroeder, G. N. (2013) LtpD is a novel *Legionella pneumophila* effector that binds phosphatidylinositol 3-phosphate and inositol monophosphatase IMPA1. *Infection and immunity* **81**, 4261-4270

Heidtman, M., Chen, E. J., Moy, M. Y., and Isberg, R. R. (2009) Large-scale identification of *Legionella pneumophila* Dot/Icm substrates that modulate host cell vesicle trafficking pathways. *Cellular microbiology* **11**, 230-248

Herbes, S. E., Allen, H. E., and Mancy, K. H. (1975) Enzymatic characterization of soluble organic phosphorus in lake water. *Science* **187**, 432-434

Hernandez, L. D., Hueffer, K., Wenk, M. R., and Galán, J. E. (2004) *Salmonella* modulates vesicular traffic by altering phosphoinositide metabolism. *Science* **304**, 1805-1807

Hilbi, H., Segal, G., and Shuman, H. A. (2001) Icm/Dot-dependent upregulation of phagocytosis by *Legionella pneumophila*. *Molecular microbiology* **42**, 603-617

Hilbi, H., Weber, S., and Finsel, I. (2011) Anchors for effectors: subversion of phosphoinositide lipids by *Legionella*. *Frontiers in microbiology* **2**

Hilbi, H., Weber, S. S., Ragaz, C., Nyfeler, Y., and Urwyler, S. (2007) Environmental predators as models for bacterial pathogenesis. *Environmental microbiology* **9**, 563-575

Hirst, P. H., Riley, A., Mills, S., Spiers, I. D., Poyner, D. R., Freeman, S., Potter, B., and Smith, A. W. (1999) Inositol polyphosphate-mediated iron transport in *Pseudomonas aeruginosa*. *Journal of applied microbiology* **86**, 537-543

Holden, E. P., Winkler, H. H., Wood, D. O., and Leinbach, E. D. (1984) Intracellular growth of *Legionella pneumophila* within *Acanthamoeba castellanii* Neff. *Infection and immunity* **45**, 18-24

Horwitz, M. A. (1983) Formation of a novel phagosome by the Legionnaires' disease bacterium (*Legionella pneumophila*) in human monocytes. *The Journal of experimental medicine* **158**, 1319-1331

Horwitz, M. A., and Maxfield, F. R. (1984) *Legionella pneumophila* inhibits acidification of its phagosome in human monocytes. *The Journal of cell biology* **99**, 1936-1943

Hsu, F., Luo, X., Qiu, J., Teng, Y.-B., Jin, J., Smolka, M. B., Luo, Z.-Q., and Mao, Y. (2014) The *Legionella* effector SidC defines a unique family of ubiquitin ligases important for bacterial phagosomal remodeling. *Proceedings of the National Academy of Sciences* **111**, 10538-10543

Hsu, F., Zhu, W., Brennan, L., Tao, L., Luo, Z.-Q., and Mao, Y. (2012) Structural basis for substrate recognition by a unique *Legionella* phosphoinositide phosphatase. *Proceedings of the National Academy of Sciences* **109**, 13567-13572

Hubber, A., and Roy, C. R. (2010) Modulation of host cell function by *Legionella pneumophila* type IV effectors. *Annual review of cell and developmental biology* **26**, 261-283

Hughes, W. E., Woscholski, R., Cooke, F. T., Patrick, R. S., Dove, S. K., McDonald, N. Q., and Parker, P. J. (2000) SAC1 encodes a regulated lipid phosphoinositide phosphatase, defects in which can be suppressed by the homologous Inp52p and Inp53p phosphatases. *Journal of Biological Chemistry* **275**, 801-808

Ikonomov, O. C., Sbrissa, D., Foti, M., Carpentier, J.-L., and Shisheva, A. (2003) PIKfyve controls fluid phase endocytosis but not recycling/degradation of endocytosed receptors or sorting of procathepsin D by regulating multivesicular body morphogenesis. *Molecular biology of the cell* **14**, 4581-4591

Ikonomov, O. C., Sbrissa, D., Ijuin, T., Takenawa, T., and Shisheva, A. (2009) Sac3 is an Insulin-regulated PtdIns(3,5)P_2 phosphatase: gain in insulin responsiveness through Sac3 downregulation in adipocytes. *Journal of Biological Chemistry*, jbc. M109. 025361

Ikonomov, O. C., Sbrissa, D., Mlak, K., Kanzaki, M., Pessin, J., and Shisheva, A. (2002) Functional dissection of lipid and protein kinase signals of PIKfyve reveals the role of PtdIns3,5P_2 production for endomembrane integrity. *Journal of Biological Chemistry* **277**, 9206-9211

Ile, K. E., Schaaf, G., and Bankaitis, V. A. (2006) Phosphatidylinositol transfer proteins and cellular nanoreactors for lipid signaling. *Nature chemical biology* **2**, 576-583

Ingmundson, A., Delprato, A., Lambright, D. G., and Roy, C. R. (2007) *Legionella pneumophila* proteins that regulate Rab1 membrane cycling. *Nature* **450**, 365-369

Irvine, R. F., Letcher, A. J., and Dawson, R. (1984) Phosphatidylinositol-4,5-bisphosphate phosphodiesterase and phosphomonoesterase activities of rat brain. Some properties and possible control mechanisms. *Biochem. J* **218**, 177-185

Jank, T., Böhmer, K. E., Tzivelekidis, T., Schwan, C., Belyi, Y., and Aktories, K. (2012) Domain organization of *Legionella* effector SetA. *Cellular microbiology* **14**, 852-868

Jefferies, H. B., Cooke, F. T., Jat, P., Boucheron, C., Koizumi, T., Hayakawa, M., Kaizawa, H., Ohishi, T., Workman, P., and Waterfield, M. D. (2008) A selective PIKfyve inhibitor blocks PtdIns(3,5)P_2 production and disrupts endomembrane transport and retroviral budding. *EMBO reports* **9**, 164-170

Jones, D. R., Bultsma, Y., Keune, W.-J., Halstead, J. R., Elouarrat, D., Mohammed, S., Heck, A. J., D'Santos, C. S., and Divecha, N. (2006) Nuclear PtdIns5*P* as a transducer of stress signaling: an *in vivo* role for PIP4Kbeta. *Molecular cell* **23**, 685-695

Kagan, J. C., and Roy, C. R. (2002) *Legionella* phagosomes intercept vesicular traffic from endoplasmic reticulum exit sites. *Nat Cell Biol* **4**, 945-954

Kagan, J. C., Stein, M.-P., Pypaert, M., and Roy, C. R. (2004) *Legionella* subvert the functions of Rab1 and Sec22b to create a replicative organelle. *The Journal of experimental medicine* **199**, 1201-1211

Kamen, L. A., Levinsohn, J., and Swanson, J. A. (2007) Differential association of phosphatidylinositol 3-kinase, SHIP-1, and PTEN with forming phagosomes. *Molecular biology of the cell* **18**, 2463-2472

Katso, R., Okkenhaug, K., Ahmadi, K., White, S., Timms, J., and Waterfield, M. D. (2001) Cellular function of phosphoinositide 3-kinases: implications for development, immunity, homeostasis, and cancer. *Annual review of cell and developmental biology* **17**, 615-675

Kessler, A., Schell, U., Sahr, T., Tiaden, A., Harrison, C., Buchrieser, C., and Hilbi, H. (2013) The *Legionella pneumophila* orphan sensor kinase LqsT regulates competence and pathogen-host interactions as a component of the LAI-1 circuit. *Environmental microbiology* **15**, 646-662

Khelef, N., Shuman, H. A., and Maxfield, F. R. (2001) Phagocytosis of wild-type *Legionella pneumophila* occurs through a wortmannin-insensitive pathway. *Infection and immunity* **69**, 5157-5161

Kong, A. M., Speed, C. J., O'Malley, C. J., Layton, M. J., Meehan, T., Loveland, K. L., Cheema, S., Ooms, L. M., and Mitchell, C. A. (2000) Cloning and characterization of a 72-kDa inositol-polyphosphate 5-phosphatase localized to the Golgi network. *Journal of Biological Chemistry* **275**, 24052-24064

Ku, B., Lee, K.-H., Park, W. S., Yang, C.-S., Ge, J., Lee, S.-G., Cha, S.-S., Shao, F., Do Heo, W., and Jung, J. U. (2012) VipD of *Legionella pneumophila* targets activated Rab5 and Rab22 to interfere with endosomal trafficking in macrophages. *PLoS pathogens* **8**, e1003082

Kubori, T., Hyakutake, A., and Nagai, H. (2008) *Legionella* translocates an E3 ubiquitin ligase that has multiple U-boxes with distinct functions. *Molecular microbiology* **67**, 1307-1319

Kular, G. S., Chaudhary, A., and Prestwich, G. (2002) Co-operation of phosphatidylinositol transfer protein with phosphoinositide 3-kinase γ *in vitro*. *Advances in enzyme regulation* **42**, 53

Kuspa, A., and Loomis, W. F. (1992) Tagging developmental genes in *Dictyostelium* by restriction enzyme-mediated integration of plasmid DNA. *Proceedings of the National Academy of Sciences* **89**, 8803-8807

Laporte, J., Bedez, F., Bolino, A., and Mandel, J.-L. (2003) Myotubularins, a large disease-associated family of cooperating catalytically active and inactive phosphoinositides phosphatases. *Human molecular genetics* **12**, R285-R292

Laussmann, T., Pikzack, C., Thiel, U., Mayr, G. W., and Vogel, G. (2000) Diphospho-*myo*-inositol phosphates during the life cycle of *Dictyostelium* and *Polysphondylium*. *European Journal of Biochemistry* **267**, 2447-2451

Laussmann, T., Reddy, K., Falck, J., and Vogel, G. (1997) Diphospho-*myo*-inositol phosphates from *Dictyostelium* identified as D-6-diphospho-*myo*-inositol pentakisphosphate and D-5,6-bisdiphospho-*myo*-inositol tetrakisphosphate. *Biochem. J* **322**, 31-33

Lemmon, M. A. (2008) Membrane recognition by phospholipid-binding domains. *Nature reviews Molecular cell biology* **9**, 99-111

Levi, S., Polyakov, M., and Egelhoff, T. T. (2000) Green fluorescent protein and epitope tag fusion vectors for *Dictyostelium discoideum*. *Plasmid* **44**, 231-238

Li, J., Yen, C., Liaw, D., Podsypanina, K., Bose, S., Wang, S. I., Puc, J., Miliaresis, C., Rodgers, L., and McCombie, R. (1997) PTEN, a putative protein tyrosine phosphatase gene mutated in human brain, breast, and prostate cancer. *Science* **275**, 1943-1947

Lim, B. L., Yeung, P., Cheng, C., and Hill, J. E. (2007) Distribution and diversity of phytate-mineralizing bacteria. *ISME J* **1**, 321-330

Liu, Y., and Luo, Z.-Q. (2007) The *Legionella pneumophila* effector SidJ is required for efficient recruitment of endoplasmic reticulum proteins to the bacterial phagosome. *Infection and immunity* **75**, 592-603

Loewus, F. A., and Murthy, P. P. (2000) *myo*-Inositol metabolism in plants. *Plant science* **150**, 1-19

Lomasney, J. W., Cheng, H.-F., Wang, L.-P., Kuan, Y.-S., Liu, S.-M., Fesik, S. W., and King, K. (1996) Phosphatidylinositol 4,5-bisphosphate binding to the pleckstrin homology domain of phospholipase C-δ1 enhances enzyme activity. *Journal of Biological Chemistry* **271**, 25316-25326

Loovers, H. M., Kortholt, A., de Groote, H., Whitty, L., Nussbaum, R. L., and Van Haastert, P. J. (2007) Regulation of phagocytosis in *Dictyostelium* by the inositol 5-phosphatase OCRL homolog Dd5P4. *Traffic* **8**, 618-628

Lott, J., Ockenden, I., Raboy, V., and Batten, G. D. (2000) Phytic acid and phosphorus in crop seeds and fruits: a global estimate. *Seed Science Research* **10**, 11-34

Lowe, C., Terrey, M., and MacLachlan, E. (1952) Organic-aciduria, decreased renal ammonia production, hydropthalmos, and mental retardation. A Clinical Entity. *AMA American journal of diseases of children* **83**, 164-184

Lu, H., and Clarke, M. (2005) Dynamic properties of *Legionella*-containing phagosomes in *Dictyostelium* amoebae. *Cellular microbiology* **7**, 995-1007

Lung, S.-C., and Lim, B. L. (2006) Assimilation of phytate-phosphorus by the extracellular phytase activity of tobacco (*Nicotiana tabacum*) is affected by the availability of soluble phytate. *Plant and soil* **279**, 187-199

Luo, H. R., Huang, Y. E., Chen, J. C., Saiardi, A., Iijima, M., Ye, K., Huang, Y., Nagata, E., Devreotes, P., and Snyder, S. H. (2003) Inositol pyrophosphates mediate chemotaxis in *Dictyostelium* via pleckstrin homology domain-PtdIns(3,4,5)P_3 Interactions. *Cell* **114**, 559-572

Machner, M. P., and Isberg, R. R. (2006) Targeting of host Rab GTPase function by the intravacuolar pathogen *Legionella pneumophila*. *Developmental cell* **11**, 47-56

Macklon, A., Grayston, S., Shand, C., Sim, A., Sellars, S., and Ord, B. (1997) Uptake and transport of phosphorus by *Agrostis capillaris* seedlings from rapidly hydrolysed organic sources extracted from ^{32}P-labelled bacterial cultures. *Plant and Soil* **190**, 163-167

Maehama, T., and Dixon, J. E. (1998) The tumor suppressor, PTEN/MMAC1, dephosphorylates the lipid second messenger, phosphatidylinositol 3,4,5-trisphosphate. *Journal of Biological Chemistry* **273**, 13375-13378

Majumder, A. L., Johnson, M. D., and Henry, S. A. (1997) 1L-*myo*-Inositol-1-phosphate synthase. *Biochimica et Biophysica Acta (BBA)-Lipids and Lipid Metabolism* **1348**, 245-256

Malchow, D., Nagele, B., Schwarz, H., and Gerisch, G. (1972) Membrane-bound cyclic AMP phosphodiesterase in chemotactically responding cells of *Dictyostelium discoideum*. *European journal of biochemistry / FEBS* **28**, 136-142

Mallo, G. V., Espina, M., Smith, A. C., Terebiznik, M. R., Alemán, A., Finlay, B. B., Rameh, L. E., Grinstein, S., and Brumell, J. H. (2008) SopB promotes phosphatidylinositol 3-phosphate formation on *Salmonella* vacuoles by recruiting Rab5 and Vps34. *The Journal of cell biology* **182**, 741-752

Mampel, J., Spirig, T., Weber, S. S., Haagensen, J. A., Molin, S., and Hilbi, H. (2006) Planktonic replication is essential for biofilm formation by *Legionella pneumophila* in a complex medium under static and dynamic flow conditions. *Applied and environmental microbiology* **72**, 2885-2895

Manstein, D. J., Schuster, H. P., Morandini, P., and Hunt, D. M. (1995) Cloning vectors for the production of proteins in *Dictyostelium discoideum*. *Gene* **162**, 129-134

Martin, J.-B., Foray, M.-F., Klein, G., and Satre, M. (1987) Identification of inositol hexaphosphate in ^{31}P-NMR spectra of *Dictyostelium discoideum* amoebae. Relevance to intracellular pH determination. *Biochimica et Biophysica Acta (BBA)-Molecular Cell Research* **931**, 16-25

McConnachie, G., Pass, I., Walker, S., and Downes, C. (2003) Interfacial kinetic analysis of the tumour suppressor phosphatase, PTEN: evidence for activation by anionic phospholipids. *Biochem. J* **371**, 947-955

McDade, J. E., Shepard, C. C., Fraser, D. W., Tsai, T. R., Redus, M. A., and Dowdle, W. R. (1977) Legionnaires' disease: isolation of a bacterium and demonstration of its role in other respiratory disease. *The New England journal of medicine* **297**, 1197-1203

Menniti, F., Miller, R., Putney, J., and Shears, S. (1993) Turnover of inositol polyphosphate pyrophosphates in pancreatoma cells. *Journal of Biological Chemistry* **268**, 3850-3856

Moffat, J. F., and Tompkins, L. S. (1992) A quantitative model of intracellular growth of *Legionella pneumophila* in *Acanthamoeba castellanii*. *Infection and immunity* **60**, 296-301

Molmeret, M., and Abu Kwaik, Y. (2002) How does *Legionella pneumophila* exit the host cell? *Trends in microbiology* **10**, 258-260

Molmeret, M., Alli, O. T., Zink, S., Flieger, A., Cianciotto, N. P., and Kwaik, Y. A. (2002) *icmT* is essential for pore formation-mediated egress of *Legionella pneumophila* from mammalian and protozoan cells. *Infection and immunity* **70**, 69-78

Molmeret, M., Bitar, D. M., Han, L., and Kwaik, Y. A. (2004) Disruption of the phagosomal membrane and egress of *Legionella pneumophila* into the cytoplasm during the last stages of intracellular infection of macrophages and *Acanthamoeba polyphaga*. *Infection and immunity* **72**, 4040-4051

Molofsky, A. B., and Swanson, M. S. (2004) Differentiate to thrive: lessons from the *Legionella pneumophila* life cycle. *Molecular microbiology* **53**, 29-40

Muder, R. R., Yu, V. L., and Woo, A. H. (1986) Mode of transmission of *Legionella pneumophila*: A critical review. *Archives of internal medicine* **146**, 1607-1612

Mukherjee, S., Liu, X., Arasaki, K., McDonough, J., Galán, J. E., and Roy, C. R. (2011) Modulation of Rab GTPase function by a protein phosphocholine transferase. *Nature* **477**, 103-106

Mullaney, E. J., and Ullah, A. H. (2003) The term phytase comprises several different classes of enzymes. *Biochemical and biophysical research communications* **312**, 179-184

Müller, M. P., Peters, H., Blümer, J., Blankenfeldt, W., Goody, R. S., and Itzen, A. (2010) The *Legionella* effector protein DrrA AMPylates the membrane traffic regulator Rab1b. *Science* **329**, 946-949

Müller-Taubenberger, A., Kortholt, A., and Eichinger, L. (2012) Simple system - substantial share: The use of *Dictyostelium* in cell biology and molecular medicine. *Eur J Cell Biol*

Müller-Taubenberger, A., Lupas, A. N., Li, H., Ecke, M., Simmeth, E., and Gerisch, G. (2001) Calreticulin and calnexin in the endoplasmic reticulum are important for phagocytosis. *The EMBO journal* **20**, 6772-6782

Murata, T., Delprato, A., Ingmundson, A., Toomre, D. K., Lambright, D. G., and Roy, C. R. (2006) The *Legionella pneumophila* effector protein DrrA is a Rab1 guanine nucleotide-exchange factor. *Nature cell biology* **8**, 971-977

Murga, R., Forster, T. S., Brown, E., Pruckler, J. M., Fields, B. S., and Donlan, R. M. (2001) Role of biofilms in the survival of *Legionella pneumophila* in a model potable-water system. *Microbiology* **147**, 3121-3126

Nagai, H., Cambronne, E. D., Kagan, J. C., Amor, J. C., Kahn, R. A., and Roy, C. R. (2005) A C-terminal translocation signal required for Dot/Icm-dependent delivery of the *Legionella* RalF protein to host cells. *Proceedings of the National Academy of Sciences of the United States of America* **102**, 826-831

Nagai, H., Kagan, J. C., Zhu, X., Kahn, R. A., and Roy, C. R. (2002) A bacterial guanine nucleotide exchange factor activates ARF on *Legionella phagosomes*. *Science* **295**, 679-682

Nakano, N., Kubori, T., Kinoshita, M., Imada, K., and Nagai, H. (2010) Crystal structure of *Legionella* DotD: insights into the relationship between type IVB and type II/III secretion systems. *PLoS pathogens* **6**, e1001129

Nakatsu, F., Perera, R. M., Lucast, L., Zoncu, R., Domin, J., Gertler, F. B., Toomre, D., and De Camilli, P. (2010) The inositol 5-phosphatase SHIP2 regulates endocytic clathrin-coated pit dynamics. *The Journal of cell biology* **190**, 307-315

Nash, T., Libby, D., and Horwitz, M. (1984) Interaction between the legionnaires' disease bacterium (*Legionella pneumophila*) and human alveolar macrophages. Influence of antibody, lymphokines, and hydrocortisone. *Journal of Clinical Investigation* **74**, 771

Nasuhoglu, C., Feng, S., Mao, J., Yamamoto, M., Yin, H. L., Earnest, S., Barylko, B., Albanesi, J. P., and Hilgemann, D. W. (2002) Nonradioactive analysis of phosphatidylinositides and other anionic phospholipids by anion-exchange high-performance liquid chromatography with suppressed conductivity detection. *Analytical biochemistry* **301**, 243-254

Neunuebel, M. R., Chen, Y., Gaspar, A. H., Backlund, P. S., Yergey, A., and Machner, M. P. (2011) De-AMPylation of the small GTPase Rab1 by the pathogen *Legionella pneumophila*. *Science* **333**, 453-456

Neunuebel, M. R., Mohammadi, S., Jarnik, M., and Machner, M. P. (2012) *Legionella pneumophila* LidA affects nucleotide binding and activity of the host GTPase Rab1. *Journal of bacteriology* **194**, 1389-1400

Newsome, A. L., Baker, R., Miller, R., and Arnold, R. (1985) Interactions between *Naegleria fowleri* and *Legionella pneumophila*. *Infection and immunity* **50**, 449-452

Newton, H. J., Sansom, F. M., Bennett-Wood, V., and Hartland, E. L. (2006) Identification of *Legionella pneumophila*-specific genes by genomic subtractive hybridization with *Legionella micdadei* and identification of *lpnE*, a gene required for efficient host cell entry. *Infection and immunity* **74**, 1683-1691

Nguyen, T. M. N., Ilef, D., Jarraud, S., Rouil, L., Campese, C., Che, D., Haeghebaert, S., Ganiayre, F., Marcel, F., and Etienne, J. (2006) A community-wide outbreak of legionnaires disease linked to industrial cooling towers—how far can contaminated aerosols spread? *Journal of Infectious Diseases* **193**, 102-111

Nicot, A. S., and Laporte, J. (2008) Endosomal phosphoinositides and human diseases. *Traffic* **9**, 1240-1249

Niebuhr, K., Giuriato, S., Pedron, T., Philpott, D. J., Gaits, F., Sable, J., Sheetz, M. P., Parsot, C., Sansonetti, P. J., and Payrastre, B. (2002) Conversion of PtdIns(4,5)P_2 into PtdIns(5)*P* by the *S. flexneri* effector IpgD reorganizes host cell morphology. *The EMBO journal* **21**, 5069-5078

Ninio, S., Zuckman-Cholon, D. M., Cambronne, E. D., and Roy, C. R. (2005) The *Legionella* IcmS–IcmW protein complex is important for Dot/Icm-mediated protein translocation. *Molecular microbiology* **55**, 912-926

Odriozola, L., Singh, G., Hoang, T., and Chan, A. M. (2007) Regulation of PTEN activity by its carboxyl-terminal autoinhibitory domain. *Journal of Biological Chemistry* **282**, 23306-23315

Pan, X., Lührmann, A., Satoh, A., Laskowski-Arce, M. A., and Roy, C. R. (2008) Ankyrin repeat proteins comprise a diverse family of bacterial type IV effectors. *Science* **320**, 1651-1654

Parent, C. A., Blacklock, B. J., Froehlich, W. M., Murphy, D. B., and Devreotes, P. N. (1998) G protein signaling events are activated at the leading edge of chemotactic cells. *Cell* **95**, 81-91

Pendaries, C., Tronchère, H., Arbibe, L., Mounier, J., Gozani, O., Cantley, L., Fry, M. J., Gaits-Iacovoni, F., Sansonetti, P. J., and Payrastre, B. (2006) PtdIns(5)*P* activates the host cell PI3-kinase/Akt pathway during *Shigella flexneri* infection. *The EMBO journal* **25**, 1024-1034

Peracino, B., Balest, A., and Bozzaro, S. (2010) Phosphoinositides differentially regulate bacterial uptake and Nramp1-induced resistance to *Legionella* infection in *Dictyostelium*. *J Cell Sci* **123**, 4039-4051

Peracino, B., Buracco, S., and Bozzaro, S. (2013) The Nramp (Slc11) proteins regulate development, resistance to pathogenic bacteria and iron homeostasis in *Dictyostelium discoideum*. *Journal of cell science* **126**, 301-311

Pisani, F., Livermore, T., Rose, G., Chubb, J. R., Gaspari, M., and Saiardi, A. (2014) Analysis of *Dictyostelium discoideum* inositol pyrophosphate metabolism by gel electrophoresis. *PloS one* **9**, e85533

Raboy, V. (2003) *myo*-Inositol-1,2,3,4,5,6-hexakisphosphate. *Phytochemistry* **64**, 1033-1043

Ragaz, C., Pietsch, H., Urwyler, S., Tiaden, A., Weber, S. S., and Hilbi, H. (2008) The *Legionella pneumophila* phosphatidylinositol-4 phosphate-binding type IV substrate SidC recruits endoplasmic reticulum vesicles to a replication-permissive vacuole. *Cellular microbiology* **10**, 2416-2433

Raucher, D., Stauffer, T., Chen, W., Shen, K., Guo, S., York, J. D., Sheetz, M. P., and Meyer, T. (2000) Phosphatidylinositol 4,5-bisphosphate functions as a second messenger that regulates cytoskeleton–plasma membrane adhesion. *Cell* **100**, 221-228

Redfern, R. E., Redfern, D., Furgason, M. L., Munson, M., Ross, A. H., and Gericke, A. (2008) PTEN phosphatase selectively binds phosphoinositides and undergoes structural changes. *Biochemistry* **47**, 2162-2171

Reeves, M., Pine, L., Hutner, S., George, J., and Harrell, W. (1981) Metal requirements of *Legionella pneumophila*. *Journal of clinical microbiology* **13**, 688-695

Robinson, C. G., and Roy, C. R. (2006) Attachment and fusion of endoplasmic reticulum with vacuoles containing *Legionella pneumophila*. *Cellular microbiology* **8**, 793-805

Ross, C. A., Meldolesi, J., Milner, T. A., Satoh, T., Supattapone, S., and Snyder, S. H. (1989) Inositol 1,4,5-trisphosphate receptor localized to endoplasmic reticulum in cerebellar Purkinje neurons.

Rowbotham, T. J. (1980) Preliminary report on the pathogenicity of *Legionella pneumophila* for freshwater and soil amoebae. *Journal of clinical pathology* **33**, 1179-1183

Roy, C. R., Berger, K. H., and Isberg, R. R. (1998) *Legionella pneumophila* DotA protein is required for early phagosome trafficking decisions that occur within minutes of bacterial uptake. *Molecular microbiology* **28**, 663-674

Rutherford, A. C., Traer, C., Wassmer, T., Pattni, K., Bujny, M. V., Carlton, J. G., Stenmark, H., and Cullen, P. J. (2006) The mammalian phosphatidylinositol 3-phosphate 5-kinase (PIKfyve) regulates endosome-to-TGN retrograde transport. *Journal of cell science* **119**, 3944-3957

Sabria, M., and Yu, V. L. (2002) Hospital-acquired legionellosis: solutions for a preventable infection. *The Lancet infectious diseases* **2**, 368-373

Sadosky, A. B., Wiater, L. A., and Shuman, H. A. (1993) Identification of *Legionella pneumophila* genes required for growth within and killing of human macrophages. *Infection and immunity* **61**, 5361-5373

Schoebel, S., Oesterlin, L. K., Blankenfeldt, W., Goody, R. S., and Itzen, A. (2009) RabGDI displacement by DrrA from *Legionella* is a consequence of its guanine nucleotide exchange activity. *Molecular cell* **36**, 1060-1072

Segal, G., Feldman, M., and Zusman, T. (2005) The Icm/Dot type-IV secretion systems of *Legionella pneumophila* and *Coxiella burnetii*. *FEMS microbiology reviews* **29**, 65-81

Segal, G., Russo, J. J., and Shuman, H. A. (1999) Relationships between a new type IV secretion system and the icm/dot virulence system of *Legionella pneumophila*. *Molecular microbiology* **34**, 799-809

Segal, G., and Shuman, H. A. (1998) Intracellular multiplication and human macrophage killing by *Legionella pneumophila* are inhibited by conjugal components of IncQ plasmid RSF1010. *Molecular microbiology* **30**, 197-208

Shohdy, N., Efe, J. A., Emr, S. D., and Shuman, H. A. (2005) Pathogen effector protein screening in yeast identifies *Legionella* factors that interfere with membrane trafficking. *Proceedings of the National Academy of Sciences of the United States of America* **102**, 4866-4871

Smith, A. W., Poyner, D. R., Hughes, H. K., and Lambert, P. A. (1994) Siderophore activity of *myo*-inositol hexakisphosphate in *Pseudomonas aeruginosa*. *Journal of bacteriology* **176**, 3455-3459

Solomon, J. M., Rupper, A., Cardelli, J. A., and Isberg, R. R. (2000) Intracellular growth of *Legionella pneumophila* in *Dictyostelium discoideum*, a system for genetic analysis of host-pathogen interactions. *Infection and immunity* **68**, 2939-2947

Sprong, H., Van der Sluijs, P., and Van Meer, G. (2001) How proteins move lipids and lipids move proteins. *Nature Reviews Molecular Cell Biology* **2**, 504-513

Stephens, L., and Irvine, R. (1990) Stepwise phosphorylation of *myo*-inositol leading to *myo*-inositol hexakisphosphate in *Dictyostelium*.

Stephens, L., Radenberg, T., Thiel, U., Vogel, G., Khoo, K.-H., Dell, A., Jackson, T., Hawkins, P., and Mayr, G. (1993) The detection, purification, structural characterization, and metabolism of diphosphoinositol pentakisphosphate(s) and bisdiphosphoinositol tetrakisphosphate(s). *Journal of Biological Chemistry* **268**, 4009-4015

Stokoe, D., Stephens, L. R., Copeland, T., Gaffney, P. R., Reese, C. B., Painter, G. F., Holmes, A. B., McCormick, F., and Hawkins, P. T. (1997) Dual role of phosphatidylinositol-3,4,5-trisphosphate in the activation of protein kinase B. *Science* **277**, 567-570

Suchy, S. F., Olivos-Glander, I. M., and Nussbaum, R. L. (1995) Lowe Syndrome, a deficiency of a phosphatidyl-inositol 4,5-bisphosphate 5-phosphatase in the Golgi apparatus. *Human molecular genetics* **4**, 2245-2250

Suzumura, M., and Kamatani, A. (1995) Origin and distribution of inositol hexaphosphate in estuarine and coastal sediments. *Limnology and oceanography* **40**, 1254-1261

Swanson, M. S., and Isberg, R. R. (1995) Association of *Legionella pneumophila* with the macrophage endoplasmic reticulum. *Infection and immunity* **63**, 3609-3620

Tang, J., Leung, A., Leung, C., and Lim, B. L. (2006) Hydrolysis of precipitated phytate by three distinct families of phytases. *Soil Biology and Biochemistry* **38**, 1316-1324

Tato, I., Zunzunegui, S., De La Cruz, F., and Cabezon, E. (2005) TrwB, the coupling protein involved in DNA transport during bacterial conjugation, is a DNA-dependent ATPase. *Proceedings of the National Academy of Sciences of the United States of America* **102**, 8156-8161

Terebiznik, M. R., Vieira, O. V., Marcus, S. L., Slade, A., Yip, C. M., Trimble, W. S., Meyer, T., Finlay, B. B., and Grinstein, S. (2002) Elimination of host cell PtdIns(4,5)P_2 by bacterial SigD promotes membrane fission during invasion by *Salmonella*. *Nature Cell Biology* **4**, 766-773

Tiaden, A., Spirig, T., Sahr, T., Walti, M. A., Boucke, K., Buchrieser, C., and Hilbi, H. (2010) The autoinducer synthase LqsA and putative sensor kinase LqsS regulate phagocyte interactions, extracellular filaments and a genomic island of *Legionella pneumophila*. *Environmental microbiology* **12**, 1243-1259

Tiaden, A., Spirig, T., Weber, S. S., Bruggemann, H., Bosshard, R., Buchrieser, C., and Hilbi, H. (2007) The *Legionella pneumophila* response regulator LqsR promotes host cell interactions as an element of the virulence regulatory network controlled by RpoS and LetA. *Cellular microbiology* **9**, 2903-2920

Tilney, L. G., Harb, O. S., Connelly, P. S., Robinson, C. G., and Roy, C. R. (2001) How the parasitic bacterium *Legionella pneumophila* modifies its phagosome and transforms it into rough ER: implications for conversion of plasma membrane to the ER membrane. *Journal of Cell Science* **114**, 4637-4650

Toulabi, L., Wu, X., Cheng, Y., and Mao, Y. (2013) Identification and structural characterization of a *Legionella* phosphoinositide phosphatase. *Journal of Biological Chemistry* **288**, 24518-24527

Tsai, T. F., Finn, D. R., Plikaytis, B. D., McCauley, W., Martin, S. M., and Fraser, D. W. (1979) Legionnaires' disease: clinical features of the epidemic in Philadelphia. *Annals of internal medicine* **90**, 509-517

Turner, B. L., Paphazy, M. J., Haygarth, P. M., and McKelvie, I. D. (2002) Inositol phosphates in the environment. *Philosophical Transactions of the Royal Society of London. Series B: Biological Sciences* **357**, 449-469

Ungewickell, A., Ward, M. E., Ungewickell, E., and Majerus, P. W. (2004) The inositol polyphosphate 5-phosphatase Ocrl associates with endosomes that are partially coated with clathrin. *Proceedings of the National Academy of Sciences of the United States of America* **101**, 13501-13506

Urwyler, S., Brombacher, E., and Hilbi, H. (2009) Endosomal and secretory markers of the *Legionella*-containing vacuole. *Communicative & integrative biology* **2**, 107-109

Urwyler, S., Nyfeler, Y., Ragaz, C., Lee, H., Mueller, L. N., Aebersold, R., and Hilbi, H. (2009) Proteome analysis of *Legionella* vacuoles purified by magnetic immunoseparation reveals secretory and endosomal GTPases. *Traffic* **10**, 76-87

Van der Kaay, J., Wesseling, J., and Van Haastert, P. (1995) Nucleus-associated phosphorylation of Ins(1,4,5)P_3 to InsP_6 in *Dictyostelium*. *Biochem. J* **312**, 911-917

Van Haastert, P. J., and Van Dijken, P. (1997) Biochemistry and genetics of inositol phosphate metabolism in *Dictyostelium*. *FEBS letters* **410**, 39-43

Vergne, I., Chua, J., Lee, H.-H., Lucas, M., Belisle, J., and Deretic, V. (2005) Mechanism of phagolysosome biogenesis block by viable *Mycobacterium tuberculosis*. *Proceedings of the National Academy of Sciences of the United States of America* **102**, 4033-4038

Victor, L. Y., Plouffe, J. F., Pastoris, M. C., Stout, J. E., Schousboe, M., Widmer, A., Summersgill, J., File, T., Heath, C. M., and Paterson, D. L. (2002) Distribution of *Legionella* species and serogroups isolated by culture in patients with sporadic community-acquired legionellosis: an international collaborative survey. *Journal of Infectious Diseases* **186**, 127-128

Victor, L. Y., Zuravleff, J. J., Gavlik, L., and Magnussen, M. H. (1983) Lack of evidence for person-to-person transmission of Legionnaires' disease. *Journal of Infectious Diseases* **147**, 362-362

Vieira, O. V., Botelho, R. J., Rameh, L., Brachmann, S. M., Matsuo, T., Davidson, H. W., Schreiber, A., Backer, J. M., Cantley, L. C., and Grinstein, S. (2001) Distinct roles of class I and class III phosphatidylinositol 3-kinases in phagosome formation and maturation. *The Journal of cell biology* **155**, 19-26

Vincent, C. D., Friedman, J. R., Jeong, K. C., Buford, E. C., Miller, J. L., and Vogel, J. P. (2006) Identification of the core transmembrane complex of the *Legionella* Dot/Icm type IV secretion system. *Molecular microbiology* **62**, 1278-1291

Vincent, C. D., Friedman, J. R., Jeong, K. C., Sutherland, M. C., and Vogel, J. P. (2012) Identification of the DotL coupling protein subcomplex of the *Legionella* Dot/Icm type IV secretion system. *Molecular microbiology* **85**, 378-391

Vogel, J. P., Andrews, H. L., Wong, S. K., and Isberg, R. R. (1998) Conjugative transfer by the virulence system of *Legionella pneumophila*. *Science* **279**, 873-876

Walch-Solimena, C., and Novick, P. (1999) The yeast phosphatidylinositol-4-OH kinase pik1 regulates secretion at the Golgi. *Nature cell biology* **1**, 523-525

Watarai, M., Derre, I., Kirby, J., Growney, J. D., Dietrich, W. F., and Isberg, R. R. (2001) *Legionella pneumophila* is internalized by a macropinocytotic uptake pathway controlled by the Dot/Icm system and the mouse Lgn1 locus. *The Journal of experimental medicine* **194**, 1081-1096

Watts, D. J., and Ashworth, J. M. (1970) Growth of myxameobae of the cellular slime mould *Dictyostelium discoideum* in axenic culture. *Biochem J* **119**, 171-174

Weber, S., Wagner, M., and Hilbi, H. (2014) Live-cell imaging of phosphoinositide dynamics and membrane architecture during *Legionella* infection. *mBio* **5**, e00839-00813

Weber, S. S., Ragaz, C., and Hilbi, H. (2009) The inositol polyphosphate 5-phosphatase OCRL1 restricts intracellular growth of *Legionella*, localizes to the replicative vacuole and binds to the bacterial effector LpnE. *Cellular microbiology* **11**, 442-460

Weber, S. S., Ragaz, C., Reus, K., Nyfeler, Y., and Hilbi, H. (2006) *Legionella pneumophila* exploits PI(4)*P* to anchor secreted effector proteins to the replicative vacuole. *PLoS pathogens* **2**, e46

Wen, P. J., Osborne, S. L., Morrow, I. C., Parton, R. G., Domin, J., and Meunier, F. A. (2008) Ca^{2+}-regulated pool of phosphatidylinositol-3-phosphate produced by phosphatidylinositol 3-kinase C2α on neurosecretory vesicles. *Molecular biology of the cell* **19**, 5593-5603

Whiteford, C., Brearley, C., and Ulug, E. (1997) Phosphatidylinositol 3,5-bisphosphate defines a novel PI 3-kinase pathway in resting mouse fibroblasts. *Biochem. J* **323**, 597-601

Wisniewski, D., Strife, A., Swendeman, S., Erdjument-Bromage, H., Geromanos, S., Kavanaugh, W. M., Tempst, P., and Clarkson, B. (1999) A novel SH2-containing phosphatidylinositol 3,4,5-trisphosphate 5-phosphatase (SHIP2) is constitutively tyrosine phosphorylated and associated with src homologous and collagen gene (SHC) in chronic myelogenous leukemia progenitor cells. *Blood* **93**, 2707-2720

Xu, D., Joglekar, A. P., Williams, A. L., and Hay, J. C. (2000) Subunit structure of a mammalian ER/Golgi SNARE complex. *Journal of Biological Chemistry* **275**, 39631-39639

Xu, L., Shen, X., Bryan, A., Banga, S., Swanson, M. S., and Luo, Z.-Q. (2010) Inhibition of host vacuolar H^+-ATPase activity by a *Legionella pneumophila* effector. *PLoS pathogens* **6**, e1000822

Yamada, K. M., and Araki, M. (2001) Tumor suppressor PTEN: modulator of cell signaling, growth, migration and apoptosis. *Journal of cell science* **114**, 2375-2382

Yamaga, M., Fujii, M., Kamata, H., Hirata, H., and Yagisawa, H. (1999) Phospholipase C-δ1 contains a functional nuclear export signal sequence. *Journal of Biological Chemistry* **274**, 28537-28541

Zhang, X., Jefferson, A. B., Auethavekiat, V., and Majerus, P. W. (1995) The protein deficient in Lowe syndrome is a phosphatidylinositol-4,5-bisphosphate 5-phosphatase. *Proceedings of the National Academy of Sciences* **92**, 4853-4856

Zusman, T., Aloni, G., Halperin, E., Kotzer, H., Degtyar, E., Feldman, M., and Segal, G. (2007) The response regulator PmrA is a major regulator of the *icm/dot* type IV secretion system in *Legionella pneumophila* and *Coxiella burnetii*. *Molecular microbiology* **63**, 1508-1523

Acknowledgements

I would like thank

- Prof. Dr. Hubert Hilbi for the opportunity to complete this four-year Ph D thesis in his laboratory at the Max von Pettenkofer-Institut der LMU München

- Friends and co-workers in the Hilbi group (in order of arrival: Gudrun Pfaffinger, Ivo Finsel, Eva Rothmeier, Stephanie Dolinsky, Aline Kessler, Ursula Schell, Christine Hoffmann, Christopher Harrison, Maria Wagner, Sylvia Simon, Ina Haneburger, Christian Manske, Johanna Schmölders and Bernhard Steiner) for support, engaging scientific discussion, engaging scientific collaboration, and engaging scientific parties

- Friends and members of the Max von Pettenkofer-Institut who made this PhD adventure what it was

- Parents and Grandparents for making the first stages of studying abroad possible

- Family and friends for all their encouragement